ANNUAL TECHNICAL REPORT

Contract AF 19(628)-5100
1 September 1967

Department of Geophysics and Geophysical Engineering

Saint Louis University

ARPA Order Number: 292, Amendment 45
Project Code Number: 5810
Contractor: Saint Louis University
Date of Contract: 1 September 1965
Contract Number: AF 19(628)-5100
Amount of Contract: $530,985
Contract Expiration Date: 31 August 1969
Project Director: Carl Kisslinger, JE 5-3300/540
Title of Work: Research in Seismology

Table of Contents

A. Work in progress or nearing completion

1. Travel times and amplitudes of long period body shear waves from nuclear explosions 1

2. The use of amplitude data in focal mechanism studies 11

3. Azimuthal variation of the P wave particle motion from the great circle path 24

4. P time delays and continental uplift 31

5. The mechanism of the earthquakes of the Rat Island earthquake sequence of 4 February 1965 50

6. Model studies of decoupling of explosions 61

7. Determination of depth of an earthquake focus from the spectrum of body waves 76

8. Factors affecting the determination of phase velocities 83

B. Work already published or submitted for publication 95

Annual Technical Report and Geophysical Engineering

The report contains reports by the Department of Geophysics & Planetary Physics of the University of California

Introduction

During the course of the year the following studies were conducted: body wave studies of special effects related to path of propagation and station site, the focal mechanism of earthquakes, model studies of the relation between cavity size and decoupling of explosive sources, the determination of depth of focus, and the phase velocity of surface waves. Some of these studies have been completed and are published or submitted for publication. Others are still under investigation or are as yet in the process of preparation for publication. Accordingly, this summary is divided into two sections corresponding to the completion status of the work.

A. Work in progress or nearing completion.

1. Travel Times and Amplitudes of Long Period Body Shear Waves from Nuclear Explosions

The nuclear events Half-Beak and Greeley, which took place at the Nevada Test Site on 30 June and 20 December 1966, respectively, generated relatively large amplitude long-period shear waves. In particular they provided data for determining travel times and amplitudes of long-period body shear (S) waves; until this time no nuclear explosions had produced useful data of this type. To the best of our knowledge the travel times and amplitudes included in this report are the first of this kind for explosion-generated S waves.

Seismograms which supplied the data discussed in this report were obtained from WWSS, LRSM, and Saint Louis University network stations. Additional seismograms from the LRSM and Canadian network stations have been requested by us; they will be analyzed in the coming months as a continuation of the work contained in this report.

For the purpose of determining the velocity structure of the earth's mantle the use of S waves has one decided advantage over the use of P waves. At those distances where the travel-time curve is multi-valued, the arrivals corresponding to the different branches can often be recognized by a change in polarization of the S motion. This distinctive feature does not apply to P waves, for they are all linearly polarized. The identification of later P arrivals can be accomplished only by detecting changes in amplitude or period, which are often difficult or impossible to discern. Thus the later arrivals of the multi-branched travel-time curves are more readily determined for the S waves than for their P wave counterparts.

Identification of changes in polarization and of onsets of S waves is best accomplished by employing particle motion diagrams, as was demonstrated for earthquake-generated S waves by Ibrahim and Nuttli (1967). This method of analysis does present practical problems, because large amounts of time are required for digitizing the seismograms and constructing the particle motion diagrams.

Travel Times. The travel-time data are presented in the form of a reduced time-distance graph (Fig. 1). The solid

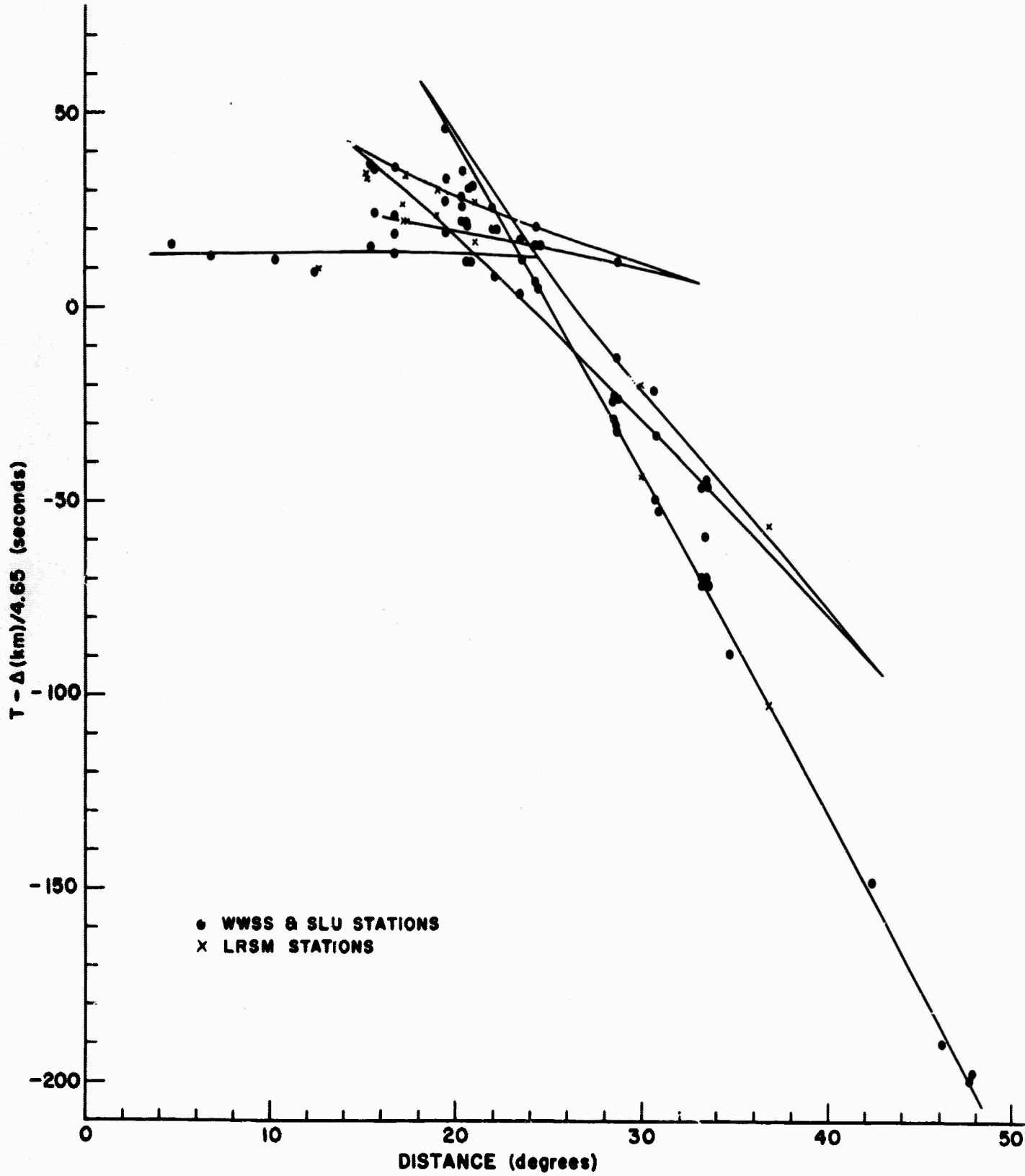
50
0
-50
-100
-150
-200
T - Δ(km)/4.65 (seconds)
0
10
20
30
40
50
DISTANCE (degrees)
• WWSS & SLU STATIONS
× LRSM STATIONS

Fig 1

line is a computed travel-time curve, based on the S velocity model of Ibrahim and Nuctli (1967), for a surface focus. Circles are used to represent the arrival times of WWSS or Saint Louis University network stations, and crosses for the LRSM stations.

An immediate conclusion which follows from an inspection of Fig. 1 is that all the data points do not lie on the curves. Much of the scatter is reduced if one applies a station anomaly correction as determined by Doyle and Hales (1967) for stations in the United States. For example, between 19° and 22° the circles correspond to S arrivals at ROL, DBQ, FLO, SLM, and OXF; these are stations in the central United States for which Doyle and Hales found the S arrivals to be 4 or 5 seconds too early. After correction the points would fall on branches 4, 3,and 6, the branches of the largest amplitude arrivals in this distance interval.

Generally it is not possible to identify arrivals corresponding to all the branches of the travel-time curve at a particular station. There are a variety of reasons for this, but the principal ones are 1) that at certain distances the amplitude of a wave of a particular branch can become very small, and 2) that the low frequency of the S wave motion usually does not permit a time resolution of events whose beginnings are separated by less than ten seconds, especially if the earlier of the two arrivals has a larger amplitude than the later one.

Table 1 contains the time difference between the first

TABLE 1. TRAVEL TIME DIFFERENCES
(Adopted Times Minus Jeffreys-Bullen Times)
For First S Arrivals and A Surface Focus

	Branch	Time Difference		Branch	Time Difference
5°	1	- 4.5 sec.	28°	6	+ 5.1 sec.
6	1	- 5.6	29	6	+ 4.4
7	1	- 6.6	30	6	+ 3.8
8	1	- 7.6	31	6	+ 3.0
9	1	- 8.4	32	6	+ 2.5
10	1	- 9.2	33	6	+ 2.2
11	1	- 9.7	34	6	+ 2.0
12	1	-10.0	35	6	+ 1.8
13	1	-10.4	36	6	+ 1.2
14	1	-10.3	37	6	+ 1.0
15	1	- 9.9	38	6	+ 0.8
16	1	- 9.8	39	6	+ 0.8
17	1	- 8.9	40	6	+ 0.7
18	1	- 8.1	41	6	+ 0.7
19	1	- 6.8	42	6	+ 0.8
20	1	- 5.2	43	6	+ 0.9
21	1	- 1.8	44	6	+ 1.3
22	4	- 1.7	45	6	+ 1.6
23	4	- 0.5	46	6	+ 1.9
24	4	+ 1.3	47	6	+ 2.0
25	4	+ 3.4	48	6	+ 2.5
26	4	+ 5.8	49	6	+ 2.8
27	6	+ 5.8	50	6	+ 3.4

arrival of our travel-time curve and the Jeffreys-Bullen tables. The time differences are negative out to 23°, and positive beyond that. Out to 15° the large negative time differences probably can be explained by the fact that the S wave (branch 1, usually called S_n) has a small amplitude compared to the higher-mode surface waves which begin impulsively five to ten seconds later at these distances. This higher-mode surface wave most likely is mistakenly identified as S in the majority of cases. From 15° to 25° the Jeffreys-Bullen tables likely refer to branch 2 rather than branch 1, which is the earlier but which is characterized by very small amplitudes.

Amplitudes. Amplitude and period measurements were made of the first half-cycle of the S motion, and where possible of the next half-cycle as well. Fig. 2 demonstrates the method used to obtain these quantities. The zero to peak amplitude is A_1; the corresponding period is $4t_1$, where t_1 is the time from the beginning of the phase to the first peak. The amplitude of the second half-cycle of motion is taken to be the average of the amplitudes of the first and second peaks, namely $(A_1 + A_2)/2$; the corresponding period is $2(t_2 - t_1)$, where $t_2 - t_1$ is the time difference between the peaks of motion.

Tables 2 and 3 contain the amplitude data for Half-Beak and Greeley, respectively. Several important observations or conclusions follow from the data included in these tables. First, both explosions generated a large amount of SH energy, comparable in size to the SV energy. Second, the amplitude

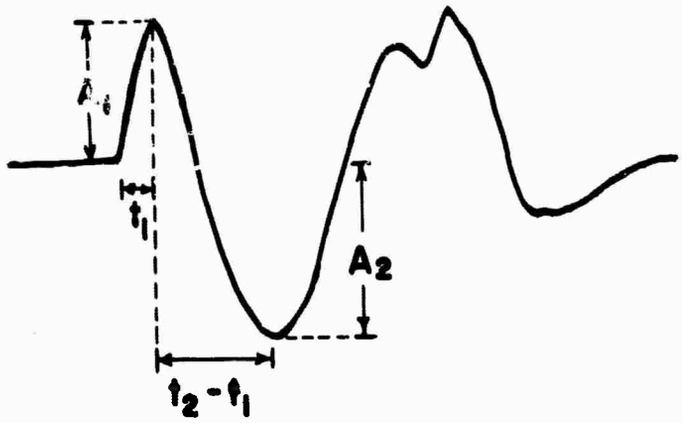

Fig 2

TABLE 2. AMPLITUDES AT S WAVES FOR HALF-BEAK.

Branch	Station	Distance	Component	Amplitude (zero-peak)	Period	Amplitude (peak-peak)/2	Period
1	TUC	6.764°	SH	0.1 microns	6 seconds	0.1 microns	6 seconds
			R	0.2	6	0.2	6
	LUB	12.342	SH	0.3	6	-	-
			Z	0.2	6	-	-
	RGSD	12.419	SH	0.3	22	-	-
2	MHT	15.605	SH	0.2	6	0.6	8
	PGBC	17.229	Z	0.1	17	-	-
	RKON	21.033	SH	0.4	20	-	-
			R	0.4	20	-	-
3	PGBC	17.229	SH	0.2	23	0.7	20
			R	0.1	23	-	-
			Z	0.1	23	0.1	20
	SIBC	18.983	SH	0.4	22	0.6	16
			R	0.2	22	0.3	16
	ROL	19.353	R	0.2	8	0.4	6
	DBQ	20.287	SH	0.4	16	-	-
			R	0.7	8	-	-
			Z	0.7	8	-	-
	SLM	20.569	SH	0.9	10	1.0	10
	RKON	21.033	Z	0.1	24	-	-
	OXF	21.930	SH	0.8	7	-	-
			R	1.2	6	-	-
			Z	0.8	5	-	-
	SHA	24.205	SH	0.8	8	-	-
			R	-	-	1.7	1.0
4	CRNB	15.484	Z	0.3	22	0.2	22
	MHT	15.605	SH	0.7	8	0.6	8
			Z	0.6	8	0.7	8
	JPAT	15.631	SH	0.2	16	0.5	16
			R	0.1	16	0.1	16
			Z	0.1	16	0.1	16
	KCMO	17.089	SH	0.2	22	0.2	12
			Z	0.1	22	0.1	12
	SIBC	18.983	Z	0.4	40	-	-
	ROL	19.353	SH	0.4	8	-	-
			Z	0.3	8	0.5	6
	SLM	20.569	Z	0.5	4	0.4	4
	BLO	23.427	R	1.0	28	2.9	12
	AX2AL	25.055	R	0.1	16	-	-
			Z	0.1	16	-	-
	BLA	28.450	SH	0.2	24	0.2	24
			R	1.4	28	-	-
	LPS	33.274	R	0.5	12	0.4	12
	COL	33.287	R	0.3	10	-	-

Table 2 (Cont'd)

Branch	Station	Distance	Component	Amplitude (zero-peak)	Period	Amplitude (peak-peak)	Period
				2			
5	BLO	23.427°	SH	0.4 microns	8 seconds	0.7 microns	6 seconds
	SHA	24.205	SH	1.2	17	-	-
	HNME	26.629	Z	0.1	32	-	-
6	ROL	19.353	SH	0.1	4	-	-
	SLM	20.569	R	2.0	10	2.0	8
			Z	0.6	8	1.0	8
	OXF	21.930	SH	2.1	15	1.9	17
			R	1.7	15	0.8	17
	BLO	23.427	SH	0.3	12	-	-
	SHA	24.205	SH	0.5	11	-	-
	AX2AL	25.055	R	0.6	16	0.6	16
	BLA	28.450	SH	0.4	6	0.4	6
			R	0.5	6	-	-
	BEFL	29.751	SH	0.2	20	0.3	12
			R	0.1	20	0.2	12
	LPS	33.274	R	0.3	8	0.4	11
	COL	33.287	SH	0.1	10	-	-
			R	0.1	10	-	-
			Z	0.1	10	-	-
	HNME	36.629	Z	0.1	22	-	-

TABLE 3. AMPLITUDES OF S WAVES FOR GREELEY

Branch	Station	Distance	Component	Amplitude (zero-peak)	Period	Amplitude (peak-peak)	Period
1	LON	10.257°	SH	-	-	0.2 microns	9 seconds
	JCT	15.368	Z	-	-	0.1	12
	DAL	16.664	Z	0.4 microns	6 sec.	0.4	10
2	DAL	16.664	R	-	-	0.7	4
	BLA	28.539	SH	-	-	0.7	9
3	DAL	16.664	SH	1.7	4	-	-
	FLO	20.542	SH	3.4	12	3.0	12
	SLM	20.658	SH	5.9	12	4.6	10
	OXF	22.018	SH	3.5	24	4.5	22
			R	2.3	24	2.0	22
			Z	1.1	24	0.9	22
4	JCT	15.368	Z	-	-	0.2	12
	SLM	20.658	R	0.6	8	0.8	8
	OXF	22.018	R	0.4	9	0.5	9
	AAM	25.500	SH	0.7	7	0.4	10
	BLA	28.539	R	-	-	1.0	11
	CMC	30.591	SH	0.7	5	0.6	8
	COL	33.264	SH	0.4	10	-	-
5	SHA	24.290	SH	2.2	14	2.4	14
			R	4.6	14	5.5	14
	AAM	25.500	SH	-	-	0.8	11
			R	0.6	7	0.9	11
			Z	0.2	7	0.4	11
	BLA	28.539	SH	-	-	1.2	14
			R	2.4	16	1.8	14
			Z	0.8	16	0.9	14
	CMC	30.591	SH	0.9	16	-	-
			Z	0.7	16	-	-
6	FLO	20.542	R	1.2	7	1.0	10
	SLM	20.658	R	3.8	8	3.5	
	SHA	24.290	SH	1.6			
	AAM		R	0.4	8	-	-
	BLA	28.539	SH	0.9	11	0.9	8
	CMC	30.591	SH	0.9	10	0.8	8
	GEO	30.840	SH	0.3	10	-	-
	COL	33.264	SH	0.4	11	-	-
			R	0.2	11	-	-
			Z	0.3	11	-	-
	GDH	46.103	SH	0.2	8	-	-
			R	0.3	8	-	-
			Z	0.3	8	-	-
	SJG	47.706	SH	0.2	8	0.2	8
			R	0.1	8	0.1	8

of the waves of branch 1 from 5° to 20° is about one order of magnitude less than those of branches 3, 4, 5, and 6 from about 20° to 30°. The amplitude of the waves of branch 2 is also comparatively small, but not as small as those of branch 1. Third, the waves of branch 3 appear to have the largest amplitude. This seems surprising in terms of our velocity model, for they correspond to a narrow beam of rays leaving the focus at angles of incidence between 41° and 45°; these rays bottom in the mantle at a depth of about 380 km. Our calculations of the transfer function for a crustal layer show that for these particular frequencies and angles of incidence a large amplification effect of the crust on the surface motion may occur for the SV component of motion. However, this would not explain the large SH motion.

One point should be kept in mind when one attempts to analyze these amplitude data. Amplitudes and periods are difficult to measure at those distances at which the travel-time curve is multi-valued. One may be dealing with the superposition of two or more waves arriving at approximately the same time, rather than a single wave.

References

Doyle, H. A. and A. L. Hales (1967). An analysis of the travel times of S waves to North American stations, in the distance range 28° to 82°, Bull. Seism. Soc. Am. 57, 761-772.

Ibrahim, A. K. and O. W. Nuttli (1967). Travel time curves and upper mantle structure from long-period S waves. (To be published in October issue of Bull. Seism. Soc. Am.)

2. The Use of Amplitude Data in Focal Mechanism Studies

Commonly focal mechanism studies are based upon the signs of the first motion of the P waves. Because the distribution of seismographic stations seldom is adequate to determine uniquely the orientation of the nodal planes (or of the x and y axes, the lines normal to these planes), Stauder and his students have included S wave polarization data in their focal mechanism studies. In this manner they have greatly improved the resolution of the nodal planes. However, in an appreciable number of earthquakes it is still possible to assign a range of values to one of the parameters of the focal mechanism solution, e.g. the strike of the y axis. The purpose of this study is to determine if amplitude data can provide an additional constraint on the focal mechanism solution, so that a more nearly unique solution can be established.

Theory. Our model of the focal mechanism is a double couple with moment, the so-called Type II force model. The displacements at large distances from the source in an infinite, homogeneous medium are (Stauder, 1962):

$$U_p = \frac{xy}{4\pi a^3 R^3} K'(t - R/a) \qquad (1)$$

$$U_{sh} = \frac{c}{4\pi b^3 R^3} K'(t - R/b) \qquad (2)$$

where x,y,z are coordinates referred to the system of forces, R is the distance from a point (x,y,z) to the focus, a and b are velocities of the P and S waves, respectively, t is time, and K(t) is a function of the amplitude and time history at

the source. The x and y axes have the direction of the forces of the couple acting at the origin, and z is orthogonal to them so as to form a right-handed system.

In addition we require a geographic coordinate system, $\bar{x}$, $\bar{y}$, $\bar{z}$, also with the focus as origin. The coordinates are related by the equations

$$x = \alpha_x \bar{x} + \beta_x \bar{y} + \gamma_x \bar{z}$$

$$y = \alpha_y \bar{x} + \beta_y \bar{y} + \gamma_y \bar{z}$$

where

$$\bar{x} = \cos AZ_{es} \sin i_h$$

$$\bar{y} = \sin AZ_{es} \sin i_h$$

$$\bar{z} = \cos i_h \ .$$

In these equations i_h is the angle of incidence at the focus and AZ_{es} is the azimuth from the epicenter to the point (x, y, z).

The direction cosines are given by

$$\alpha_x = \cos AZ_x \cos PL_x$$

$$\beta_x = \sin AZ_x \cos PL_x$$

$$\gamma_x = \sin PL_x$$

$$\alpha_y = \cos AZ_y \cos PL_y$$

$$\beta_y = \sin AZ_y \cos PL_y$$

$$\gamma_y = \sin PL_y \ ,$$

where AZ_x and PL_x are the azimuth and plunge of the x-axis, respectively. Similarly AZ_y and PL_y are the azimuth and plunge of the y-axis. The condition that the x and y axes be perpen-

dicular leads to the equation

$$\tan PL_x \tan PL_y = - \cos (AZ_x - AZ_y).$$

Finally, c, which appears in eq. (2), is given by

$$c = \frac{(\alpha_x y + \alpha_y x)\,\bar{y} - (\beta_x y + \beta_y x)\,\bar{x}}{\sin i_h} .$$

The assumptions made in deriving eqs. (1) and (2) do not apply to the real earth. We must take account of the fact that it is a finite, bounded non-homogeneous sphere rather than an infinite, homogeneous space. This produces an additional dependence of amplitude on epicentral distance, owing both to geometrical spreading and to absorption. The effect of geometrical spreading, which can be calculated, is larger than that of absorption for the low-frequency body waves with which we are concerned.

The free surface and the crustal layers cause the motion at a point on the surface of the earth to differ from that at a neighboring point just below the crust. This effect, which depends both on the angle of incidence and the frequency content of the incident wave motion, is much more severe for the SV component of motion than for P and SH. Accordingly we restrict our amplitude studies to P and SH.

For a specified epicentral distance all the terms in eqs. (1) and (2) except for x, y, and c will be constant. Thus, if the observed P wave amplitudes are divided by the product xy, a plot of these adjusted amplitudes versus epicentral distance

should show a more-or-less smooth, continuous change in amplitude with distance, as for a uniform radiating source. A large amount of scatter of the data, particularly for stations near a nodal line, indicates that the focal mechanism parameters should be revised. In this manner P wave amplituder can be used to refine focal mechanism solutions. For SH waves one adjusts the observed amplitude by dividing it by the value of c.

Examples. We consider here two earthquakes whose focal mechanism solutions have been given by Stauder and Bollinger (1966, 1965). The first is the Kodiak Island earthquake of February 6, 1964, a foreshock of the great Alaskan earthquake of the following month. The second is an earthquake which occurred in the Kurile Islands on June 28, 1963. Table 1 lists the hypocentral coordinates and the focal mechanism solutions for these earthquakes.

Table 1

Date	Feb. 6, 1964		June 28, 1963	
Location	Kodiak Islands		Kurile Islands	
Latitude	55.7N		46.5N	
Longitude	155.8W		153.2E	
Origin Time	13-07-25		21-55-39	
Focal Depth	33 km		33 km	
Magnitude	7		6-3/4	
	Stauder & Bollinger	Revised	Stauder & Bollinger	Revised
AZ_x	336°	339°	162°	154°
PL_x	9	12	74	76
AZ_y	130.5	118	298	320
PL_y	80	75.5	12	13.5

For the Kodiak Island earthquake we read the amplitudes of the P waves from the long-period seismograms of fifty WWSS stations. Total ground amplitudes were obtained by taking the square root of the sum of the squares of the vertical and horizontal components. In some cases where horizontal data were lacking the total amplitude was obtained by dividing the vertical component by the cosine of the apparent angle of incidence. The amplitudes, uncorrected for focal mechanism, are plotted as a function of distance in Fig. 1. The data scatter widely in this figure, and show no observable dependence on epicentral distance.

Fig. 2 illustrates the marked reduction in the scatter of amplitudes which occurs after the amplitudes have been adjusted according to the focal mechanism solution of Stauder and Bollinger. However, three points have large amplitudes and plot off-scale. In addition, six points (indicated by broken x's in the figure) have the wrong sense of motion. The size of the symbols is an indication of the distance of a station from a nodal line; small symbols are for stations near nodal lines, and large ones for stations more removed from them. The adjusted amplitudes of stations near nodal lines are most sensitive to the proper focal mechanism solution.

By a judicious trial and error procedure we have modified the values of the azimuth and plunge of the x and y axes to further reduce the scatter in the amplitude data. Our best solution, from a set of eighty considered solutions, is given as the revised solution in Table 1. Adjusted amplitudes using

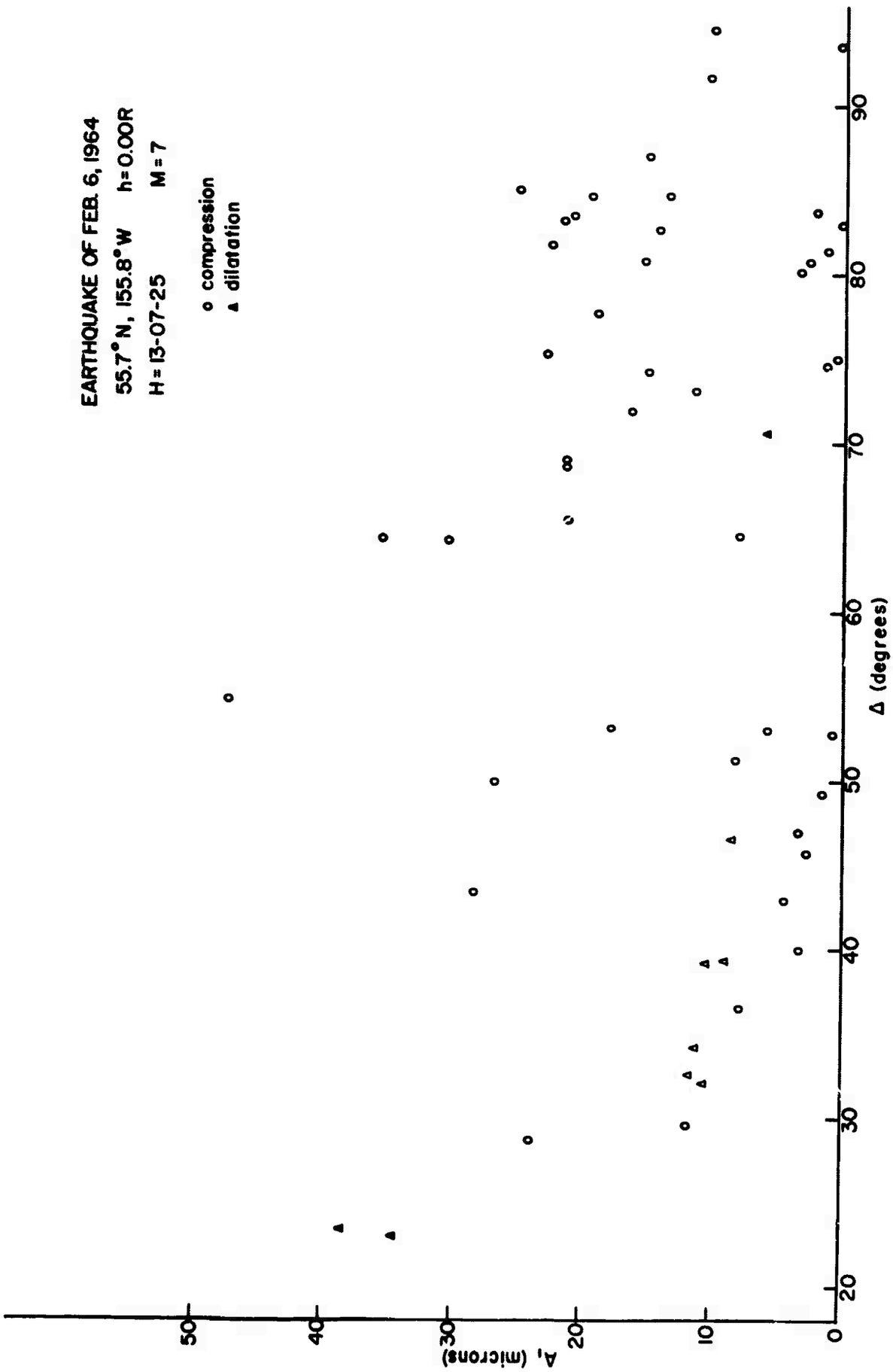
EARTHQUAKE OF FEB. 6, 1964
55.7° N, 155.8° W h=0.00R
H=13-07-25 M=7
o compression
▲ dilatation
A, (microns)
0
10
20
30
40
50
Δ (degrees)
20
30
40
50
60
70
80
90

Fig. 1

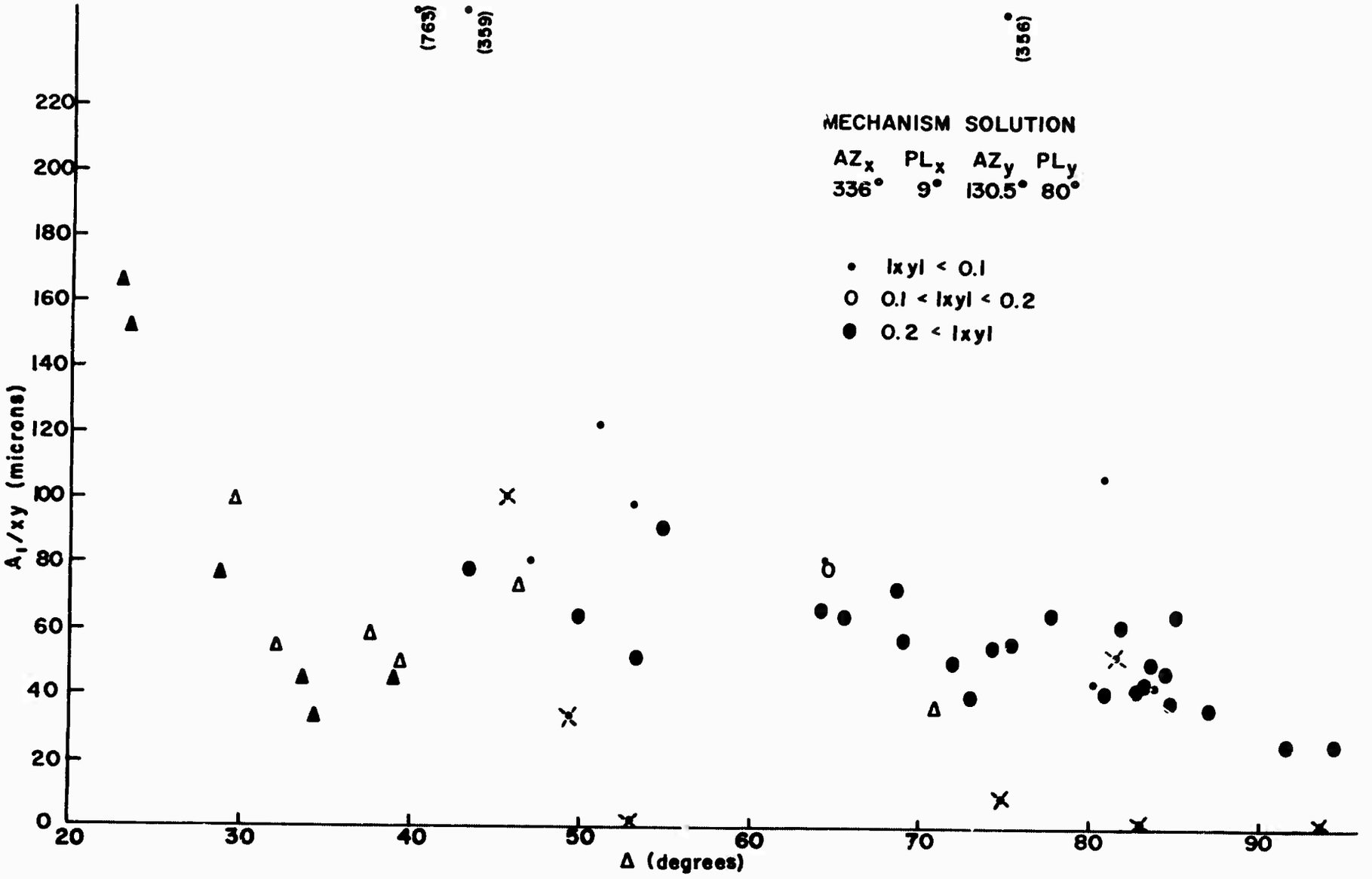
(765)
(359)
(356)
MECHANISM SOLUTION
AZx PLx AZy PLy
336° 9° 130.5° 80°
• |xyl < 0.1
O 0.1 < |xyl < 0.2
● 0.2 < |xyl
A1/xy (microns)
Δ (degrees)
0
20
40
60
80
100
120
140
160
180
200
220
20
30
40
50
60
70
80
90

Fig. 2

this solution are presented in Fig. 3. For this solution no stations have an incorrect sense of first P motion, and the adjusted amplitudes for stations near nodal lines are reasonably similar to those for stations far removed from them but at the same epicentral distance. The solid line in this figure is a theoretical curve showing the expected decrease in amplitude owing to geometrical spreading, calculated from the Jeffreys-Bullen travel time tables. Because absolute amplitudes for this theoretical curve are unknown, it was arbitrarily made to fit our data at 80°. Its remarkably close agreement with the observed data leads us to conclude that geometrical spreading is the principal cause of amplitude attenuation for long-period P waves.

Fig. 4 presents the SH amplitudes adjusted for the focal mechanism, based upon the revised solution given in Table 1. The scatter is reasonably small, less than for any other focal mechanism solution which we considered. We speculate that the increase in amplitude which is observed beyond 70° is caused by the superposition of ScS motion with that of S.

Fig. 5 contains the adjusted P wave amplitude data for the Kurile Islands earthquake. Although there is more scatter of these data than for the Kodiak Island earthquake, the scatter for this solution is significantly less than for most of the eighty other solutions which we considered. The same statement applies for the adjusted SH amplitudes, which are given in Fig. 6.

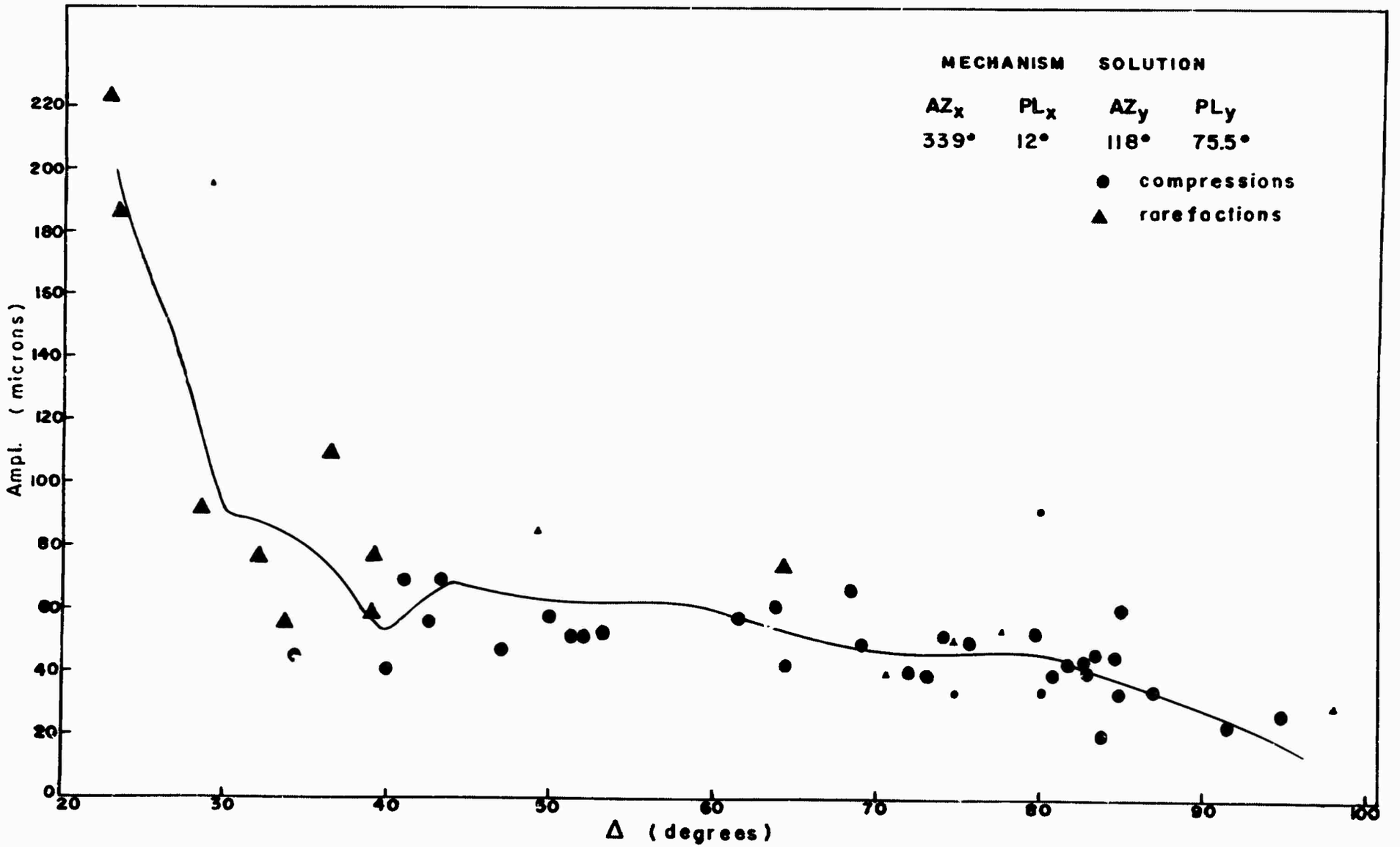
MECHANISM SOLUTION
AZx PLx AZy PLy
339° 12° 118° 75.5°
compressions
rarefactions
Ampl. (microns)
0
20
40
60
80
100
120
140
160
180
200
220
20
30
40
50
60
70
80
90
100
Δ (degrees)

Fig. 3

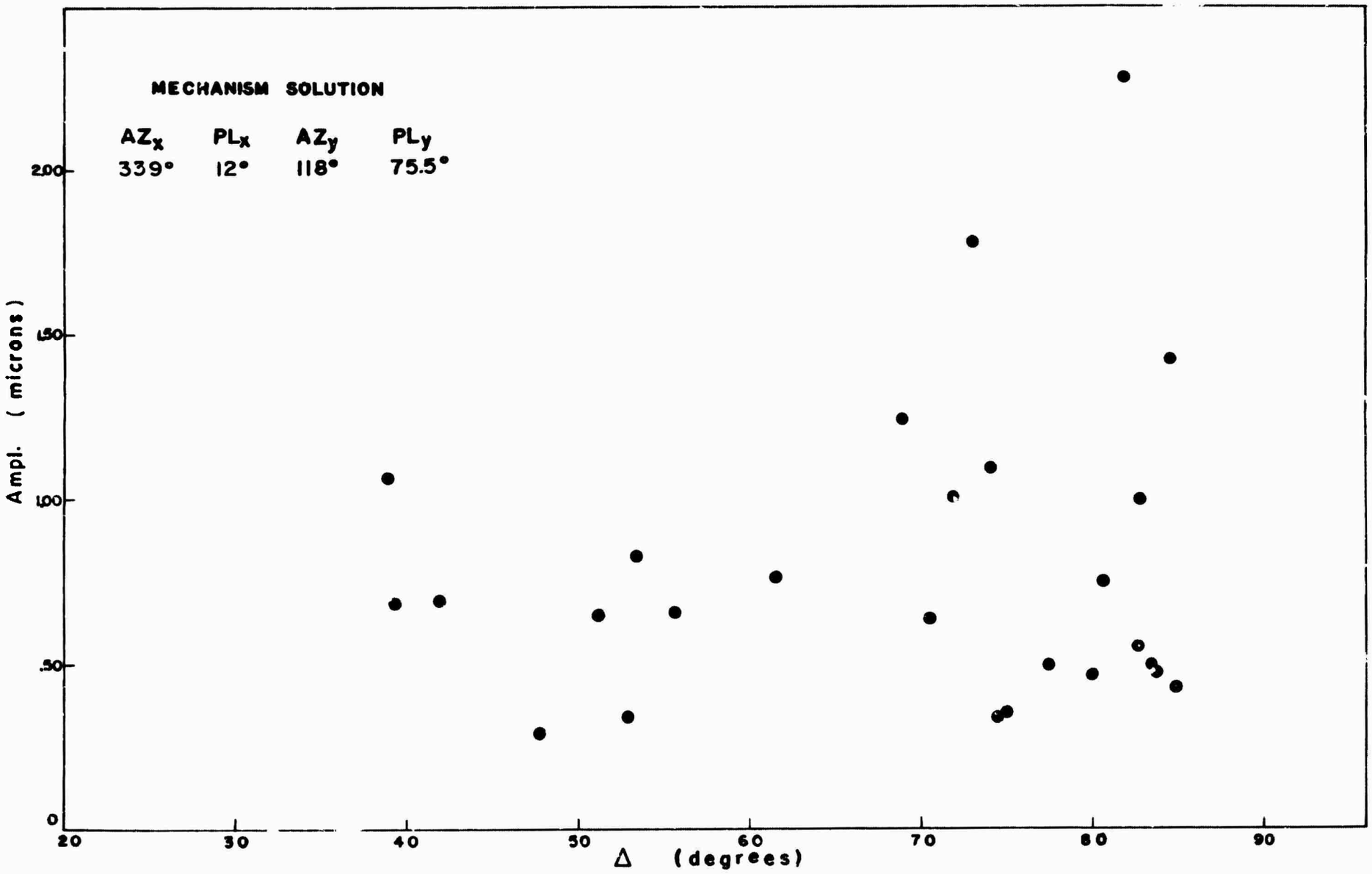
MECHANISM SOLUTION
AZx PLx AZy PLy
339° 12° 118° 75.5°
Ampl. (microns)
200
150
100
50
0
20
30
40
50
60
70
80
90
Δ (degrees)

Fig. 4

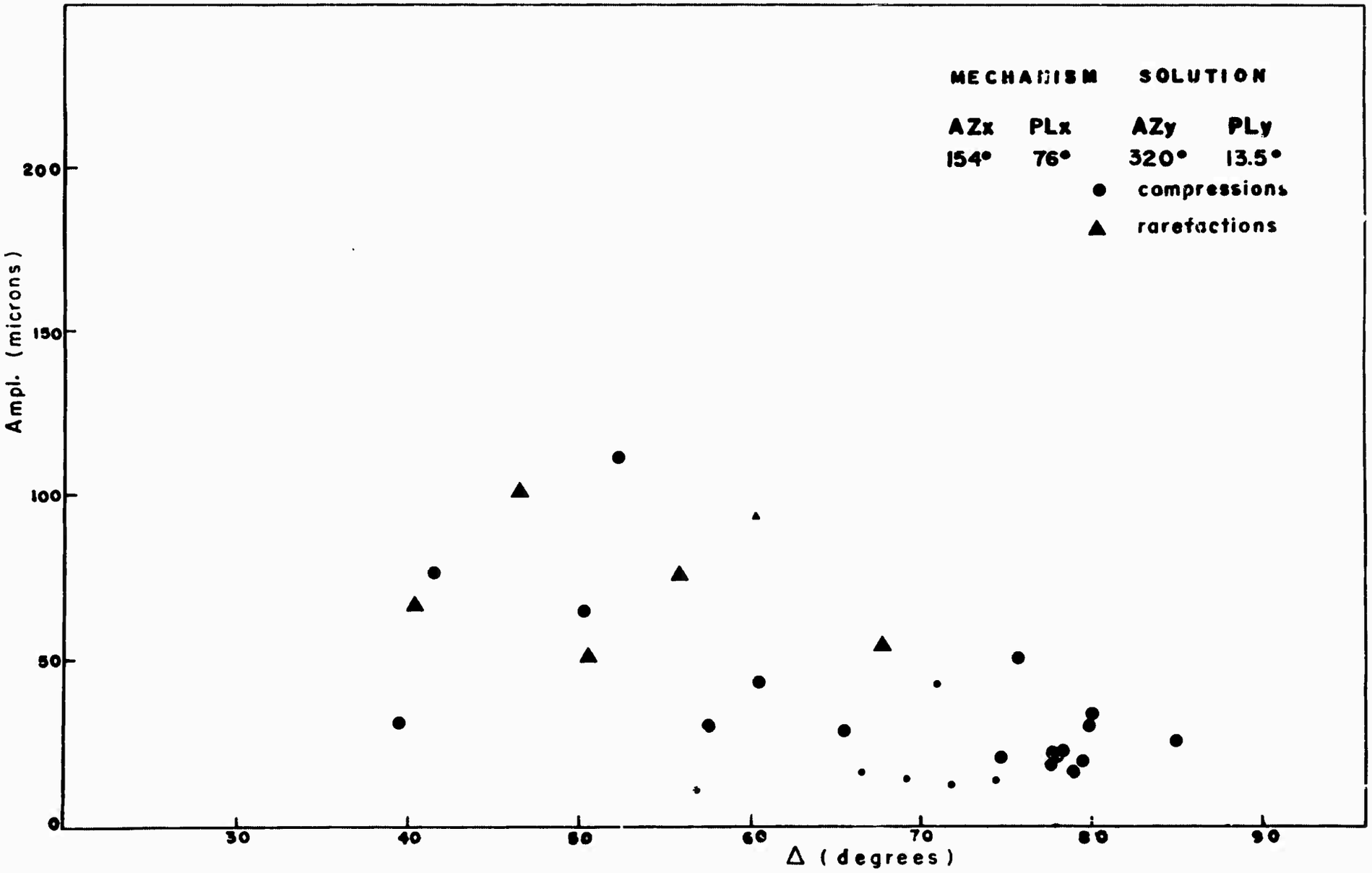
MECHANISM SOLUTION
AZx PLx AZy PLy
154° 76° 320° 13.5°
compressions
rarefactions
Ampl. (microns)
200
150
100
50
0
30
40
50
60
70
80
90
Δ (degrees)

Fig. 5

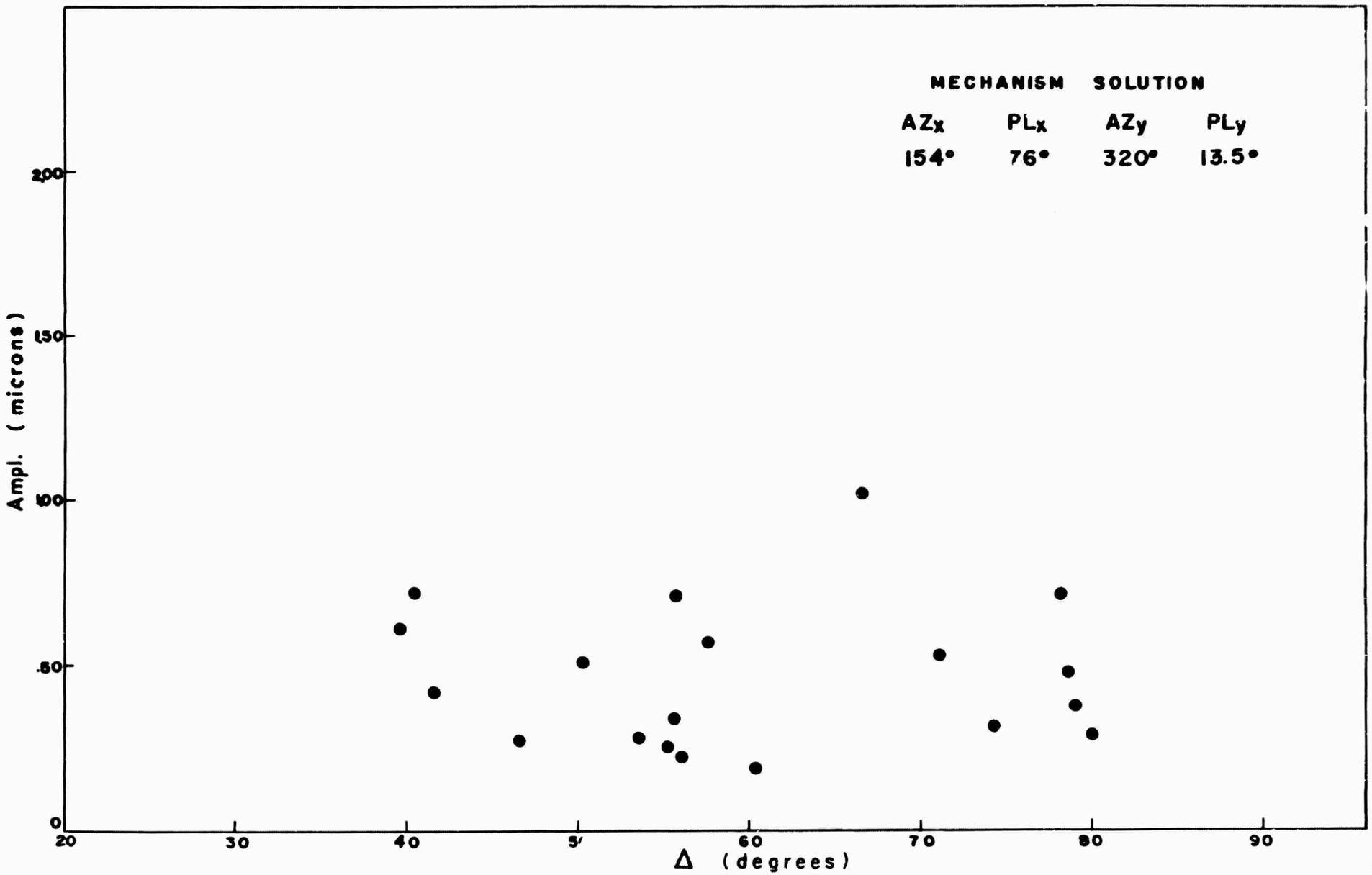
MECHANISM SOLUTION
AZx PLx AZy PLy
154° 76° 320° 13.5°
Ampl. (microns)
200
150
100
50
0
20
30
40
50
60
70
80
90
Δ (degrees)

Fig. 6

Future Work. We intend to continue our studies of the type reported here, paying particular attention to earthquakes located in regions where a knowledge of the focal mechanism parameters can assist in a better understanding of the geology of these regions.

From our present studies it is apparent that no meaningful amplitude-distance studies can be undertaken without correcting for the earthquake radiation pattern, and that even small errors in the focal mechanism parameters can produce large errors and large scatter in the adjusted amplitude data. We now are in a position to obtain much better amplitude attenuation data, which was the primary purpose for our undertaking these amplitude studies.

References

Stauder, William (1962). The focal mechanism of earthquakes, Advances in Geophysics, 9, 1-76.

Stauder, William and G. A. Bollinger (1965). The S Wave Project for Focal Mechanism Studies: Earthquakes of 1963, Scientific Report prepared under Grant AF-AFOSR 62-458 for Air Force Office of Scientific Research, Project VELA-Uniform.

Stauder, William and G. A. Bollinger (1966). The S Wave Project for Focal Mechanism Studies: The Alaska Earthquake Sequence of 1964, Scientific Report prepared under Contract AF 19(628)-5100 for Air Force Cambridge Research Laboratories, Project VELA-Uniform.

3. Azimuthal Variation of the P Wave Particle Motion from the Great Circle Path.

P wave amplitudes contain information about the structure of the crust and upper mantle at the recording site. This information may be used to supplement that obtained from refraction and surface wave dispersion studies or, when these are lacking, to assign preliminary values to the crust and upper mantle parameters. In this study we are employing the departure of the direction of the horizontal component of the P wave motion from the great circle path, and in particular its dependence on the azimuth of the approaching wave, to infer the earth structure at selected WWSS stations.

In cases where the distance from the epicenter is considerable, a longitudinal wave may be regarded as plane where it emerges. When a longitudinal wave strikes the earth's crust, if such boundaries are horizontal, the refracted or reflected waves which are formed will always be polarized in such a way that the displacements will remain in the vertical station to epicenter plane. It follows that it is possible to determine the azimuth towards the epicenter from the station, using the horizontal components of the vibrations in the P wave. That is, the azimuth α is given by

$$\tan \alpha = \frac{Y_e}{Y_n} \frac{V_n}{V_e}$$

where Y_e and Y_n are amplitudes measured on the E-W and N-S seismograms during the first impulse of the longitudinal wave, and V_e and V_n are the dynamic magnifications of the seismographs. An incorrect solution for α may result from errors

in the determination of the instrumental constants or in case the inner refractive boundaries are not horizontal. The latter constitutes a matter of interest in the present investigation of the peculiarities of the structure of the earth.

The simplest earth model which can produce an azimuth anomaly is a single dipping discontinuity surface. For such a case the azimuth anomaly curve is psuedo-sinusoidal, with zero anomaly in the dip direction. Fig. 1 presents theoretical curves for a plane dipping at 15°, with a velocity of 5.6 km/sec above and 7.75 km/sec below. The solid line is for an angle of incidence of 25° (epicentral distance of about 50°) and the dashed line for angles of incidence of 45° to 60° (epicentral distance of about 20° to 25°).

Experimental studies. The experimental work consists in measuring the half amplitudes and the peak-to-peak amplitudes, as well as the periods, of the first motion on the N-S and E-W component long-period seismograms, using a digitizing machine. By applying the known constants of the instruments these measured values are converted into ground motion, to the nearest one-tenth of a micron. These values are used to determine an azimuth, which is called the observed azimuth. A calculated azimuth is obtained using a formula of spherical trigonometry, where the coordinates of the epicenter and seismograph station are known. The azimuth anomaly is defined as the observed value minus the calculated value.

Following is a brief discussion of the features of the azimuth anomaly curves constructed for certain selected WWSS stations.

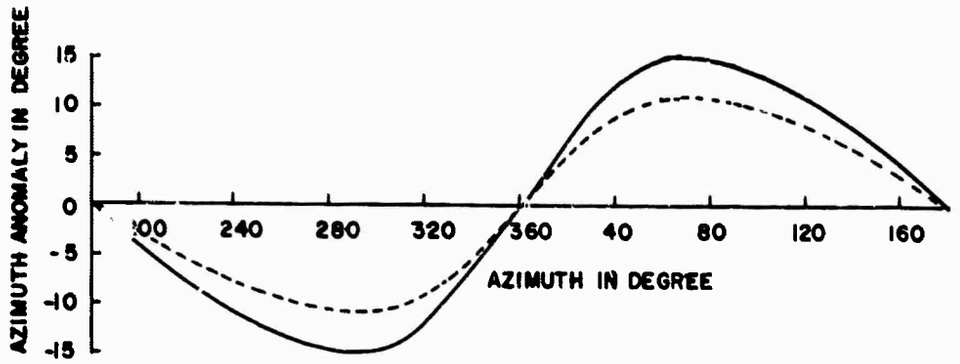

Fig. 1

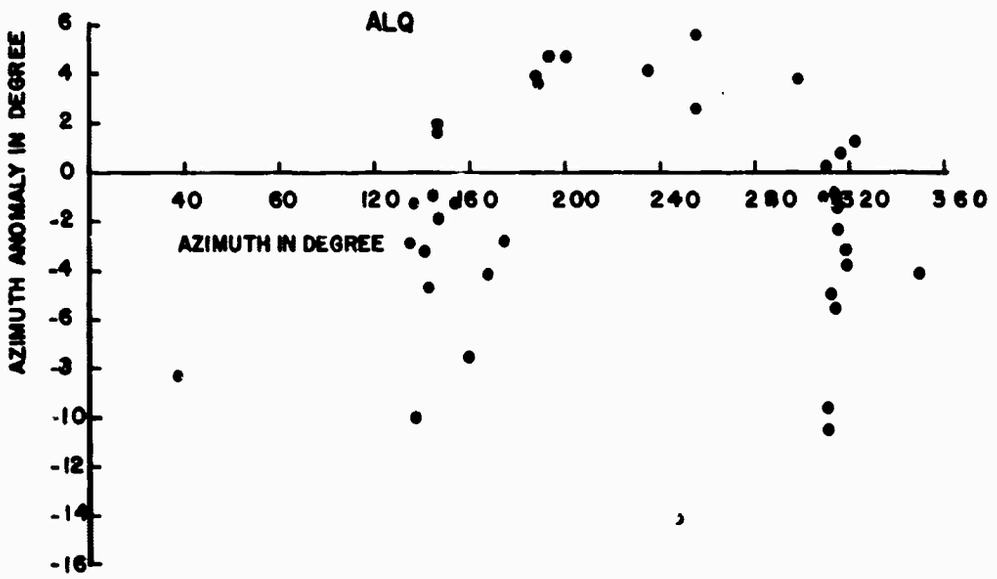

Fig. 2

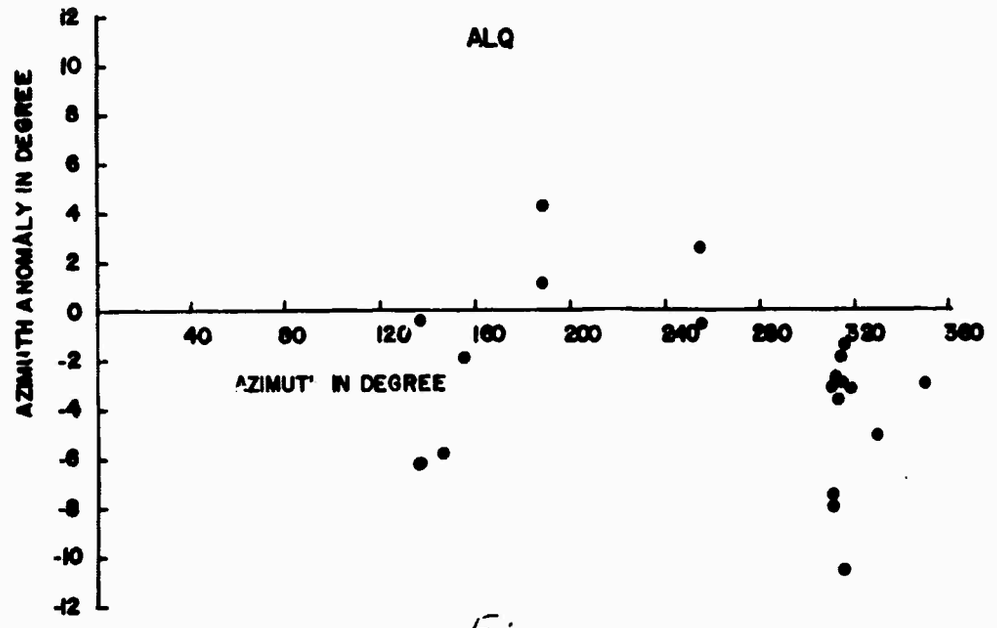

Fig. 3

ALQ (Figs. 2 and 3). For Albuquerque it was possible to divide the observations into three groups, depending on the signs of the anomaly. In Fig. 2 it can be seen that with the exception of two points all of the anomalies between 0° and 180° are negative. Positive anomalies are found between 180° and 300°, and negative beyond 300°. The maximum value of the anomaly is of the order of 5° on the positive side and 10° on the negative side. Fig. 2 is based on the first half amplitude, and Fig. 3 on the peak-to-peak amplitude data. Both show the same trends, although there are fewer data for the latter figure because in many cases the P motion is interrupted by other arrivals before one full cycle is completed.

BKS (Fig. 4) In the case of the Berkeley data the observations are more scattered, which is probably indicative of the more complex crustal and upper mantle structure at that station. Most of the points between 0° and 160° are characterized by a negative anomaly, while those from 160° to 316° are positive and those beyond 316° are negative. The maximum value of the anomaly is about 8° on both the positive and negative sides.

MDS (Fig. 5) We have fewer data for Madison because the seismograms are often disturbed by long-period noise. We have only two observations at azimuths 0° to 110°, for which both anomalies are small and positive. With one exception all the anomalies between azimuths of 130° and 330° are negative, the amplitude being as large as 24°. These large negative anomalies are surprising if one imagines the crustal structure to be simple and composed of nearly horizontal layers.

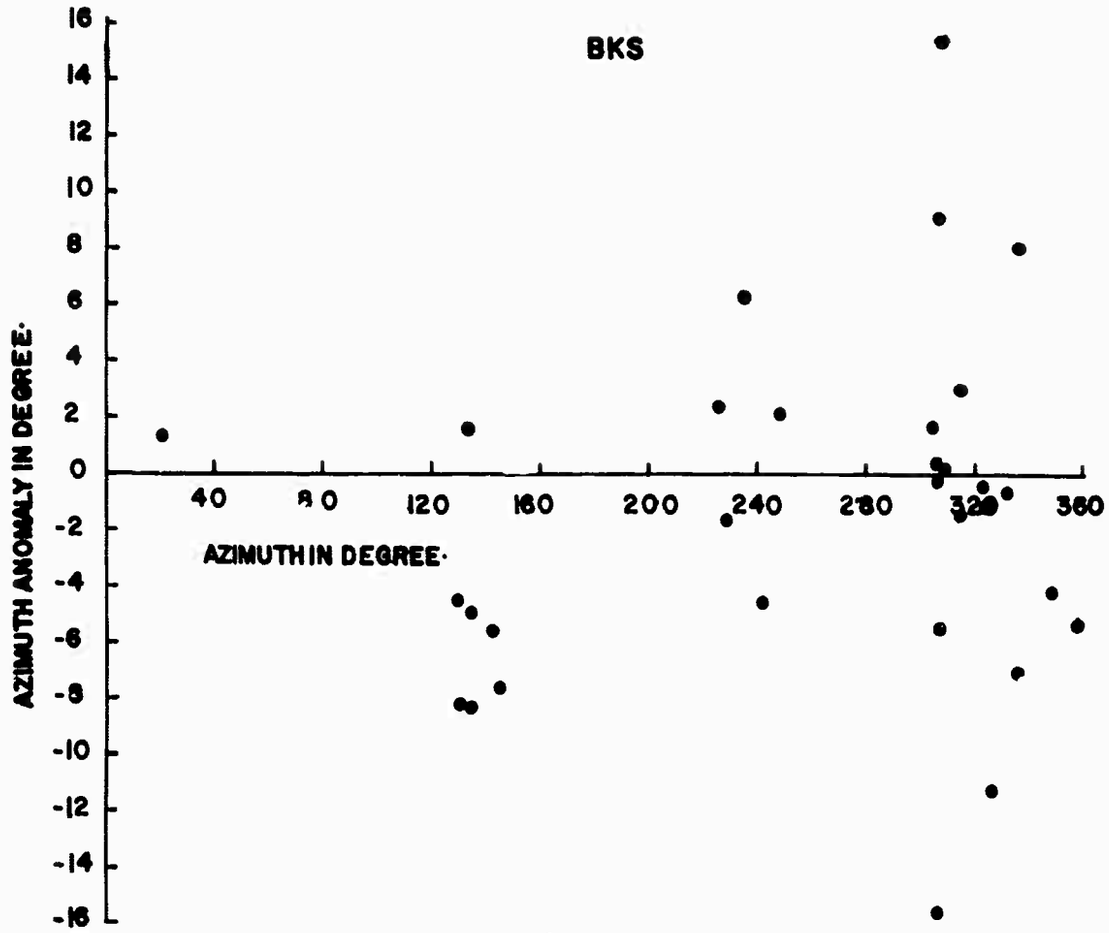
BKS
AZIMUTH ANOMALY IN DEGREE
AZIMUTH IN DEGREE
16
14
12
10
8
6
4
2
0
-2
-4
-6
-8
-10
-12
-14
-16
40
80
120
160
200
240
280
320
360

Fig. 4

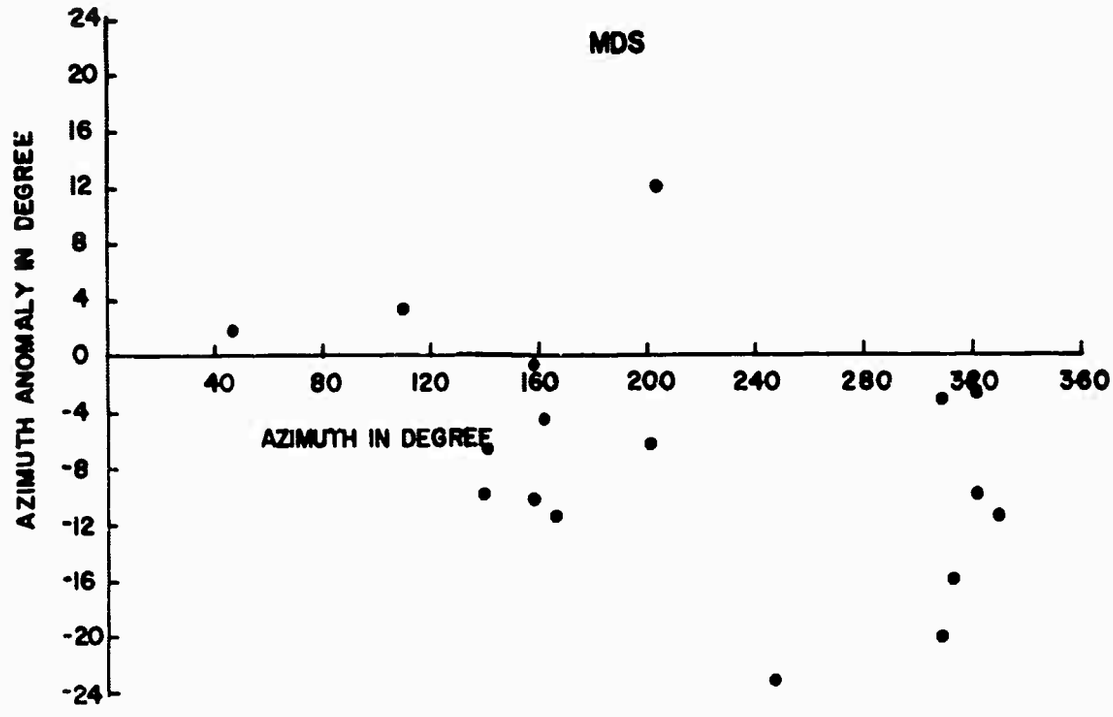
MDS
AZIMUTH ANOMALY IN DEGREE
AZIMUTH IN DEGREE
24
20
16
12
8
4
0
-4
-8
-12
-16
-20
-24
40
80
120
160
200
240
280
320
360

Fig. 5

OXF (Fig. 6) It was possible to obtain many seismograms showing impulsive P waves at Oxford. The anomalies are negative between 0° and 40°, positive between 40° and 200°, negative between 200° and 300°, and positive beyond 300°. The maximum amplitude of the anomaly is of the order of 12° on the positive side and 6° on the negative side.

It is interesting to compare Fig. 6 with Fig. 2 for Albuquerque. One is almost the mirror image of the other. That is, at azimuths where ALQ has positive anomalies, OXF has negative, and vice versa. The shapes and amplitudes are also almost the same. This indicates that the structural features at the two stations are similar and have the same strike direction, but that the dip directions differ by 180°.

TUC (Fig. 7) A good azimuthal distribution of the data could not be obtained in the case of Tucson. Most of the observations are between the azimuths of 120° to 180° and 300° to 330°. Most of the anomalies are positive between 120° and 256° and negative beyond. Maximum amplitudes are 20° on the positive side and 15° on the negative side.

Future Work. It is obvious that the theoretical curves for a single dipping layer do not satisfy our observations. We shall consider other earth models, and derive formulas for the azimuth anomaly produced by them in an attempt to get a better match to our data.

We shall apply the same techniques to the long-period LASA data from Montana. Because of the unusually low seismicity on a global scale for this year we have only found two

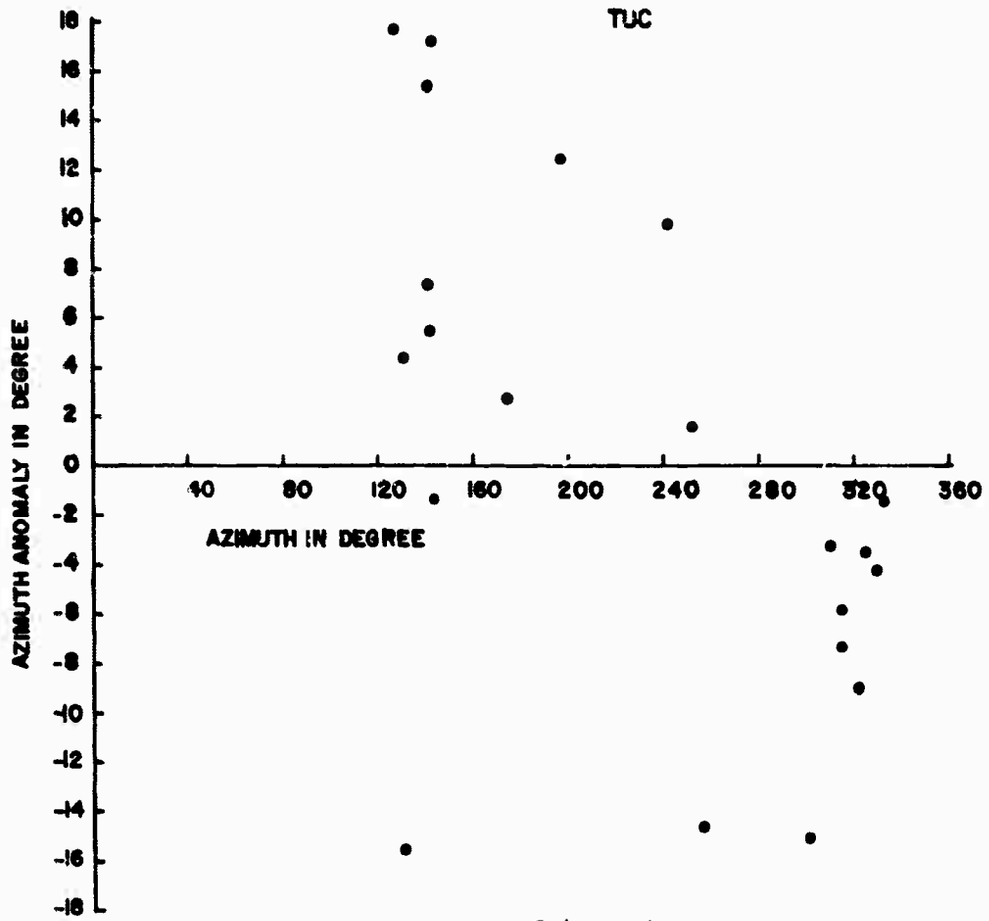
TUC
AZIMUTH ANOMALY IN DEGREE
AZIMUTH IN DEGREE
18
16
14
12
10
8
6
4
2
0
-2
-4
-6
-8
-10
-12
-14
-16
-18
40
80
120
160
200
240
280
320
360

Fig. 6

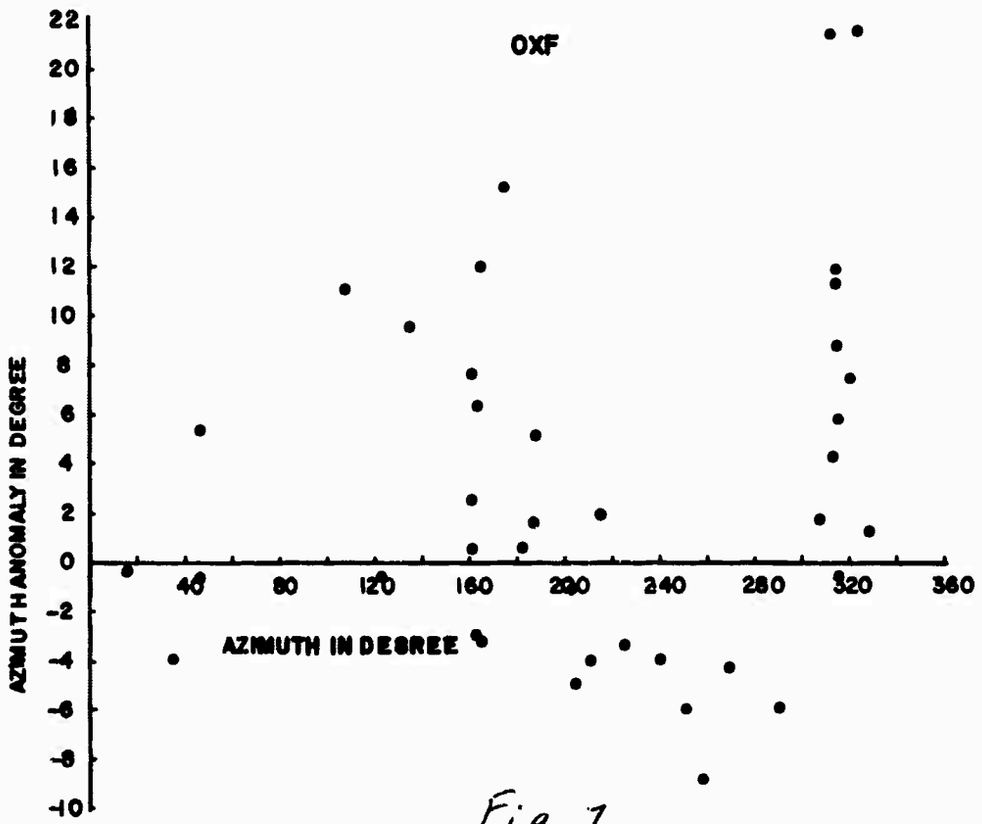
OXF
AZIMUTH ANOMALY IN DEGREE
AZIMUTH IN DEGREE
22
20
18
16
14
12
10
8
6
4
2
0
-2
-4
-6
-8
-10
40
80
120
160
200
240
280
320
360

Fig. 7

earthquakes in the first seven months of 1967 which provide satisfactory LASA data. As we wait for sufficient LASA data to accumulate we shall study other WWSS stations in the U. S. for the periods 1964-1966.

4. P Time Delays and Continental Uplift.

Introduction. The velocity versus depth profile underlying the travel time tables of seismic waves by Jeffreys and Bullen (1948) proves to be of remarkable consistence all over the world. In the past, deviations of the travel times, thought not without importance, barely exceeded the observational accuracy of most seismographic stations. This contributes certainly to the fact that the Jeffreys-Bullen travel-time tables became the most used ones, at least as far as teleseisms are concerned.

Since two parameters, the epicentral distance and the focal depth appear to be of predominant importance for the travel time, the structure of the earth is mainly concentric.

Perturbations of the travel times are of regional importance. Their causes are located in the crustal and upper mantle structure underneath the seismographic station or the source. The investigation of the perturbations was facilitated in the last years by the increased quality of the instrumentation of seismographic observatories. The present study was possible because the travel times at some seismographic stations are measured and reported with an accuracy of 0.1 sec.

The objective of the study is to investigate the possible correlation between the continental uplift and the P-time delays.

Fennoscandia was chosen because:

1. It is covered by a relatively dense network of seismographic observatories,
2. It has a seismographic service of high standard, and
3. The evidence of continental uplift is well established by geologic, geodetic, and mareographic observations made over a period of decades and even centuries.

The method applied here was stimulated by a recent investigation by Bolt and Nuttli (1966). These authors found that the P-time delays at twelve seismographic stations in central and northern California, if related to a reference station, Berkeley, vary cyclically with the azimuth from the station to the epicenter. In the present study the P-time delays at 15 Scandinavian stations were investigated. Uppsala and Umeå were used as reference stations. This produced 28 sets of relative P-time delays.

Observational Material. In the time from January 1, 1963 to December 31, 1965, 15 seismographic stations were operational in Norway, Sweden, and Finland, for which station bulletins were available. The length of the interval guaranteed a sufficiently large sample of data. The beginning of the interval was chosen to coincide with the time when most of the stations started to report the arrival times of P-waves with an accuracy of 0.1 sec. The names, coordinates, elevations above sea level of the stations, and intervals for which the bulletins were available, are given in Table 1. The location of the stations is seen in Fig. 1.

Table 1

STATION NAME		LATITUDE AND LONGITUDE	ELEVATION ABOVE SEA LEVEL	TIME INTERVAL INVESTIGATED	NUMBER OF P-TIME DELAYS			
					TOTAL	WITH WEIGHT 1.0	WITH WEIGHT 0.5	WITH WEIGHT 0.25
Uppsala	UPP	59°51.5'N 17°37.6'E	14m	Jan. 1, 1963 - Dec. 31, 1965				
Kiruna	KIR	67°50.4'N 20°25.0'E	390m	Jan. 1, 1963 - Dec. 31, 1965	285	235	49	1
Skalstugan	SKA	63°34.8'N 12°16.8'E	580m	Jan. 1, 1963 - Dec. 31, 1965	279	231	47	1
Göteborg	GOT	57°41.9'N 11°58.7'E	66m	Jan. 1, 1963 - Dec. 31, 1965	272	225	46	1
Umea	UME	63°48.9'N 20°14.2'E	16m	Jan. 1, 1963 - Dec. 31, 1965	297	247	47	3
Karlskrona	KLS	56°09.9'N 15°35.5'E	11m	Jan. 1, 1963 - Dec. 31, 1965	269	221	43	5
Helsinki	HEL	60°10.5'N 24°57.4'E	20m	Jan. 1, 1963 - Jan. 31, 1964	53	16	30	7
Nurmijarvi	NUR	60°30.5'N 24°39.3'E	102m	Jan. 1, 1963 - Dec. 31, 1965	259	193	59	7
Sodankyla	SOD	67°22.3'N 26°37.8'E	181m	Jan. 1, 1963 - Dec. 31, 1965	262	201	58	3
Kajaani	KJN	64.1° N 27.7° E	250m	Jan. 1, 1963 - Dec. 31, 1965	235	176	53	6
Kevo	KEV	69°45.4'N 27°00.9'E	97m	Jan. 1, 1963 - Dec. 31, 1965	225	148	67	10
Kongsberg	KON	59°40' N 9°40' E	200m	Jan. 1, 1964 - Dec. 31, 1965	151	132	17	2
Tromso	TRO	69°38.0'N 18°55.7'E	1[illegible]m	Jan. 1, 1964 - Dec. 31, 1965	126	110	15	1
Kirkenes	KRK	69°43.5'N 30°03.8'E		April 15, 1964 - Dec. 31, 1965	67	58	9	0
Lillehammer	LIL	61°03.3'N 10°52.0'E	560m	Aug. 1, 1963 - Feb. 28, 1965 April 1, 1965 - Dec. 31, 1965	147	119	27	1

The arrival times of P waves from more than 300 earthquakes have been extracted from the bulletins of the 15 stations. For the most part the earthquakes were in the epicentral distance range between 30° and 100°, and were selected so as to cover possibly all azimuths. Obviously, the distribution of seismic regions limits an even coverage of the azimuths. For the same reason, the epicentral distances of the earthquakes studied change with azimuths, and the assumption had to be made that P-time delays are independent of the epicentral distance.

The P-time delays found at each station over a period of 3 years may be expected to scatter about the calculated values, especially since the readings were performed in course of routine work. The relative P-time delays, involving readings at two stations, will scatter even more. However it is clear that with a sufficiently large amount of readings significant conclusions can be drawn with regard to the relative P-time delays.

We found the greatest uniformity of readings at the Swedish stations Uppsala (UPP), Kiruna (KIR), Skalstugan (SKA), Göteborg (GOT), Umeå (UME), Karlskrona (KLS). Two of these stations, Uppsala and Umeå, were taken as reference stations for all the remaining stations. Further reasons for choosing them as reference stations are:

1. Neglecting the array station Lillehammer (LIL), Uppsala and Umeå recorded more earthquakes and provided more travel times than any other station.

2. Uppsala and especially Umeå are situated at places of most intensive continental uplift, granting eventually a uniformity of the structure beneath the stations, and at the same time close to the center of the Scandinavian stations involved (see Fig. 1).

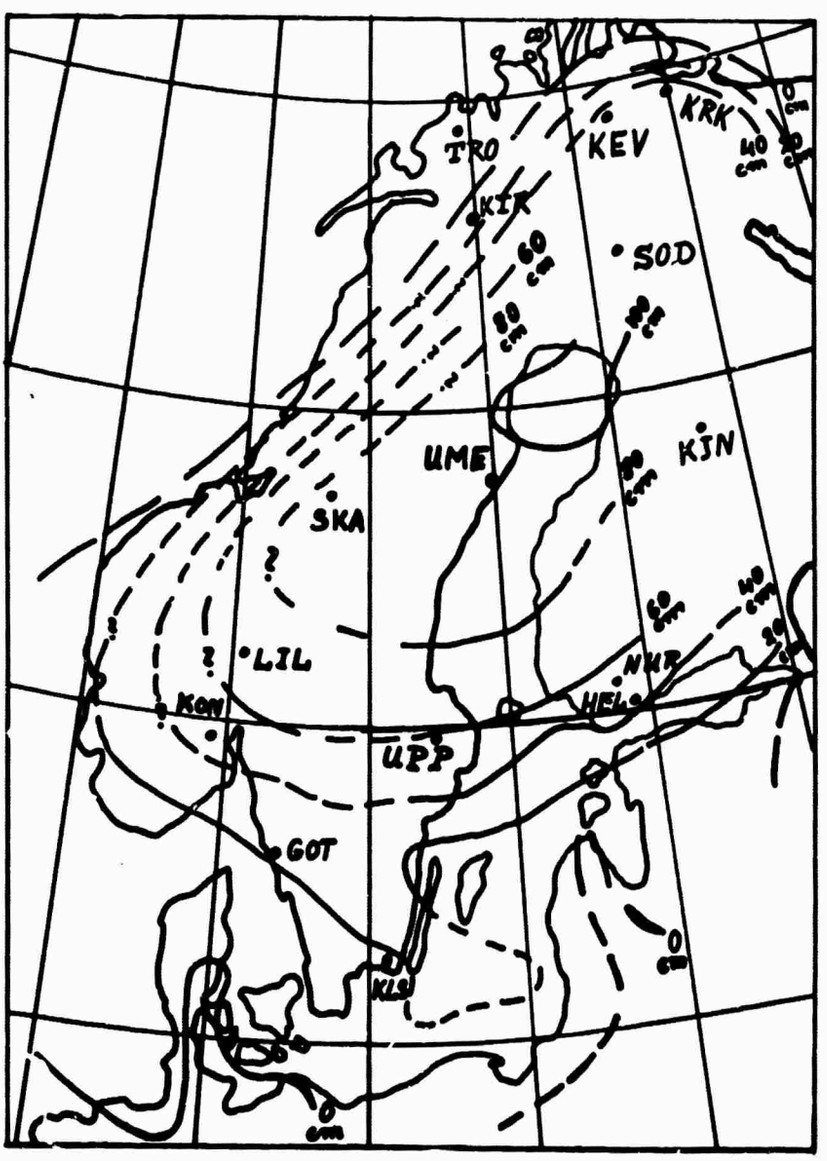

FIG. 1

Lillehammer is the only array station here. It was operated during, and bulletins were issued for, 28 out of 36 months investigated (see Table 1). The station produced, however, only 147 usable time differences, as compared with the maximum of 297 at Uppsala and Umeå.

Relative P-time Delays. The following quantity was computed for all earthquakes recorded at any of the 14 station (ST) and the reference (REF) station (Uppsala or Umeå):

$$RPD = (T_{obs} - T_{cal})_{ST} - (T_{obs} - T_{cal})_{REF} \qquad (1)$$

where T_{obs} - the observed travel time, and

T_{cal} - the travel time calculated from Jeffreys-Bullen Tables.

For both T_{obs} and T_{cal}, the origin time, epicentral coordinates, and focal depth of the event are accepted as given by the USCGS in their Seismological Bulletin.

A relative P-time delay so constructed represents a travel time anomaly. Its cause is present in that portion of the two ray paths, where the latter diverge most, i.e. in the upper mantle and crust, below the two stations involved.

Whenever the RPD exceeded $\pm$ 3 sec., it was rejected as unreliable and containing a systematic error. The total number of time differences produced in that way for each station is given in Table 1.

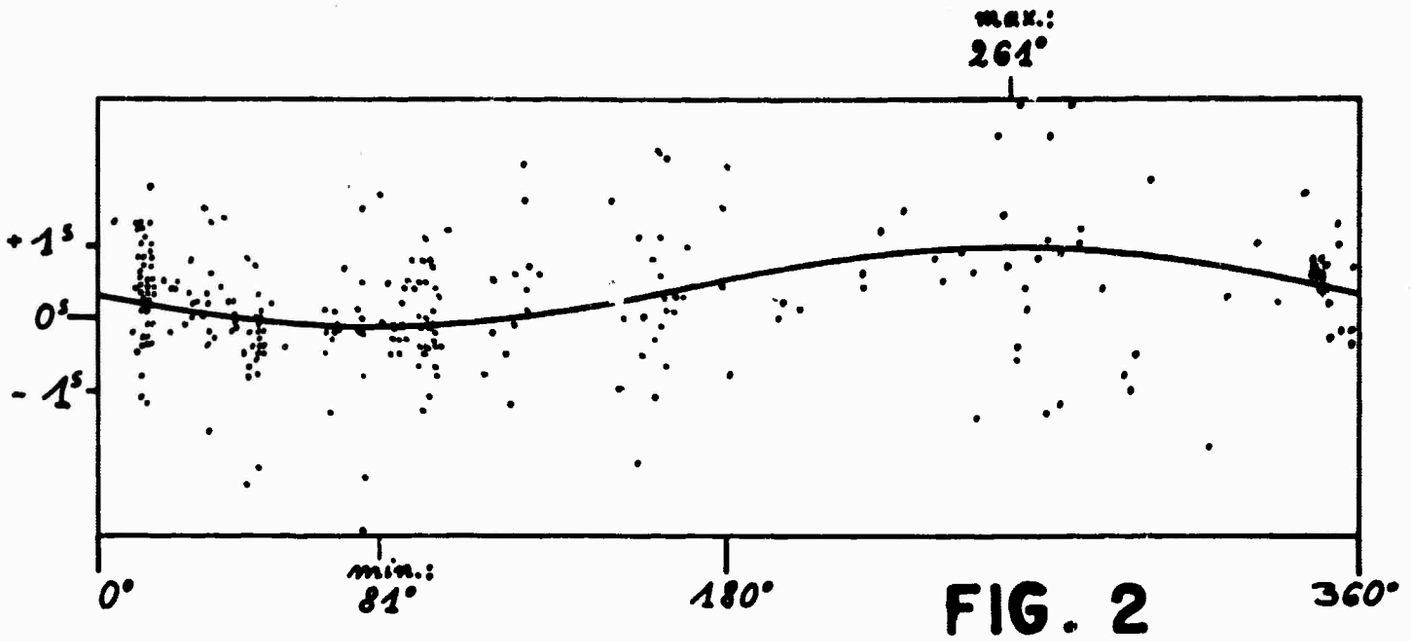

FIG. 2

The RPD were assigned a weight of 0.5 if:

1. The arrival time was reported with an accuracy of only 1.0 sec.
2. The RPD was diverging by ~1 sec. from the delays at neighboring azimuths.
3. The distance from the epicenter to a station or a reference station became smaller than 30°.

If two of the conditions applied to an RPD, the weight assigned was 0.25; if all three applied - the figure was dropped. All other RPD's were given the weight 1.0 . The number of RPD's with the weights 1.0 , 0.5 , 0.25 for the stations are given in Table 1.

The RPD were plotted as function of an angle Θ equal to the arithmetic average of the azimuths from the station and reference station to the epicenter. As illustration, Fig. 2 gives the RPD's as function of the azimuth, for Göteborg versus Uppsala.

The RPD for data sets were approximated in the least square sense by the equation

$$RPD = A + B \sin(\theta + \varepsilon) \qquad (2)$$

where A, B, ε are constants characteristic of each station. They were calculated for 14 stations, if referred to Uppsala, and again, if referred to Umeå. Table 2 contains the corresponding figures. Most remarkable is that with Uppsala as reference station all 14 A-values are positive with an average of 0.47; with Umeå as reference station 13 stations attained a positive A-value, the average amounting to 0.53. This indicates a certain similarity of the structures below Uppsala and Umeå. It might be noted here that the A-values in all approximations are closest to zero for Umeå, Uppsala, and Karlskrona (see Fig. 1), all three stations delineating a roughly NS trending axis.

The RPD were correlated with a sinusoidal curve shifted along the axis of azimuths at intervals of 2°. For the data shown in Fig. 2, the correlation coefficient amounts to 0.52 for a lag ε being equal to that found from the least square approximation within less than 10 degrees. The correlation with 272 data pairs is then significant at the 70 per cent confidence level.

Orientation of the RPD Approximations. The least square approximation of the RPD's by a sinusoidal curve has an appreciable standard deviation. In the example shown on Fig. 2, the standard deviation is 0.82. However, as mentioned earlier,

Table 2

Coefficients A, B, and ε in equation

$RPD = A + B \sin(\theta + \varepsilon)$

Reference stations:

	Uppsala (UPP)			Umeå (UME)		
	A	B	ε	A	B	ε
UPP				-0.04	0.52	95.61
KIR	0.38	0.49	-106.51	0.31	0.18	157.65
SKA	0.55	0.44	-134.99	0.45	0.46	140.65
GOT	0.45	0.53	-171.41	0.50	0.79	148.49
UME	0.04	0.52	- 84.39			
KLS	0.13	0.48	-146.33	0.03	0.54	140.02
HEL	1.02	0.23	173.18	0.84	0.57	113.65
NUR	0.45	0.24	- 58.45	0.51	0.25	99.60
SOD	0.41	0.24	- 10.83	0.38	0.48	61.38
KJN	0.45	1.02	- 45.10	0.56	0.64	- 28.85
KEV	0.34	0.23	- 22.48	0.41	0.23	85.03
KON	0.75	0.33	127.09	0.97	0.81	132.76
TRO	0.47	0.24	-174.49	0.71	0.60	162.43
KRK	0.55	0.37	- 19.24	0.75	0.10	90.51
LIL	0.53	0.46	-175.68	0.55	0.73	137.89

the RPD were obtained from routine measurements made for two stations over a time interval of 3 years, the stations having independent recording systems and clocks. A thorough analysis of variance renders, for every particular station taken individually, only a low reliability of the approximation. Nevertheless for each of the reference stations, Uppsala and Umeå, 14 approximations are available, and we may look for a systematic behavior of all the approximations even though no statistical model is available which would permit the estimation of the confidence level of conclusions drawn from the interrelated approximations.

On Figure 3 the arrows represent the azimuths of the maximum positive RPD's for all 14 stations, referred to Uppsala. Figure 4 shows the corresponding directions with Umeå as reference station. The arrows are assigned to the midpoints between the particular station and the reference station. It can be seen immediately that the arrows have a tendency to be directed away from the region of most intensive continental uplift, in the direction perpendicular to the lines of equal rate of uplift (compare Figs. 3 and 4 with Fig. 1).

Of particular interest is the bend of the directions at points situated to the W, N, and E of Umeå, around the region of most intensive uplift so as to point away from it.

This fact, together with the positive A-values pointed out earlier, indicates that seismic velocities below the reference stations are higher than below the other stations, situated at places of less intensive continental uplift, as will be discussed with greater detail below.

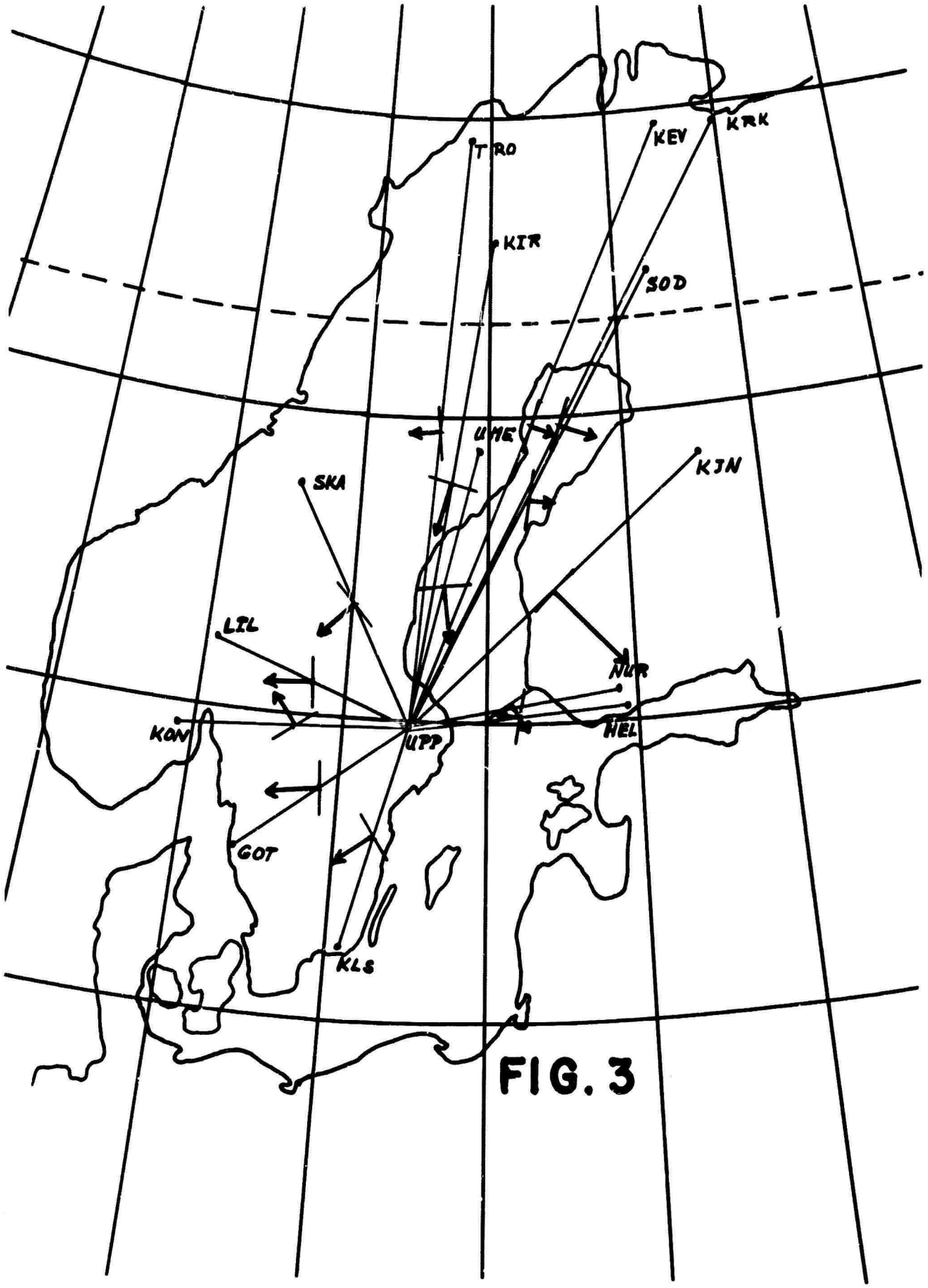

FIG. 3

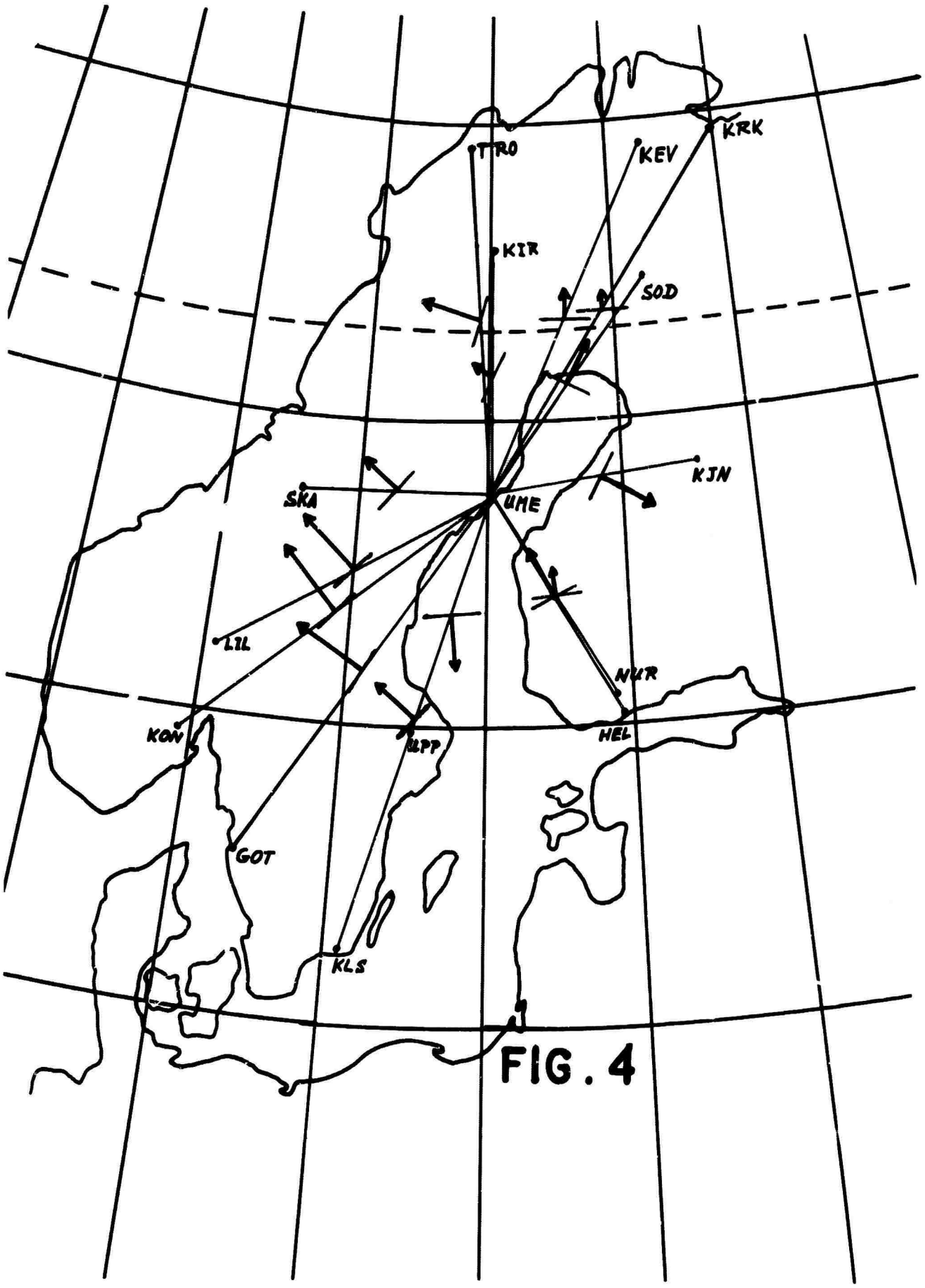

FIG. 4

Without discussing now the exceptions as seen particularly for Helsinki (HEL) on Fig. 3, and for Helsinki and Nurmijarvi (NUR) on Fig. 4, we will propose an interpretation of the general features of the RPD as function of azimuth.

Travel Times as Function of Azimuth. Let us assume two layers in contact with the outer boundaries being plane, horizontal and parallel to each other, and the plane interface to dip at an angle δ (see Fig. 5A). The velocities of P-waves are v_A and v_B in the lower and upper layer respectively. The total thickness of the layers is H.

A P-wave arriving from an azimuth ψ measured from the dip direction will be refracted at the lower boundary and at the interface, suffering in the latter case a deviation φ from the original azimuth. The deviation can be expressed as

$$\varphi = \text{arc tan} \frac{\sin \psi}{\frac{\tan i_1}{\tan \delta} - \cos \psi}$$

with i_1 = angle of refraction at the lower boundary; this angle can be found if the angle of incidence at the lower boundary and the velocities on both sides of it are known. It will be constant for a particular epicentral distance (see Fig. 5B).

The travel time across the two layers will be obviously a cyclical function of the azimuth. It can be expressed by the following formula:

$$t = \frac{1}{\cos i_1} \cdot \left[\frac{h_1}{v_A} + \frac{H - h_1}{v_B} \cdot \frac{\sin i_2 + \tan \beta \cdot \cos i_2}{\sin i_3 + \tan \beta \cos i_3} \right] \quad (2)$$

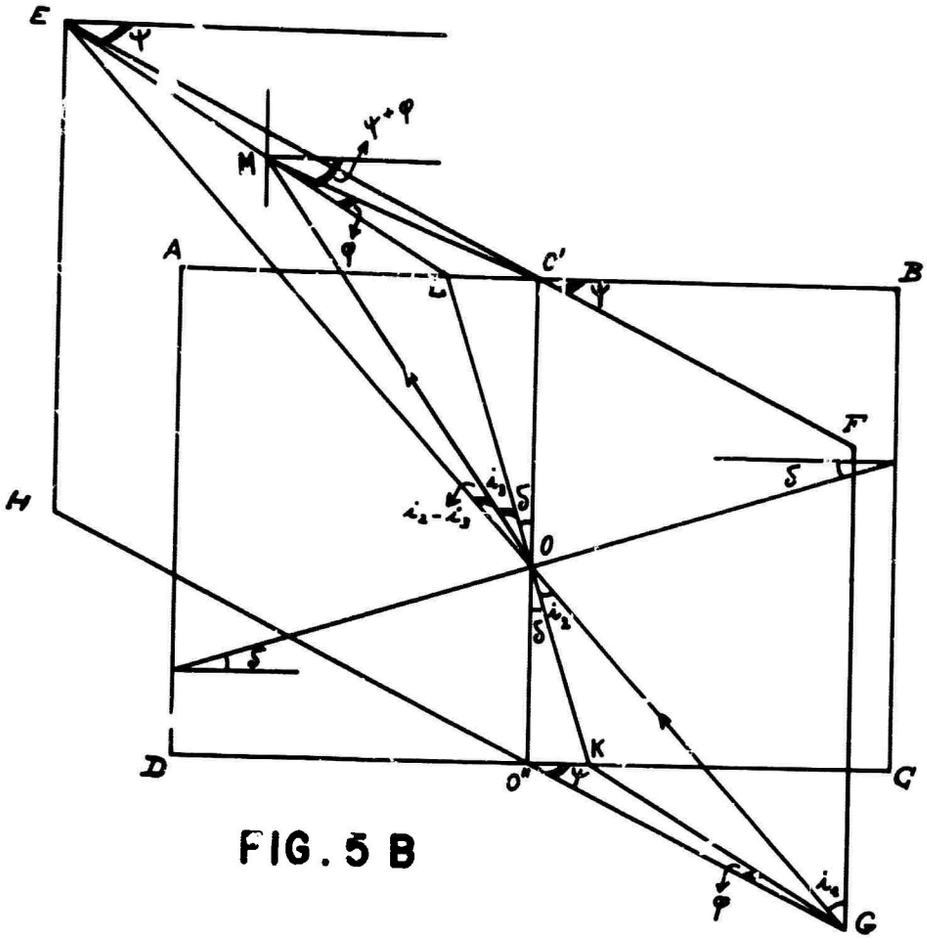

FIG. 5 B

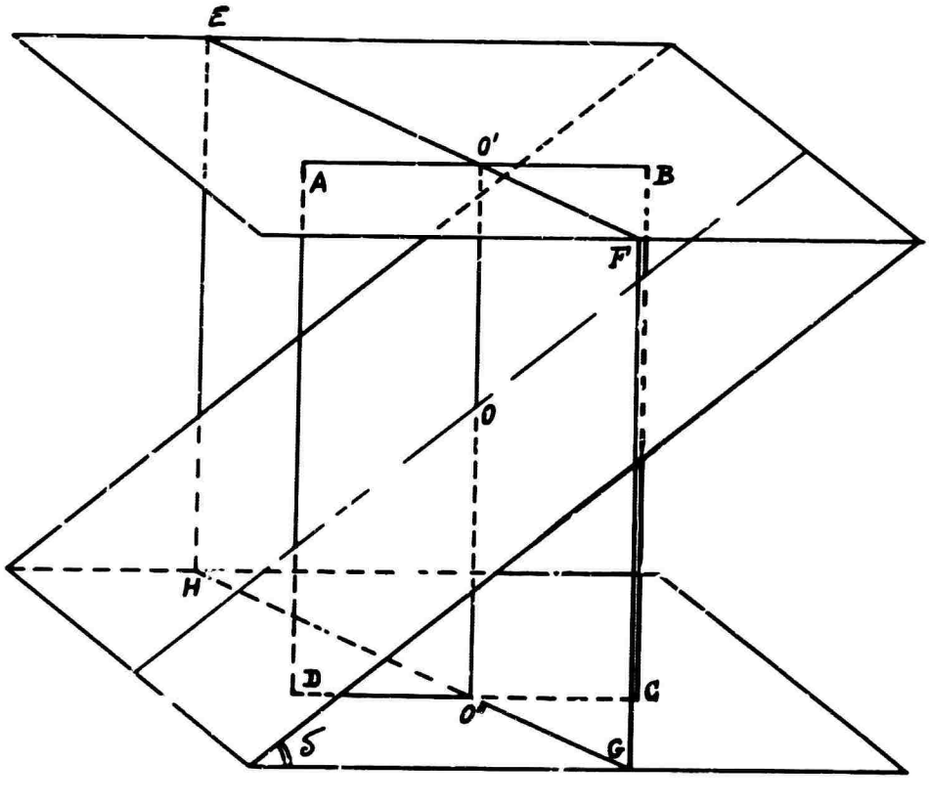

FIG 5 A

where h_1 is the depth of the refraction point at the dipping interface below the surface, i_2 and i_3 are the angles of incidence and refraction at the interface respectively, and β expressed by:

$$\beta = \arcsin \frac{\sin i_2}{\cos i_1 \cdot \sqrt{\tan^2 i_1 + 2 \tan i_1 . \tan \delta \cos \psi + \tan^2 \delta}}$$

The RPD, as calculated from the observations, are the differences of two travel times of the form (2). They will attain extremal values for $\psi = 0^\circ$, or 180°. Assuming the two stations and the epicenter to be situated along the dip direction of the interface at a relative distance of 500 km, and assuming v_A, v_B, and i_1 to be 7600 km/sec, 4500 km/sec, 1°, and 18.5° respectively, the extremal RPD can be estimated to be of the order of -0.75 and 0.75 sec. The figures are compatible with the amplitude of the RPD's observed in our investigation. The calculated range of amplitudes depends on a number of parameters which unfortunately cannot be determined uniquely from the observations.

Two remarks concerning the formula (2) are appropriate here. The thickness H considered does not coincide necessarily with any marked boundary, e.g. the Mohorovicic discontinuity. It defines only a level above which a travel time anomaly exists along the ray paths to the two stations. The dip δ of the interface does not necessarily mean a real, dipping boundary. It may be understood as a measure of a horizontal velocity inhomogeneity. This means that the medium may have a velocity gradient in the dip direction of the inter-

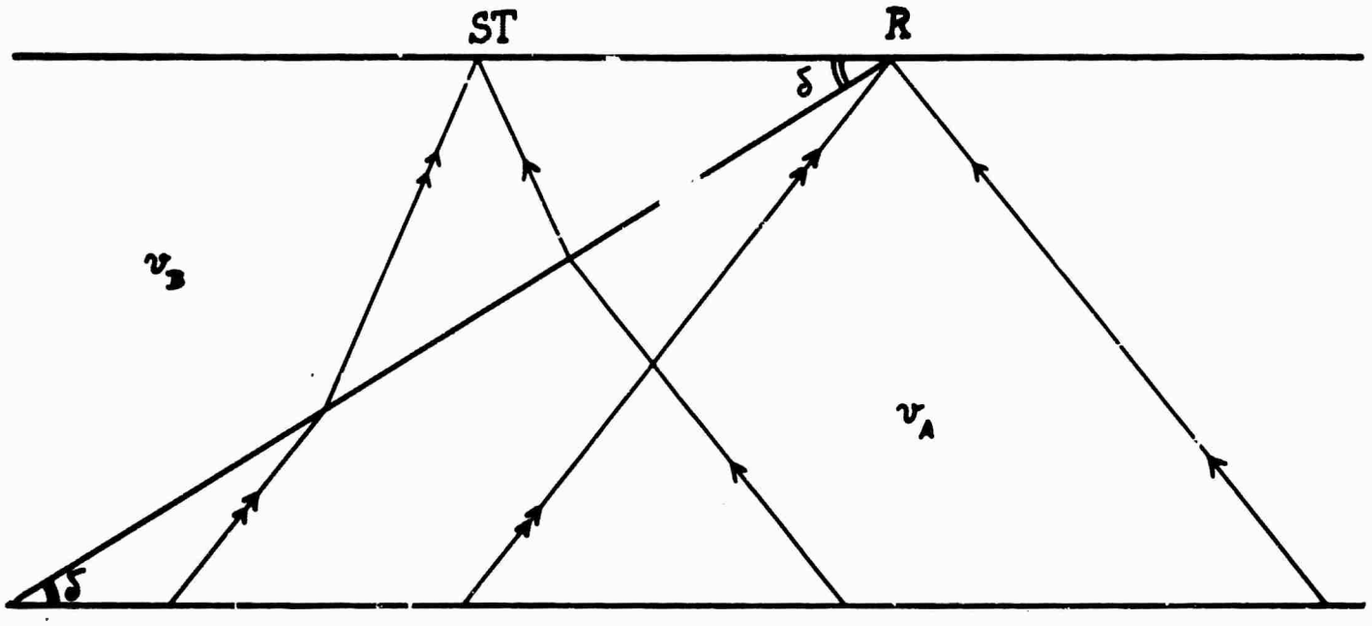

FIG. 5 C

face, different from zero. This model seems most relevant to the RPD's as observed in Scandinavia.

In Fig. 5C the station (ST), reference station (R), and the epicenter are assumed to lie in a vertical plane coinciding with the dip direction of the interface. The reference station (R) is situated close to the outcrop of the interface, so that the rays arriving at (R) travel always with the velocity v_A assumed to be larger than v_B.

In this case the RPD's will be always positive. The maximum value is obtained for waves traveling in the updip,

the minimum value - for waves traveling in the downdip direction, changing cyclically for the remaining azimuths.

It can be seen that essentially the same will apply if a horizontal velocity gradient exists in the layer, and if the reference station is situated in the direction of the horizontal velocity gradient with respect to the station. And opposite, if the reference station is situated away from the station, in the direction opposite to the horizontal velocity gradient, the average of the RPD's for all azimuths will be negative.

We shall apply this model to the RPD's as observed in Scandinavia. The A-values in formula (1) were found to be positive for Uppsala and Umeå as reference stations. This implies that the reference stations are situated in the direction of a horizontal velocity gradient. Since the reference stations are surrounded by 14 stations each, we conclude that underneath the reference stations the velocities of P waves are highest.

Interpretation. As was mentioned earlier, the reference stations Uppsala and Umeå are situated at places of most intensive continental uplift. Let us assume here the hypothesis that continental uplift in Fennoscandia is an evidence of isostatic readjustment of the crust. If isostasy alone would be involved, we would expect the horizontal velocity gradient in the crust and upper mantle to be directed away from the center of most intensive uplift, since the latter coincides with the region where the lighter, crustal material

was mostly submerged during the glacier period.

Our investigation indicates the velocity gradient to be directed towards the center of uplift. This does not contradict the isostasy as mechanism of the uplift, but since isostasy cannot explain the finding, an additional mechanism needs to be introduced.

The most obvious one seems to be the compression of the layers in consequence of loading with the icecap, the compression having been most intensive in the region of most intensive present uplift. During glaciation the material in the crust and upper mantle can be supposed to have been compressed elastically in a time-independent (perfect elasticity) and a time-dependent way, the latter having a recoverable and/or an irrecoverable component. Unloading caused a dilatation in the same order, the time-dependent dilatation eventually still going on. Compression is known to cause in general an increase of seismic velocities, and the region mostly suppressed, revealing now the most intensive uplift, should then have higher seismic velocities if compared with the surrounding.

Conclusions.

1. A cyclical variation of relative P-time delays at 14 seismographic stations in Scandinavia is found, with Uppsala and Umeå as reference stations.
2. Twenty-eight sets of relative P-time delays are constructed as function of azimuth from the station to epicenter, and the observational data are approximated by the first two terms of a Fourier series

expansion. The constant term is found to be positive, and the maximum positive delay is found for azimuths pointing away from the region of maximum continental uplift.

3. The behavior of relative P-time delays is interpreted in terms of a horizontal velocity inhomogeneity in the crust and upper mantle, such that higher velocities are found in the region of maximum continental uplift.
4. The velocity inhomogeneity does not exclude isostasy as mechanism of the continental uplift; an additional mechanism of the uplift, however, must be introduced to explain the findings.
5. As additional mechanism we propose the following. The strata were compressed during glaciation. In consequence of the removal of the icecap a dilatation took place. Both compression and dilatation had a time-independent and a time-dependent component. Part of the compression may even be irrecoverable. In regions of most intensive present uplift the compressions may be supposed to have been heaviest, and even now higher seismic velocities may be expected there, as found indeed from the relative P-time delays. Whether the time-dependent dilatation is still going on is beyond the method applied in the present investigation.

References

Bolt, B. A. and O. W. Nuttli (1966). P wave residuals as a function of azimuth, 1, Observations, J. Geophys. Res. 71, 5977-5985.

Jeffreys, H. and K. E. Bullen (1948). Seismological Tables, British Association for the Advancement of Science, 50 pp.

Gutenberg, B. (1941). Changes in sea level, postglacial uplift, and mobility of the earth's interior, Bull. Seism. Soc. Am. 52, 721-772.

5. The Mechanism of the Earthquakes of the Rat Island Earthquake Sequence of 4 February 1965.

A magnitude 7 3/4 (PAS,BRK), 8-8¼ (PAL), 7.5 (CGS-MC) earthquake occurred near Amchitka Island on 4 February 1965, 05-01-21.8 GMT. The USCGS epicenter has coordinates 51.3°N, 178.6°E, with focal depth about 40 km (restricted). The major shock was followed by a strong aftershock sequence. For example, of the many aftershocks which occurred during the first 24 days following the main shock, 750 were large enough to be located by the routine procedures of the epicenter determination program.

This study concerns the focal mechanism of the main shock and of the larger aftershocks.

Fig. 1 presents a map showing the location of the main shock, the extent of the epicentral region, and the location of the larger aftershocks which are here examined in detail. The aftershock epicenters shown on the map are those of the smaller aftershocks located by the USCGS for the first three days following the major shock, together with those of the larger shocks of the entire sequence. It is seen that the

RAT ISLANDS EARTHQUAKE, 4 FEBRUARY 1965

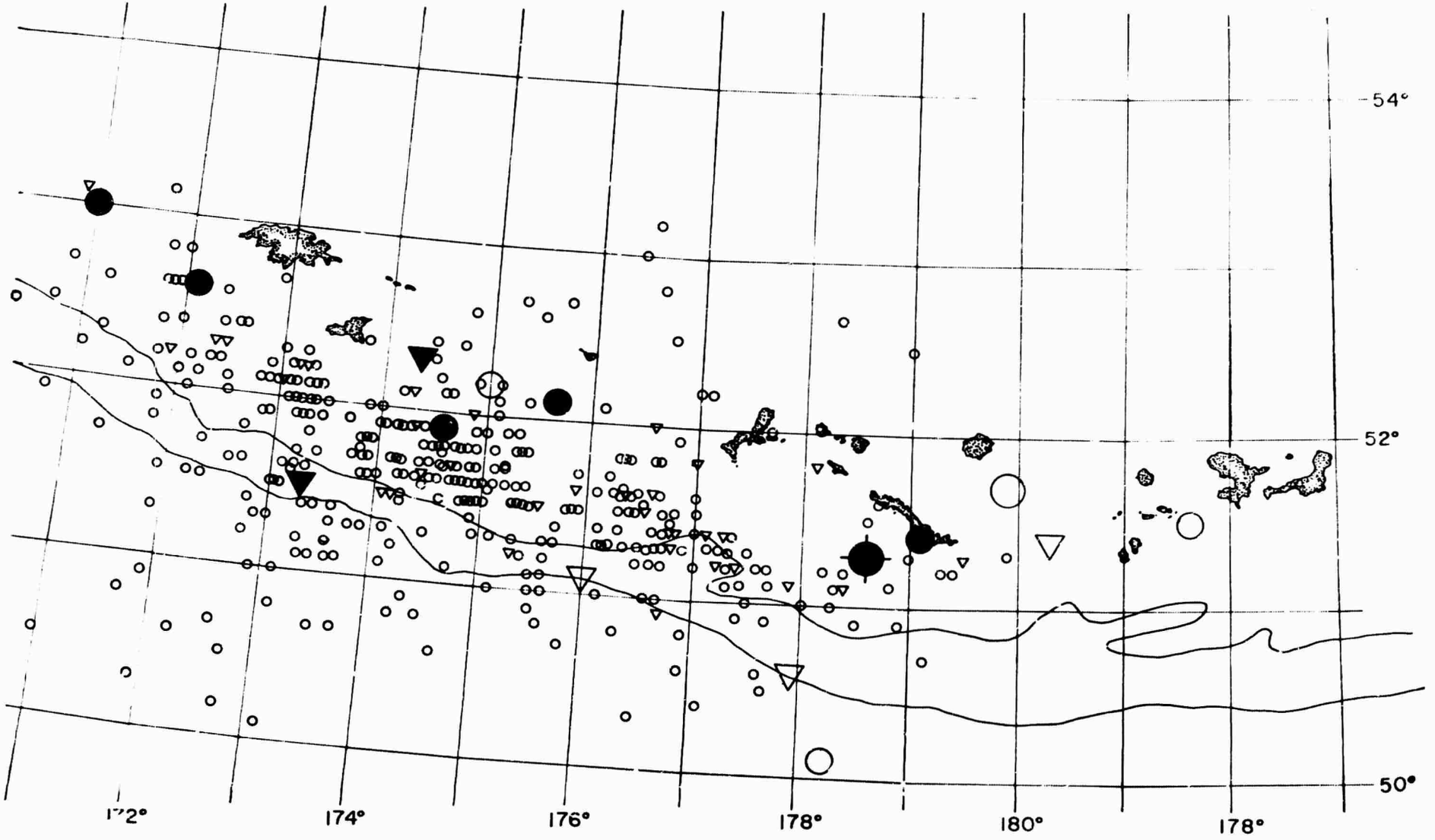

Fig. 1

major shock occurred near the eastern extremity of the activity, that the aftershock zone extends from 180° to 170°E, and that the activity extends over a zone about 200 km wide immediately to the south of the island chain. The focal depths given by the USCGS vary from 25 to 40 km. A few foci lie in the range of focal depth 40 to 50 km.

The earthquakes here examined are indicated by the larger symbols on the figure. The solid symbols represent foci of the first three days. Thereafter there were no aftershocks large enough to yield a focal mechanism solution until 30 March. The open symbols represent earthquakes occurring between 30 March 1965 and 4 July 1966. The epicentral coordinates, together with the focal mechanism solutions, for all these earthquakes are listed in Table 1.

Focal Mechanism Solutions. The focal mechanism solutions have been determined using data from the WWSSN system. In the determinations data from the long-period records only were used. Both direction of first motion of P and the polarization of the S wave were used in determining the nodal planes. In all cases a double couple mechanism was assumed; no evidence favoring or requiring any other type mechanism was observed.

Two distinct classes of foci were found. An example of the first is indicated in Fig. 2a. The observable P wave radiation pattern of this class samples only two first motion quadrants on the focal sphere. As a result, only one nodal plane of the P wave first motion is determined. On the assumption of the double couple mechanism, the S wave polarization

Table 1. Rat Island Earthquake Sequence
4 February 1965

Date	Time	Lat.	Long.	h	m_b (USCGS)	Plane 1 Dip Direc.	Plane 1 Dip	Plane 2 Dip Direc.	Plane 2 Dip
4 Feb 65	05-01-28	51.3N	178.6E	40	6.0*	150°E	78°	-	-
"	12-06-04	52.6N	172.1E	25	5.8	145°E	83°	29°E	15°
"	14-18-28	53.0N	171.0E	30	5.7	148°E	83°	33°E	17°
5 Feb	09-32-09	52.3N	174.3E	41	5.9	141°E	75°	325°E	15°
"	20-47-13	51.9N	174.6E	35	5.7	153°E	77°	310°E	14°
5 Feb	04-02-53	52.1N	175.7E	35	5.9	142°E	75°	359°E	18°
7 Feb	02-17-09	51.4N	173.4E	40	6.0	196°E	53°	58°	45°
"	09-25-51	51.4N	179.1E	30	5.3	141°E	74°	340°E	16°
30 Mar	02-27-07	50.6N	177.9E	51	7	194°E	47°	52°E	50°
23 May	23-46-12	52.2N	175.0E	22	6.1	145°E	75°	12°E	22°
1 Oct	08-52-04	50.1N	178.2E	23	6.3	185°E	50°	40°E	50°
22 Nov	20-25-13	51.4N	179.7W	40	5.9	145°E	70°	354°E	22°
15 May 66	14-46-06	51.5N	178.4W	31	5.8	136°E	61°	349°E	34°
2 June	03-27-53	51.1N	176.0E	41	6.0	211°E	51°	50°E	40°
4 July	18-33-36	51.7N	179.9E	13	6.2	97°E	85°	187°E	85°

*This is the m_b value given by the USCGS from short-period body waves. Actual magnitude is about M = 7.5. Other shocks here listed are probably in the range $6 < M < 7$.

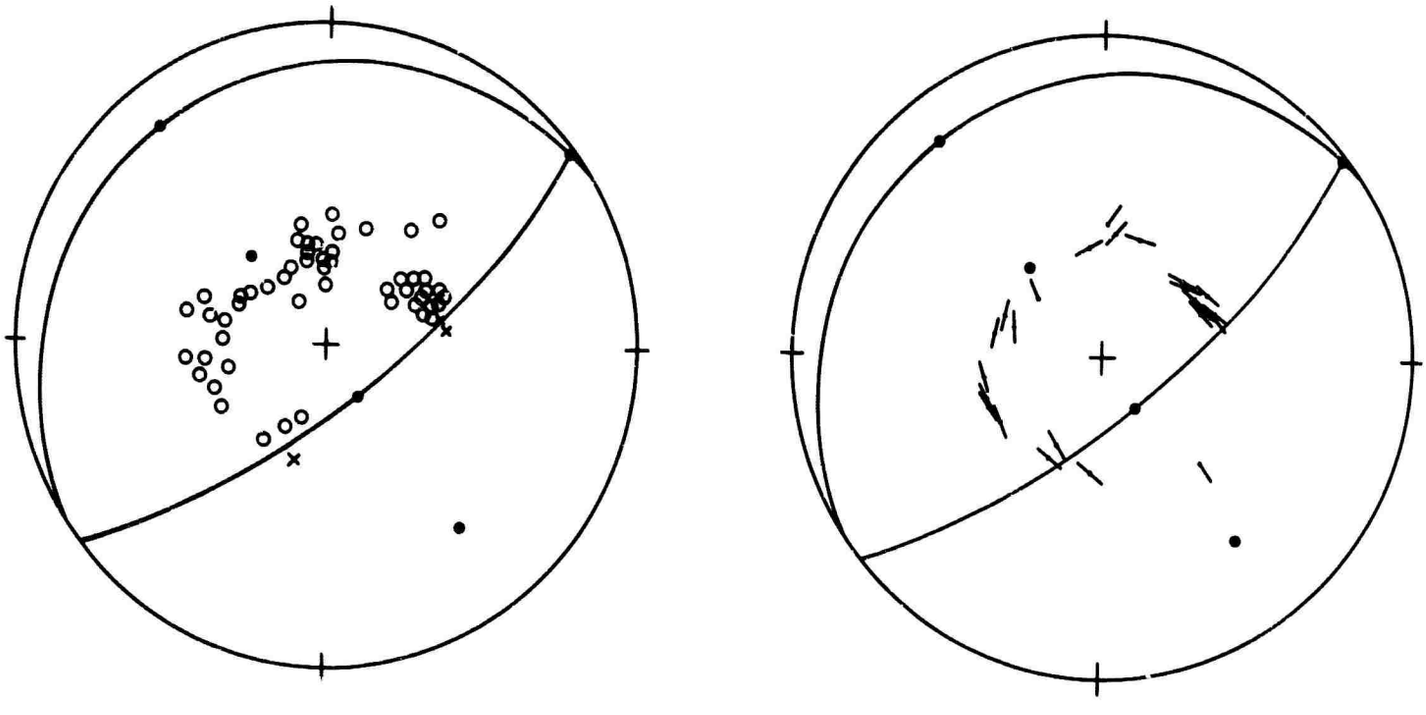

RAT ISLANDS, 5 FEBRUARY 1965, 09h

Fig. 2a

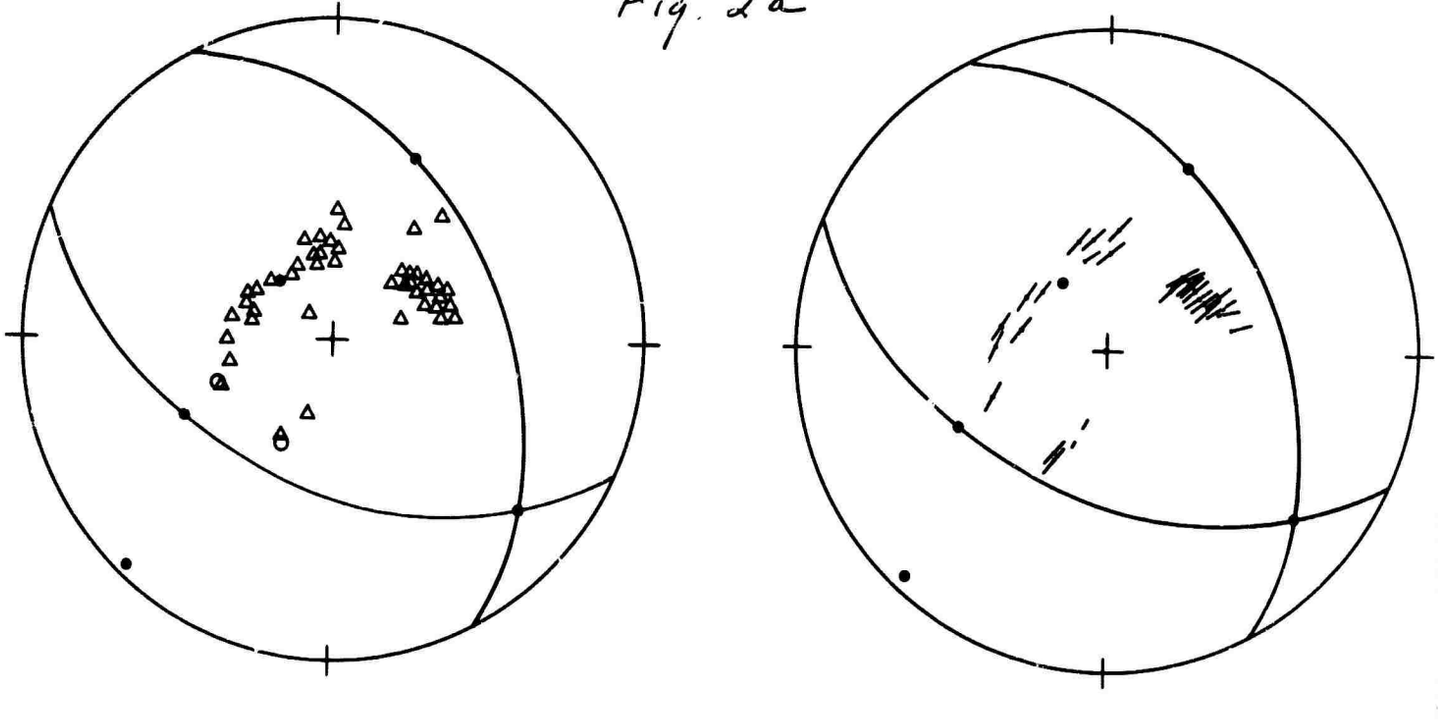

RAT ISLANDS, 7 FEBRUARY 1965, 02h

Fig. 2b

data, as presented on the right-hand portion of the figure, make possible a complete determination of both planes.

An example of the second class of foci is presented in Fig. 2b. For these earthquakes the observable P wave radiation pattern samples only a single quadrant. Neither nodal plane is determinable on the basis of the P wave data alone, though each of the nodal planes is restricted to a range of dip in the neighborhood of 45°, $\pm$ 15°. In this case, again on the assumption of a double couple mechanism, the S wave polarization data make possible a determination of both nodal planes.*

The orientation of the nodal planes for all the earthquakes studied is given in Table 1. The focal mechanisms are further indicated, together with their spatial relationship to one another, in Fig. 3. The shaded portions of the mechanism diagrams in the figure correspond to rarefaction first motion quadrants.

Discussion. Several comments may be made concerning the focal mechanism of these Rat Island earthquakes.

First, there is a distinct spatial classification of the foci. One group consists of foci located

---

* The particular configuration in question is one which corresponds to a near vertical axis of greatest compressive stress (all rarefaction first motions) or of least compressive stress (all compressions). In such cases a rotation in the strike of the nodal plane is possible with no great difference in the agreement with the S wave data. Were the principal axis to be perfectly vertical, the solution would be indeterminate, save for the restriction placed on the dip of the nodal planes.

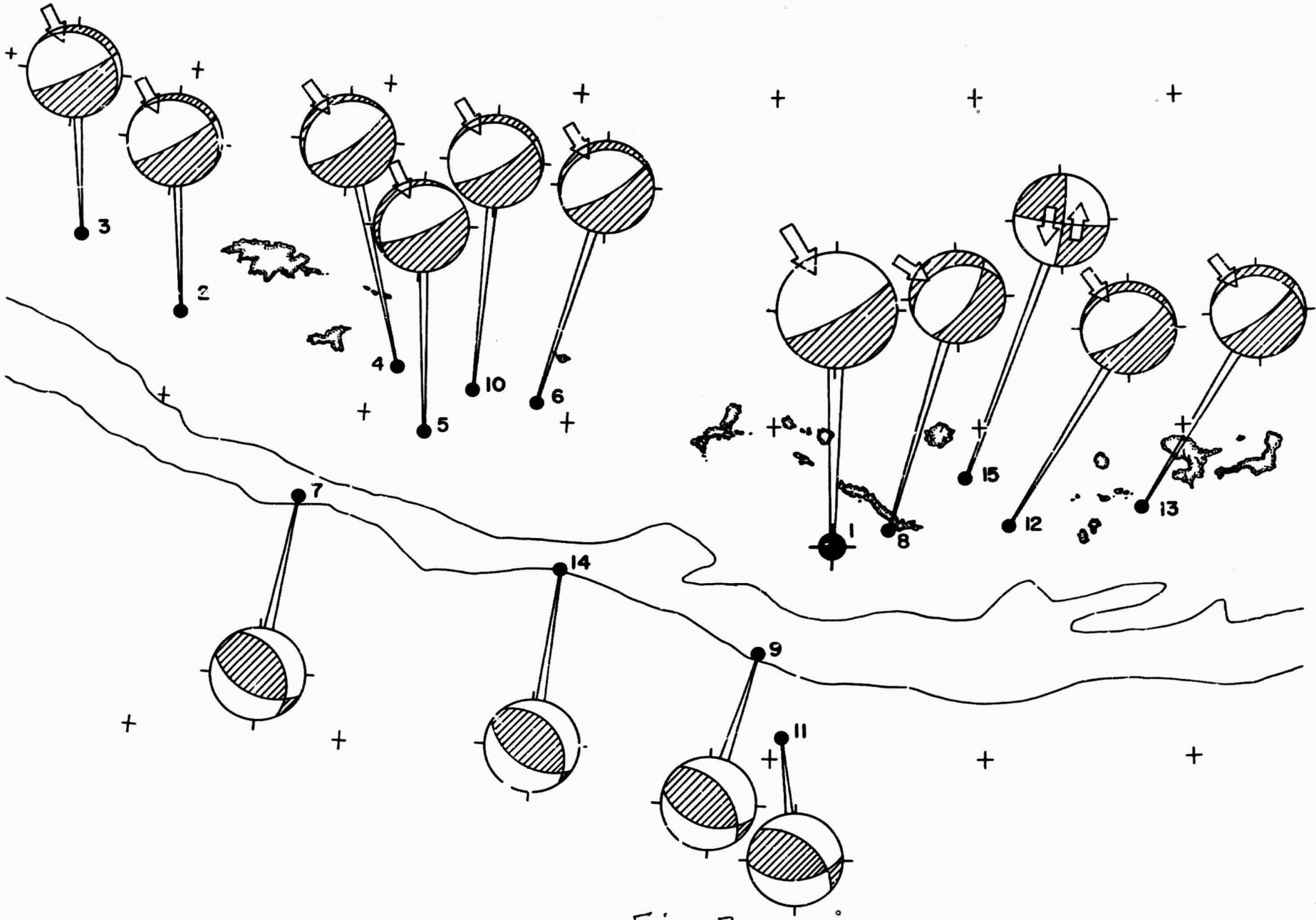

Fig. 3

near the inner or northern edge of the active zone, immediately south of the island chain. A second group consists of the foci located under or to the south of the Aleutian Trench.

The first group includes the initial shock and ten larger aftershocks. The focal mechanisms of all of these shocks, except that of the final larger shock, that of 4 July 1966, are similar to that shown in Fig. 2a. This means that each of these shocks represents a continuation of episodic fault motion of one and the same character. The fault plane solutions themselves are ambiguous as to the character of the motion: either of the nodal planes may correspond to the fault plane. If the steeply dipping plane is taken as the fault, the motion is reverse faulting along a series of faults striking obliquely to the trend of the island chain. If the nearly horizontal plane is taken as the fault plane, the motion is thrust faulting in character along a plane dipping gently (about 10° - 15°) under the island arc. In the latter hypothesis the island or landward side overthrusts the oceanic side. As indicated by the arrows in Fig. 3, the thrust block moves toward the southeast. The motion corresponds to a pressure axis approximately normal to the trend of the arc acting upward from the ocean side at an angle of about 30° from the horizontal.

The similarity of these mechanisms to those of the Alaska earthquake of 28 March 1964 and its aftershock sequence (see Stauder and Bollinger, 1966) is noteworthy. A possible special

significance to the mechanism of focus 15, that of 4 July 1966, is noted below.

The second group of earthquakes, those with foci under the trench, are all similar in character to that shown in Fig. 2b. The pressure axis for these foci is oriented nearly vertical, whereas the axis of least compressive stress is horizontal. These foci apparently do not differ significantly in focal depth from those of the first group. It is difficult to correlate the stress systems of the two groups.

The property here noted for the earthquakes with foci under the trench (first motions all rarefactions at teleseismic distances, pressure axis vertical) corresponds to a property noted previously by Evison (1967) for earthquakes under the Aleutian trench as opposed to those with foci on the interior of the arc. Foci of several other earthquakes associated with the Aleutian trench which we have studied recently have this same property.

Secondly, a noteworthy temporal classification of the foci suggests itself. Excluding the first seven hours after the main shock, during which time the traces on the WWSSN records were too tangled to interpret, seven aftershocks large enough for a focal mechanism solution occurred. There followed a lapse of fifty days before another aftershock of comparable magnitude occurred. Thereafter, seven large aftershocks were placed sporadically over the next fifteen months.

The aftershocks of the first three days are indicated in Fig. 4a. As noted above, the main shock occurred near the

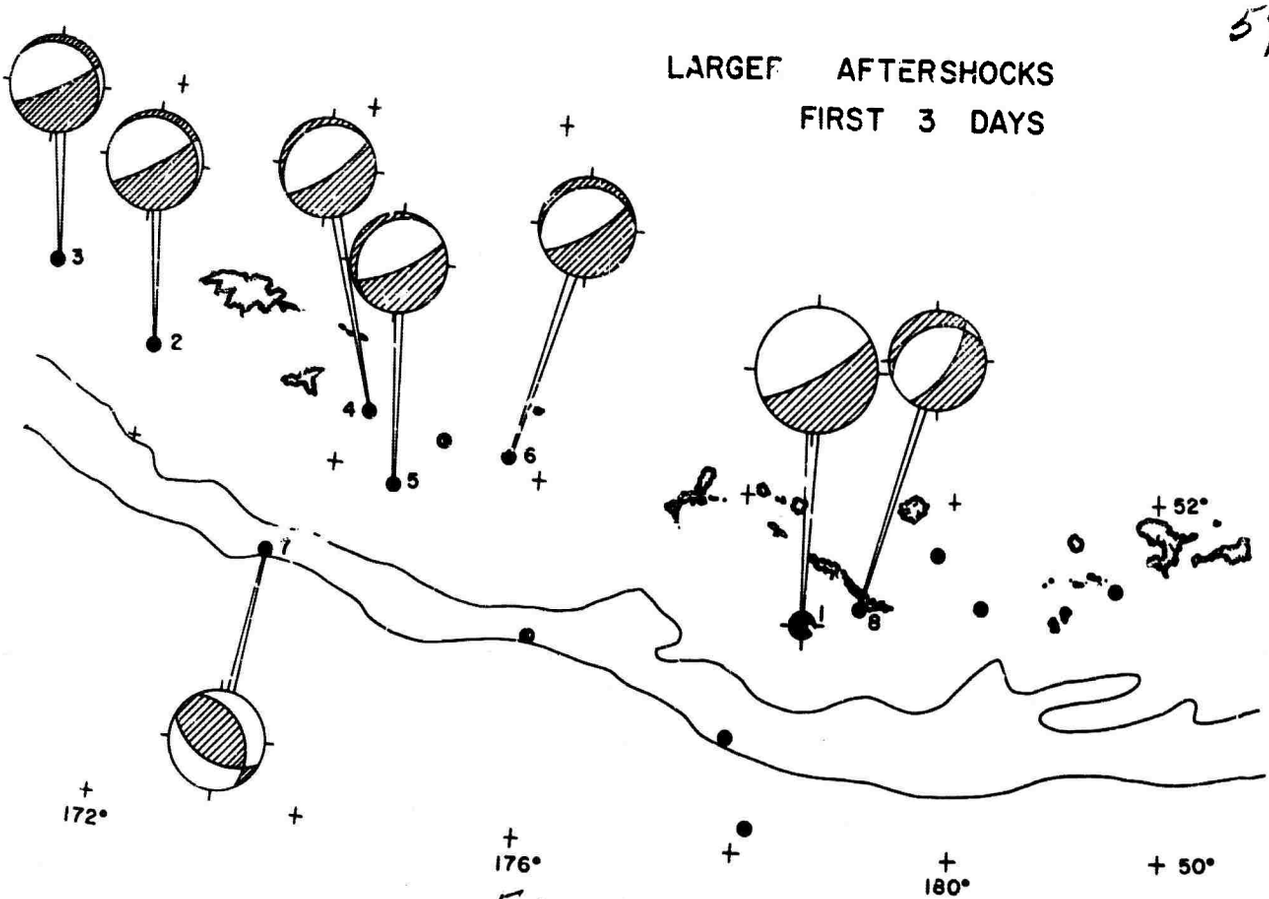
LARGER AFTERSHOCKS
FIRST 3 DAYS
1
2
3
4
5
6
7
8
172°
176°
180°
+ 52°
+ 50°

Fig. 4a

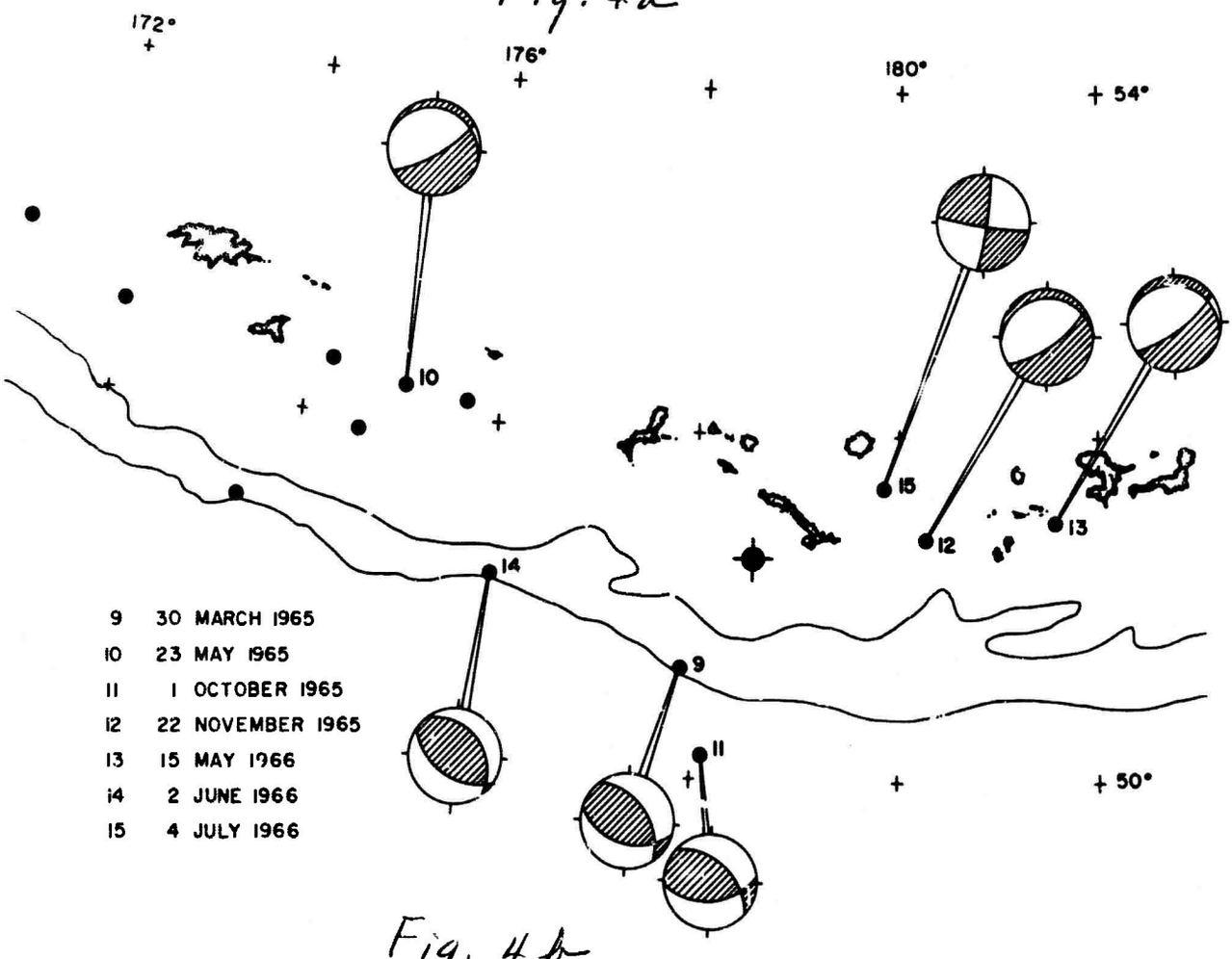
172°
176°
180°
+ 54°
+ 50°
9 30 MARCH 1965
10 23 MAY 1965
11 1 OCTOBER 1965
12 22 NOVEMBER 1965
13 15 MAY 1966
14 2 JUNE 1966
15 4 JULY 1966

Fig. 4b

eastern extremity of the epicentral zone. The larger aftershocks which followed were distributed, sequentially in time, at the opposite extremity of the active zone and toward the center. The next to last aftershock of this group took place under the trench, and the last at the right extremity of the zone. The mechanism of this last aftershock differs slightly, as if the trend of the faulting curved around at the end of the fault.

The larger aftershocks of the later group, beginning 30 March 1965, concentrate under the trench and to the east of the major epicentral region, along the continuation of the trend of the Aleutian arc in the Andreanof Islands.

The last shock of the sequence, that of 4 July 1966, is of markedly different mechanism from the others. The first motion field determines well all four first motion quadrants, and the faulting motion is strike slip - either left lateral on a north-south fault, or right lateral on an east-west fault. The former interpretation is here preferred as more in keeping with the general tectonic movement indicated in Fig. 3. Shortly after this earthquake, on 7 August 1966, a large earthquake occurred near the Fox Islands (50.6N, 171.3°W), apparently marking the initiation of a new phase of the Aleutian Island activity.

Conclusions. Two conclusions of significance for this Contract follow from this study. First, the similarity of mechanism of aftershocks of a given sequence is further

illustrated. Second, foci radiating uni-polar first motion radiation fields are probably restricted to certain definite, and relatively narrowly defined, portions of a tectonic environment.

References

Evison, F.F. (1967). On the occurrence of volume change at the earthquake source, Bull. Seism. Soc. Am. 57, 9-25.

Stauder, William and G. A. Bollinger (1966). The focal mechanism of the Alaska earthquake of March 28, 1964, and of its aftershock sequence, J. Geophys. Res. 71, 5283-5296.

6. Model Studies of Decoupling of Explosions.

During the last period, the following experiments were performed.

1. Absolute calibration of the receiving channels.
2. Decoupling of the explosion.

Receiving channels play a major role in controlling recorded wave forms. The objective of this calibration is to obtain a response curve in absolute units, in order to reduce the displacement of the wave displayed on the screen of the scope to the displacement at the surface of the model. The recording channels consist of a capacitance pick-up and a 60 cycle rejection filter. The displacement at the surface of the model produces a change in capacity of the capacitor, which is amplified, filtered, and finally displayed on the screen of the scope. In order to calibrate the receiver absolutely a source of mechanical motion is required. A piezoelectric transducer is used to furnish the mechanical motion. Transducers were sandwiched between two circular rods of

plexiglas 7/8" in diameter and equal in length. Three rods of different lengths (10, 15, and 20 cm) were used. The model is suspended by a fine wire.

In this experiment a sine wave frequency oscillator was employed. The signal frequency of the oscillator was varied constantly from five kilocycles to seventy-three kilocycles per second, keeping the oscillator output amplitude constant. The output voltage of the oscillator was fifteen volts (RMS). It was found that the amplitude of the resulting sinusoidal wave pattern on the oscilloscope screen passed through a series of maxima and minima, and the amplitude and frequency values of these maxima were measured. The maxima occurred at resonant frequencies of the rods. The value of these resonant frequencies depends on the elastic properties of the rods and the length of the rods. The resonant frequencies of a rod, free at both ends, are given by

$$f_k = \frac{KC}{2L}$$

in which f = frequency, k = an integer, L = length of the rod, and C = phase velocity of the rod material.

In the configuration in question the transducer is always located at an antinode in displacement; therefore, each rod will vibrate as if free at both ends. For the even number of modes, the free ends of the rods are 180° out of phase with the input of the transducer, while for the odd number of modes, they are in phase.

The amplitude recorded at the free end of the rod is the incident amplitude, plus the multiple reflections from the free ends of the rods. The possible number of reflections is infinite. But the attenuation in plexiglas is high enough to diminish the amplitude to a negligible amount after some number of reflections. To correct the recorded amplitude, a simplified formula is derived to reduce the recorded amplitude to one resulting from the incident wave only. This is given by

$$\bar{A}_+ = \frac{A_o^+(R+1)e^{\alpha L}}{R} \sum_{K=1}^{\infty} (-1)^{K+1} R^K e^{-2K\alpha L}$$

in which

$\bar{A}_+$ = amplitude at the ends of the rod plus reflection

A_o+ = output amplitude of the transducer

R = reflection coefficient for plexiglas air interface

L = length of the rod

α = absorption coefficient in plexiglas

k = integer

The observed amplitude on the scope = $M\bar{A}_+ = A_s$ where M = magnification factor

$$M = \frac{A_s}{\frac{A_o^+(R+1)}{R} e^{\alpha L} \sum_{K=1}^{\infty} (-1)^{K+1} R^K e^{-2K\alpha L}}$$

The absorption coefficient is obtained from another experiment, in which a rectangular pulse generator is used instead of a sine wave oscilator. The value of α is calculated from

the spectrum of the pulses reflected at the free ends of the rods.

The above series does converge. For calculation of magnification factor only 100 terms of the series were included.

The amplitude response of the receiving channels obtained is shown in Fig. 1.

Phase Response. The phase response of the receiving channels was obtained as follows. The scope was triggered internally by the output of the sine wave oscillator. The output of the scope was displayed on the scope on one of the beams. The sine wave oscillator also applied to the transducer simultaneously and the output of the channels was displayed on the upper beam of the scope. It is assumed that there is no delay between the output of the oscillator and the output of the transducer. The phase shift of the sine signal propagated through the plexiglas rod and recorded by the receiving unit, compared with the output of the oscillator will be due to the receiving channels.

The odd modes of the rods are 180° out of phase with the even mode. To measure the delay introduced by the receiving channels, the output of the oscillator is compared with the output of the receivers. For odd mode the peaks of the two outputs are compared, and for even mode the peak of one output is compared with the trough of another output. Then the delay time is multiplied by the angular frequency of the sine wave to obtain the phase delay. The phase response curve is shown in Fig. 2.

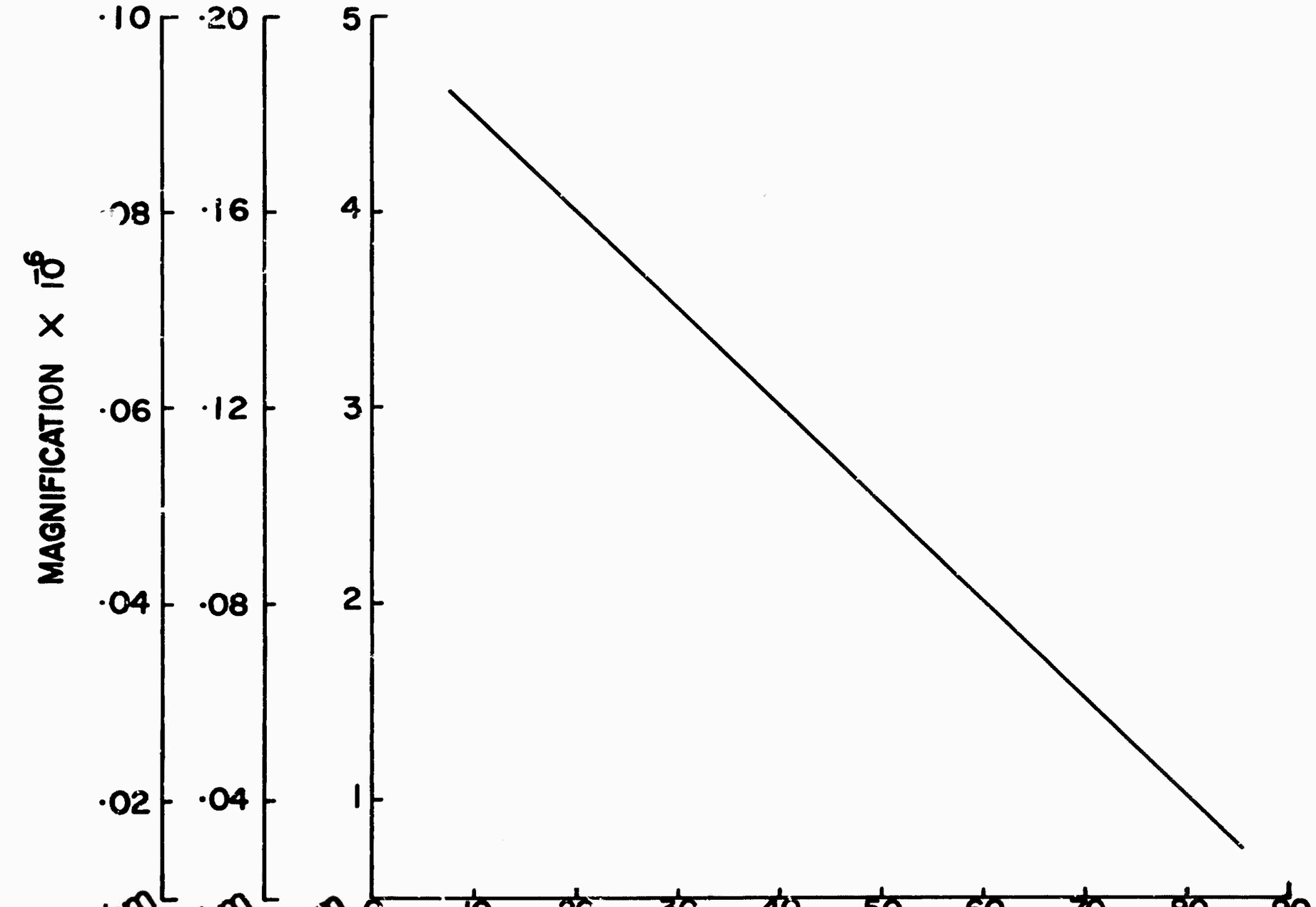

FIG-1 AMPLITUDE RESPONSE CURVE

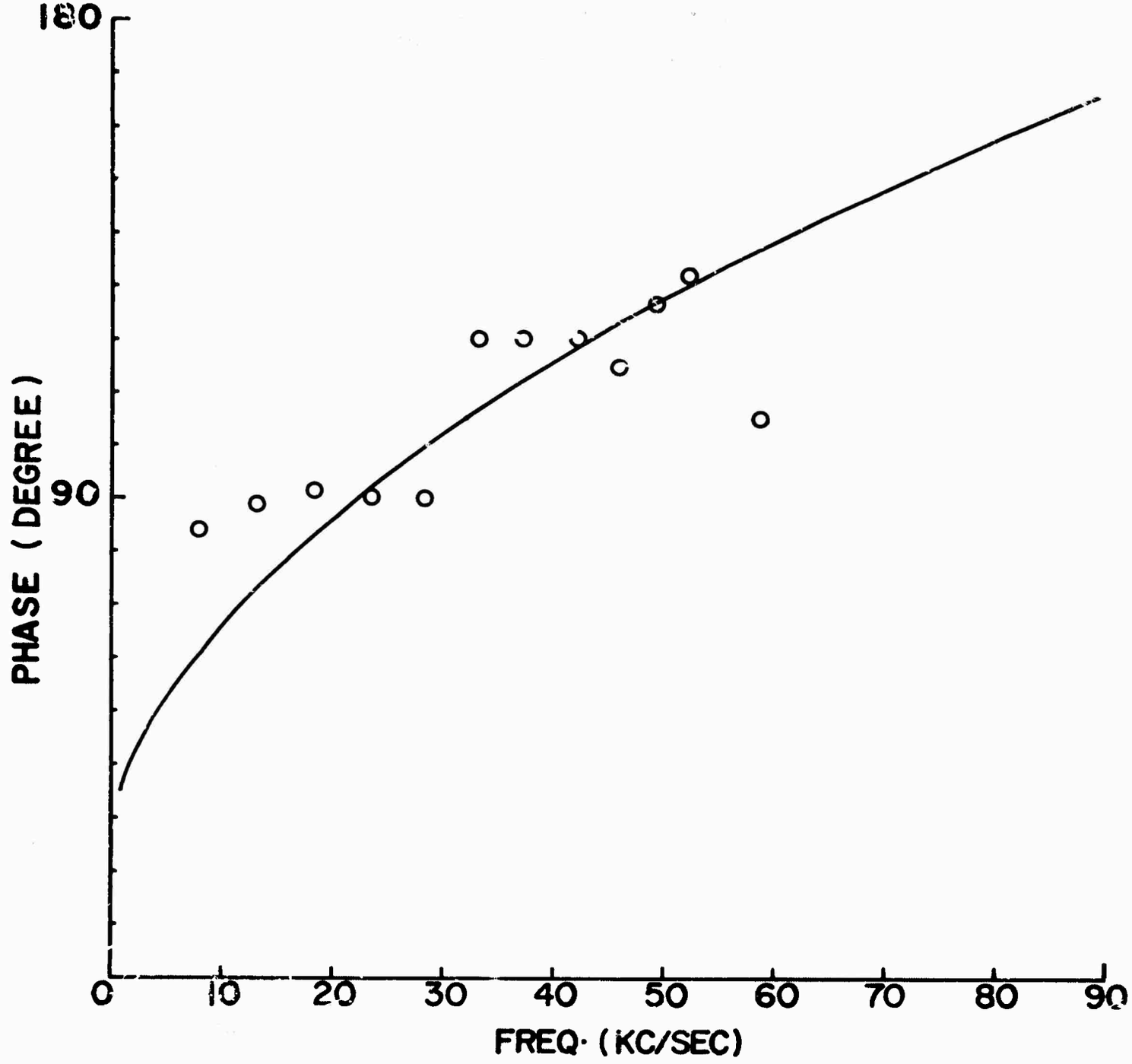

FIG·2 PHASE RESPONSE CURVE

Decoupling. This experiment was performed in a cubic foot block of plaster of paris.

The decoupling assembly was prepared in the following manner. Cylindrical tubes of plexiglas of two different diameters 50 mm and 70 mm were used to cast the cylindrical cores. Each tube consisted of two parts, one eight centimeters in length. The lower part of the specimen was casted first. During the casting of the lower part a plexiglas sphere was placed at the center of the tube. In order to prevent the sphere from sinking, a small hole about one millimeter in diameter was made through the sphere. The sphere was held at the center by a thin wire which ran through the sphere and along the edge of the tube. After putting thin aluminum foil around the sphere and over the lower part, the upper part of the core was cast. The advantage of this procedure is to get a fine contact between the two pieces in order to cement them together later on. After five minutes of setting, the mold is removed, the two pieces of the core are then separated and the plexiglas sphere is removed. This is the only way that could produce a perfect spherical cavity.

After letting the core specimen dry for a period of about two weeks, the specimens are ready for use. The drying period could be made shorter by heating the sample in an oven for twenty-four hours with 50° centigrade temperature.

The charge is hung inside the cavity by the detonation wire which runs through the charge. A fine wire was used in order to prevent any disturbance of the pressure inside the cavity. After the charge was assembled, the two core pieces

were cemented together with an epoxy cement. The samples were left overnight to let the cement dry. Weights were placed on top of the core to join the two pieces firmly together. The core can then be fitted inside the block. A hole is drilled with power-driven drilling bits. Two sizes of holes were drilled fifty millimeters and seventy millimeters in diameter. In order to cement the core to the hole, a soft mixture of plaster of paris and water was poured inside the hole before the sample was lowered. Immediately after pouring the plaster the sample was pushed inside the hole. The core squeezed the plaster out along the gap between the core and the hole cavity, and the plaster filled the gap.

The advantages of this technique are better and excellent control of the charge inside the cavity, the cavities are perfect in shape and the same block may be used as many times as one wishes without spending time preparing another block. The only thing one does is drill the hole again and lower another specimen.

To establish a spherical detonation the charge should be initiated at the center. A thin tin copper wire is filed at one point one millimeter in length. This wire is then passed through the center of the charge with the filed point at the center. Then 1900 volts are applied to the wire from a blaster to melt and initiate a spark at the center of the charge.

Experimental Results. Two series of decoupling experiments were performed in plaster of paris. In each series the

weight of the charge was kept constant. In the first series a 55 mm charge was used, and in the second series a 100 mm charge was used. The distance between the center of the charge and the receiver is kept constant. The source detector distance is 15.3 centimeters. The radial components of motion were recorded at the surface of the block. One receiver is positioned parallel to the equatorial plane of the cavity and another one perpendicular to it.

For 55 mm series the cavity radius is varied from 0.47 centimeter to 3.2 centimeters, and for 100 mm series the cavity radius is varied from 0.63 centimeter to 3.2 centimeters. The charges diameters are 0.47 centimeter and 0.6 centimeter.

Typically, the tamped shots were made in the following manner. The charge was placed at the center of the cylindrical core during the casting. To protect the charge from moisture the charge was painted with oil paint before casting inside the specimen.

The tamped shot gave small seismic signals in comparison with the cavity shots. Post shot drilling of the hole showed a crushing zone around the charge. The diameter of the cavity left after the shot is as follows: for 55 mm charge, 7 millimeters; for 100 mm charge,1.1 millimeters. This indicates that some of the energy released by the explosions was spent in crushing the material. The cracking zone cannot be be recognized. Hence, the energy released by the explosion was used in an irreversible process leaving only part of it available for the radiated seismic energy.

Nicholls and Duvall have investigated both theoretically and experimentally the effect of the ratio characteristic impedance on explosion generated strain amplitudes and strain energies. Although their theory postulated is for plane waves, observed data agree with predictions based on shock wave theory. According to their results, the stress in the medium may be calculated from

$$\text{Medium Stress} = \frac{(1+N)}{(1+NR)} \text{ detonation pressure.}$$

Where R is the ratio of characteristic impedance of explosive to rock and N is determined to be five from the experimental data. N may be defined as the ratio of mass flowing through the reflected shock front per unit area in unit time to the mass flowing through the incident shock front per unit area in unit time or as the ratio of the effective characteristic impedance of the reflected shock wave to that of incident shock wave. If these ratios are equal, N=1, and the above equation reduces to the acoustical law for the transmission of a wave across a boundary at normal incidence.

The detonation pressure of the explosive used in the experiment (silver acetylide) was calculated from the following equation (Ref. 1).

$$P = D^2 \Delta \frac{0.45}{1 + 0.8\Delta} \qquad (1)$$

where P = detonation pressure in dyne per square centimeter,

Δ = average loading density in gram per cubic centimeter,

D = detonation velocity in centimeter per second.

For the silver acetylide employed in the experiment, the load-density is 0.9 gm/cm^3 and detonation velocity 1.3 km/sec. It has to be remembered that the detonation velocity is a function of a loading density. Using the above equation, the detonation pressure is given by,

$$P = 4.0 \text{ kilobar.}$$

The plaster of paris has a density of 1.1 gram per cubic centimeter; a longitudinal propagation velocity, c, of 3.37 km/sec., and a characteristic impedance (ρ C) of 3.63 X 10^5 dyne sec/cm^3. The characteristic impedance (Δ D) of the explosive used is 1.17 X 10^5 dyne sec/cm^3. The impedance ratio is simply the characteristic impedance of the explosive, divided by the characteristic impedance of rock, and is given by R = 0.322. Using equation (1), the stress transmitted to the medium is found to equal to 9.2 kilobar.

The compressive and tensile strengths of the plaster measured in static failure are 414 and 40 bar respectively. The dynamic compressive and tensile strengths of the material are about twice the static strength.

Comparing the stress transmitted to the medium from a tamped shot with the dynamic strengths of the material, the input stress to the medium exceeded the strength of the material. The input stress is about one order of magnitude larger than compressive strength and two orders of magnitude larger than the tensile strength. Hence, the crushed and cracked zones should exist around the tamped shot.

The variation of peak amplitude with cavity diameter from two series of decoupling experiments is shown in Fig. 3 and Fig. 4. Comparing the amplitude of the signal obtained from the smallest cavity (radius = 0.47 cm for 55 mgm charge and 0.63 cm for 100 mgm charge) with the signal obtained from the largest cavity (radius = 3.2 cm), the amplitude of the smallest cavity is about twice the largest cavity. This is the same for both charge sizes. Therefore the reduction in amplitude is independent of the charge size.

By plotting the peak amplitude as a function of the radius of the cavity on logarithmic paper, a straight line can be drawn that fits the observed points. The least square method is used to get the slopes of the lines. The slopes of the lines obtained for 55 mgm charge and 100 mgm charge are -0.46 and -0.55, respectively. The slopes indicate that the peak amplitude is inversely proportional to the cavity radius raised to a power less than one.

The maximum value of amplitudes in Figs. 3 and 4 correspond to cavity radii 0.47 cm and 0.63 cm. In the regions to the left of these radii the amplitudes start decreasing with decreasing cavity radius. In this region the pressure produced by the explosion exceeds both the compressive and tensile strength of the material. For cavity radii larger than those given above the amplitude decreased as the radius increased. The pressure on the surface of the cavity is within the compressive strength of the plaster, but exceeded the tensile strength of the plaster. Therefore a cracked zone exists in the medium surrounding the cavity.

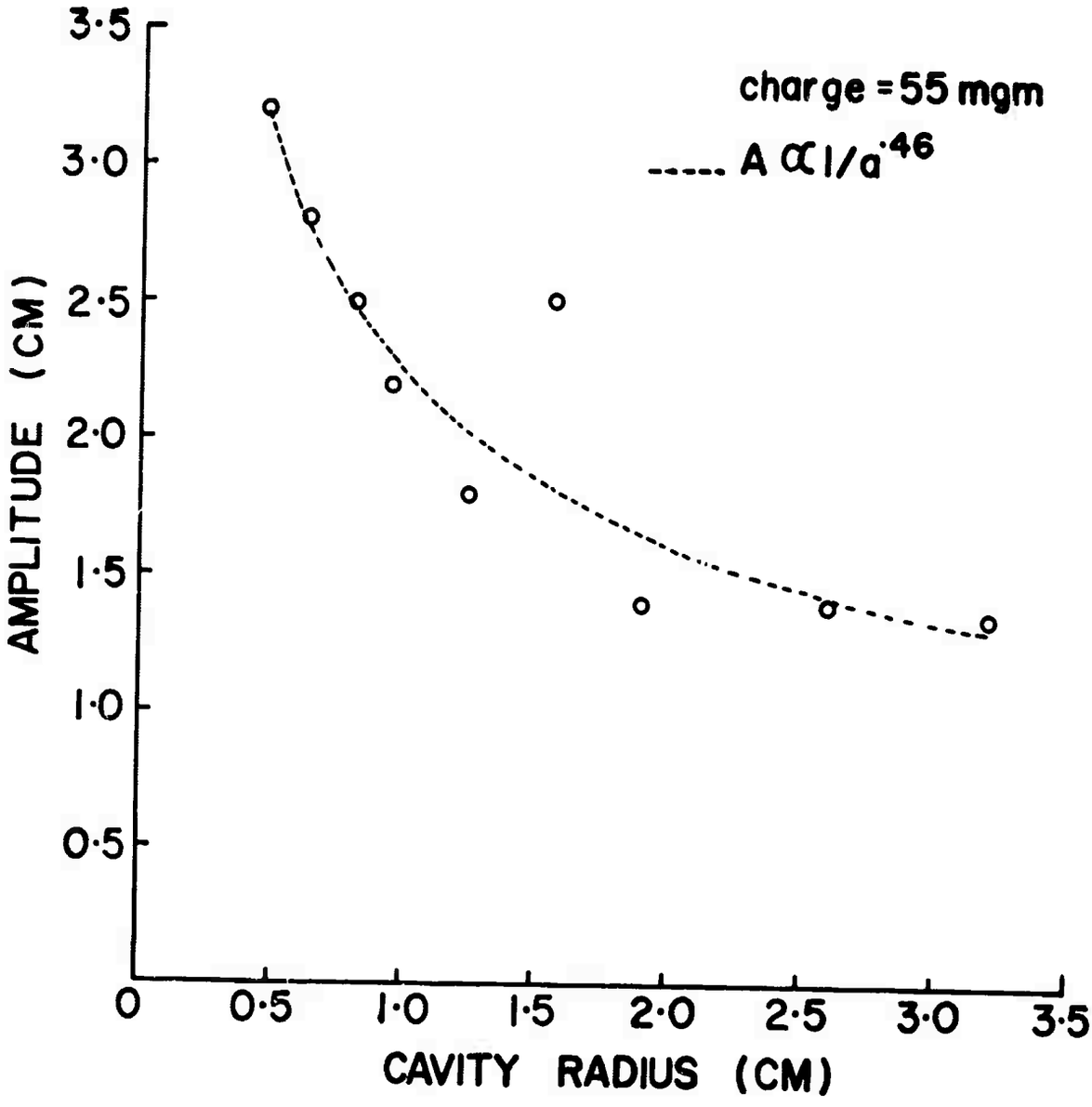

FIG. 3 PEAK AMPLITUDE OF P-WAVES AS A FUNCTION OF CAVITY RADIUS

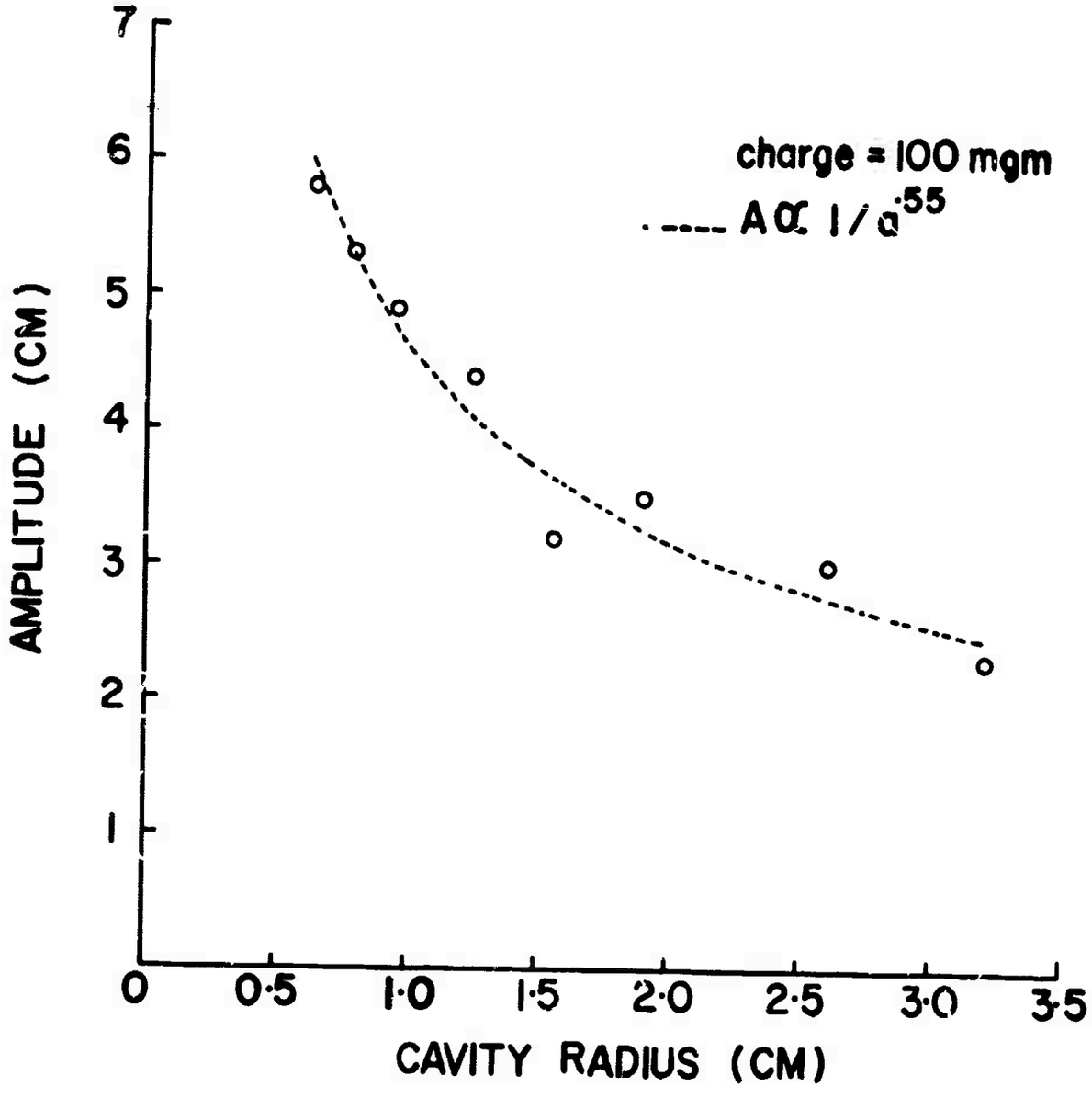

FIG·4 PEAK AMPLITUDE OF P-WAVES AS A FUNCTION OF CAVITY RADIUS

To get a quantitative value of the pressure applied on the surface of the cavity, a shock wave theory would be used to calculate the pressure decay inside the cavity. To compare this with the pressure transmitted to the medium, the amplitude and phase of the observed signal at the surface of the block would be corrected for the instrument, propagation path and geometrical divergence. Then from the reduced signal the transmitted pressure would be calculated.

References

Brown, F. W. (1956). Determination of basic performance properties of blasting explosives, First Symposium on Rock Mechanics, Colorado School of Mines Quarterly, 51, No. 3, 181.

Nicholls, H.R. and W. I. Duvall (1963). Effect of characteristic impedance on explosion-generated strain pulses in rock, Fifth Rock Mechanics Symposium, University of Minnesota, Fairhurst Editor (Pergamon Press).

7. Determination of Depth of an Earthquake Focus from the Spectrum of Body Waves.

Statement of the Problem. It is known that the spectrum of the seismic body waves as recorded at a seismographic station is influenced by several factors which include the depth of the earthquake focus. The purpose of this investigation is to find a method which will enable one to infer and hopefully determine approximate focal depth from the spectrum of seismic body waves as recorded at a single or a group of seismographic stations.

Theoretical Background of the Work. Much of the work of this investigation is based on the paper by Haskell (1953) in which he developed a matrix relation between the motion stress

vector (i.e. the horizontal and vertical components of particle velocity and the normal and tangential components of stress) at an interface of multilayered media and the amplitudes of plane waves below this interface. By an extension of Haskell's work, a matrix relation was formulated which enables one to calculate the amplitudes of plane waves in the layers of the source crust from the spectrum of body waves recorded at a seismographic station.

Since the general matrix relations developed by Haskell are familiar, the theory will not be presented in this summary. Suffice it to note that from the record of dilatational waves at a seismographic station one can calculate the frequency spectrum of $\dot{u}_o/c$ and $\dot{w}_o/c$. Using the matrix relations, one can obtain Δ_n'', the wave potential of an incident P wave at the receiver crust. By an extension of the matrix development one can then obtain the amplitudes of the plane waves, i.e. $\Delta'(P)$, $\Delta''(P)$, $\omega(P)$, and $\omega''(P)$, in the source layers which have given rise to dilatational waves in the mantle.

To obtain focal depth from these derived wave potentials two methods were considered.

> First method. If one calculates both the dilatational and rotational wave potential distribution of particular frequency at all points situated in a vertical column through the epicenter from the P waves recorded at a seismographic station i and sums the derived wave potential distribution with respect to i (i.e. one obtains the sum of the wave potential distribution derived from all seismographic stations around the epicenter), one can obtain the potential distribution in the neighborhood of the focus. If a source is present in the layered crust, theoretically one should obtain a maxima in the vicinity of the source. Therefore, the point at which the computed potential distribution shows a maxima will

roughly correspond to the position of the focus in the crust.

There are two major disadvantages which render the application of this method difficult. They are:

(a) Records from a large number of seismographic stations need to be analyzed and

(b) The travel time from the focus to the seismographic station needs to be known very accurately. The wave potential distribution should show a maxima near the focal region provided that the potential distribution at one particular instant is considered. In order to obtain the distribution of the wave potential at one particular instant in the source crust, one needs to consider both the amplitudes and phases of the wave potentials $\Delta'(P)$, $\Delta''(P)$, $\omega(P)$, and $\omega''(P)$. Since the time of transmission from the focus to the recording station affects the phases of these wave potentials, the transmission time needs to be known very accurately for all the recording stations. (Although, inaccuracy in the determination of the origin time of the earthquake will not matter, since this will affect the phases of the wave potentials for all the stations equally.)

Because of these difficulties, this method has not been tried yet.

Second method. The waveform recorded at a seismographic station is a transient time function. By a matrix formulation described earlier, one is able to calculate the wave potentials in the layers of the source crust from the recorded waveform. These wave potentials include the wave potentials of the upgoing and downgoing P waves and those of the upgoing and downgoing S waves in all the layers of the source crust. At any point in the source crust the waveform due to any of these potentials is a transient time function. However, the time of initiation of these four pulses should not be the same; it is only at the focus that all the four pulses should start at the same instant. If one calculates the waveforms due to these four waves at discrete points in a vertical column through the epicenter, theoretically only at one point should the four transients initiate at the same instant, and that point should correspond to the focus.

To test how this method works, an earthquake of magnitude 7 (depth of focus 25 Km) with epicenter near

Haiti was chosen and seismograms recorded at Golden, Colorado, were analyzed using a standard crustal model. The spectrum of the derived wave potentials indicated a focus at the crust-mantle boundary. It was at that state the underlying principle of the second method was re-examined. It appeared that the method would not work. At the present time, we are inclined to think that the chances that one will be able to obtain focal depth uniquely from observations at one single station are rather dim, since, as we shall see later, the spectrum of the body waves is influenced by factors other than the depth of earthquake focus.

Present Development. We also considered the question why the spectrum of the seismic body waves be at all influenced by the depth of the earthquake focus and the conclusion we reached is that the following factors, besides the characteristics of the recording instruments, will influence the spectrum:

(a) source spectrum and the dimension of the source - this includes (1) the (time) wave shape of the stress field at various parts of an extended source and (2) the effect of integration of waveforms radiated from different parts of the source as the recording station
(b) radiation pattern at the source region
(c) the layering of the source crust
(d) the position of the source in the layered crust.

To demonstrate the effect of factors (b), (c) and (d), let us consider a point source at A in the homogeneous crust shown below.

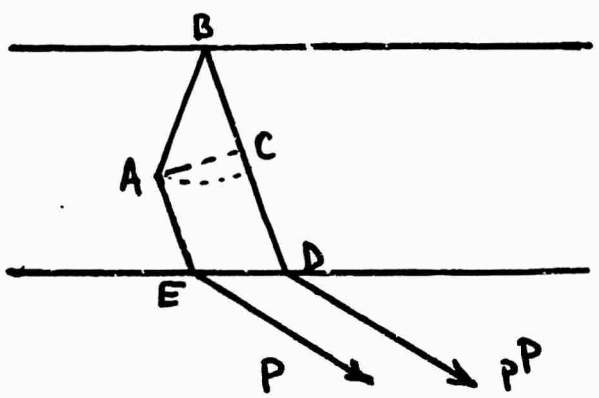

If the reflection coefficient at the free surface is -1, pP will be 180 degrees out of phase with respect to P and it will be delayed by a time T. At the receiving station one would observe a waveform which is the sum of pP and P.

Let P wave denoted as a time function $f_1(t)$ having frequency spectrum $F_1(\omega)$ and pP be denoted as $f_2(t)$ having frequency spectrum $F_2(\omega)$. Then the frequency spectrum of the sum of the two waveforms will be

$$F(\omega) = \frac{1}{\sqrt{2\pi}} \int_{-\infty}^{+\infty} e^{-i\omega t} \left[f_1(t) + f_2(t) \right] \quad dt$$

Assuming that the radiation along the directions AB and AE are the same, we have $f_2(t)$ the same as $f_1(t)$, except that $f_2(t)$ is 180 degrees out of phase and delayed by a time T with respect to $f_1(t)$. Hence,

$$F_2(\omega) = F_1(\omega) \exp\left[- i(\pi + \omega T) \right]$$

Therefore,

$$f_1(t) + f_2(t) = \frac{1}{\sqrt{2\pi}} \int_{-\infty}^{\infty} e^{i\omega t} \; F_1(\omega) \left[1 + e^{- i(\pi + \omega T)} \right] d\omega$$

Hence,

$$F(\omega) = F_1(\omega) \left[1 + e^{- i(\pi + \omega T)} \right]$$

Therefore, the effect of summing the two waveforms is the same as filtering $f_1(t)$ by a filter whose frequency response function is given by

$$K(\omega) = 1 + e^{- i(\pi + \omega T)}$$

Amplitude response function of this filter is of the form shown below

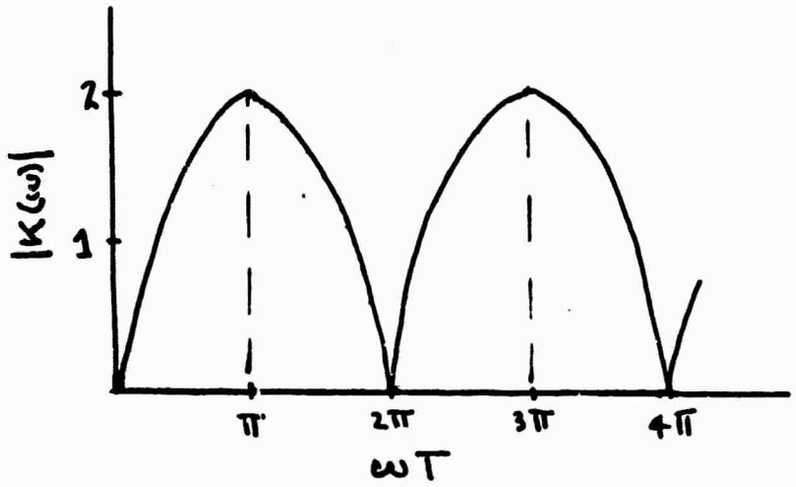

Thus one can see that certain discrete frequencies are totally eliminated in the resultant waveform. However, the picture as shown above is very simplified. In reality the filtering effect will not be as shown in the figure because of the following factors:

(1) because of influence of direction on radiation pattern, the strength of the signal propagated along the directions AB and AE are not the same

(2) the layering of the source crust will influence the relative strengths of pP and P; the layering will introduce internal reflections which will also be observed on the seismogram

(3) the reflection coefficient at the free surface, in general, is not -1.

Because of the above factors, none of the frequency components will be completely eliminated; however, there will be minima in the frequency spectrum at certain discrete frequencies. These characteristics of the frequency spectrum could

be utilized to determine focal depth. The procedure which has been recently thought about is outlined below:

(1) assume (i) an impulsive point source at some depth in the layered crust, (ii) radiation is same in all directions, and (iii) some reasonable value of reflection coefficient at the free surface

(2) calculate the dilatational waves emerging at the base of the crust at an apparent velocity c. This time function is the weighting function of the filter which results from compositing the P waves with pP, sP and internal reflections in the source layers

(3) by process of inverse filtering, remove the effect of filtering described earlier and thus obtain the frequency spectrum of the source which would have been observed at the focus had there been no reflectors, such as free surface and internal interfaces.

If the assumed focal depth, radiation pattern, reflection coefficient at the free surface are correctly chosen, one should obtain a reasonably smooth frequency spectrum. On the other hand, if these parameters, particularly the focal depth, are chosen erroneously, one should obtain maxima and minima in the spectrum at certain discrete frequencies. Thus by assuming focus at different depths in the layered crust, by a method of trial and error, one should be able to locate the most probable position of the focus by the criteria of the smoothness of the calculated frequency spectrum.

It should be pointed out that the proposed method cannot uniquely determine the focal depth. Also, in the light of the foregoing discussions, it appears that the chances that one will be able to find a method which can uniquely pinpoint the earthquake focus from observations at one single station are rather dim. The reason for this lack of uniqueness is that

the spectrum of the body waves is influenced by several factors other than the focal depth (examples of these factors: radiation pattern, spectrum at the source region, etc.) and from observations at one station it is not possible to eliminate the effect of other factors. However, the method outlined above could give the most probable position of the earthquake focus.

Reference

Haskell, N.A. (1953). The dispersion of surface waves on multilayered media, Bull. Seism. Soc. Am. 43, 17-34.

8. Factors Affecting the Determination of Phase Velocities.

Phase velocity curves obtained from seismograms are not always smooth, nor do they have the expected shape of theoretical phase velocity curves. As a result of difficulties encountered in the determination and interpretation of these curves considerable time has been spent during the last two quarters of this year in examining into the causes of these irregularities. The investigations are here summarized.

In particular, since the method of processing of data may contribute notably to the irregularities, we have examined quantitatively the effects of factors such as ramp functions and data windows on the phase velocity curves. For this purpose nine pairs of stations were selected more or less at random from sets of Rayleigh wave data for four earthquakes. The identical digitized data for each station pair were processed by different methods and the results compared. The earthquakes

and station pairs examined are given in Table 1.

In normal procedures records are digitized at approximately one second intervals. The digitized data are then filtered, smoothed and decimated using a six point filter (see Hamming, 1962, p 317) and the trend and mean removed. A Fourier analysis is then performed by applying Simpson's integration technique. Corrections for instrument magnification and phase response are made, and, finally, the phase velocity computations are performed by Sato's method (1955).

Except for a deconvolution procedure, variations in the data processing methods (that is, the way in which the digitized data are filtered and smoothed, the way in which the slope of the ramp function is determined, and the stage at which the correction for the mean is to be made) take place before the Fourier analysis.

Seven methods of data processing preceding phase velocity computations were applied.

1. The ramp angle was determined by means of a least square fit of the set of digitized data to a straight line. By correcting for the slope and intercept of the straight line the trend and the mean are removed from the data. Processing of the data then proceeded as indicated above.

2. The ramp angle was determined by computing the average of the first half of the digitized data series and the average of the second half, then passing a straight line thru the two points so located at one-fourth and three-fourths of the time duration of the data. The filtered data were corrected for this ramp angle, and then the correction for the mean made by subtracting the difference between the mean of the filtered and ramp-corrected data.

TABLE I

08 August 1963, Fox Is.	EBMT - BLA FLO - ATL
21 August 1963, Caribbean Is.	ATL - FLO
07 September 1963, Ascension Is.	ATL - RTNM MDS - FRMA
06 November 1963, New Guinea	GIMA - MDS FRMA - BLWV AAM - BRPA TDNM - DUOK

3. The ramp angle was computed as in process 2, then the filtered data were corrected for the slope and intercept of the ramp.

4. The data were filtered and the mean only was removed; no correction was made for the ramp angle.

5. The ramp was determined as in process 2, then a boxcar function with height A-(L - R)/2 was introduced. Here A is the mean of the filtered data, L is the mean of the first half of the digitized data, R the mean of the second half. This method of computing the boxcar height was chosen so that it would also be a function of the amplitudes of the data.

6. The ramp was determined as in process 2. Data processing continued as in that process but with the application of a hanning window to the filtered, and ramp and mean corrected data. The hanning window is given by

$$a(\tau_i) = 0.5\left[1 + \cos\pi\left(\frac{\tau_i - T}{T}\right)\right], \quad |\tau_i| < 2T, \quad i = 1,2,\ldots,n$$
$$= 0, \quad |\tau_i| > 2T$$

where n is the number of data points, τ_i is the time of the ith data point and T is one-half the time duration of the data (see Blackman and Tukey).

7. A deconvolution procedure was applied. This was based on the assumption that the finite length surface wave train was the product of an infinite wave train and a boxcar function in time. The resulting spectrum is the convolution of the spectrum of the infinite wave train with the spectrum of the boxcar function. Deconvolution to find the spectrum of the infinite wave train involves the solution of integral equations. Since the convolution spectrum is that obtained by Fourier analysis of the data, and since knowing the length of the data we can compute the spectrum of the boxcar function of unit height, it is possible to solve the integral equation for the spectrum of the infinite wave train.

In the deconvolution procedure the phase velocity curves obtained are in general jagged, with deep minima. There is little, if any, resemblance to the shape of theoretical phase velocity curves. From this it appears that the assumption of

multiplication by a boxcar function in time may be invalid. This implies that the physical situation of the data themselves corresponds to a signal of finite time duration.

The application of a hanning window also gave erratic phase velocities. The Fourier amplitude spectra have the same shape as without hanning, but are reduced in amplitude and are smoother. The Fourier phase spectra are generally quite different from the phase spectra found without hanning.

In short, neither deconvolution nor the application of a hanning window gave favorable results. No further discussion will be given of these two procedures.

There remain procedures 1 through 5. To examine the various parameters of the data processing procedures for their effect on phase velocity determination, computations from four representative pairs of stations from those given in Table 1 are here presented.

1. Pair ATL-FLO, 21 August 1963 (see Fig. 1*)

   Method 1. For ATL the least squares ramp angle, θ, is $+0.1^{\circ}$ and $h/\sigma = 0.001$, where h is the value of the mean and σ is the standard deviation. For FLO, $\theta = 0.0^{\circ}$ and $\sigma = 0.000$. Obviously this is a very good set of data.

   Method 2. For method $\theta = +2.2^{\circ}$ and 0.2°, respectively, which $h = 0$. This gives exactly the same phase velocities as method 1.

   In fact methods 2 through 5 give good agreement with the least squares method. The maximum ramp

*In the figures the entire phase velocity curves from 8 to 72 seconds are presented for purposes of comparison of the various processing methods. It should be noted that in some cases the curves should be terminated at periods corresponding to minima of the Fourier amplitude spectra. The amplitude spectra are indicated in the figures.

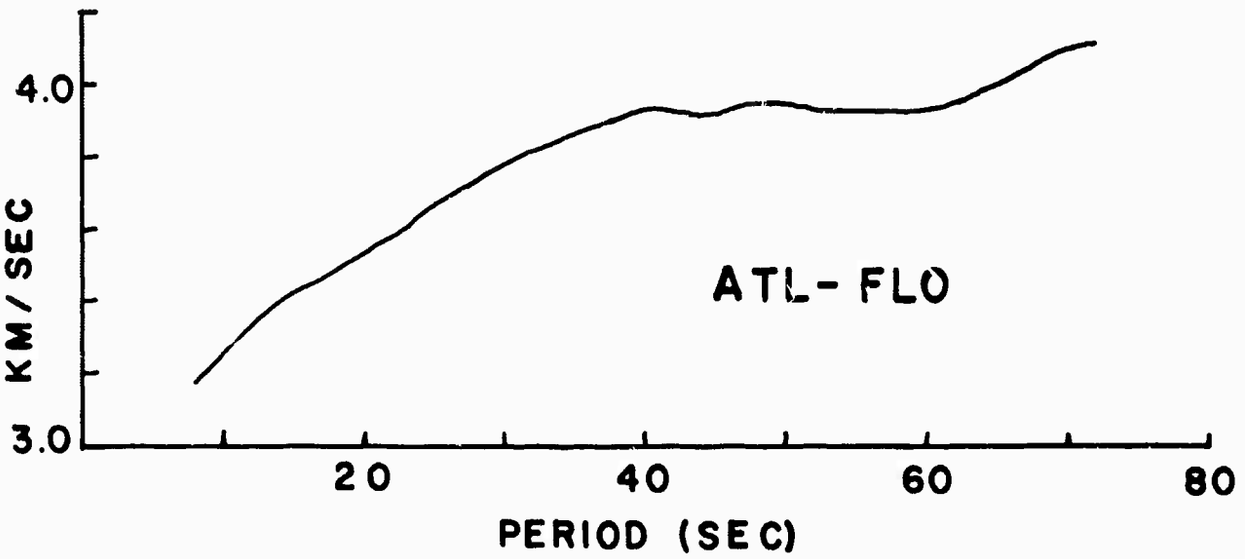
4.0
3.0
KM/SEC
ATL- FLO
20
40
60
80
PERIOD (SEC)

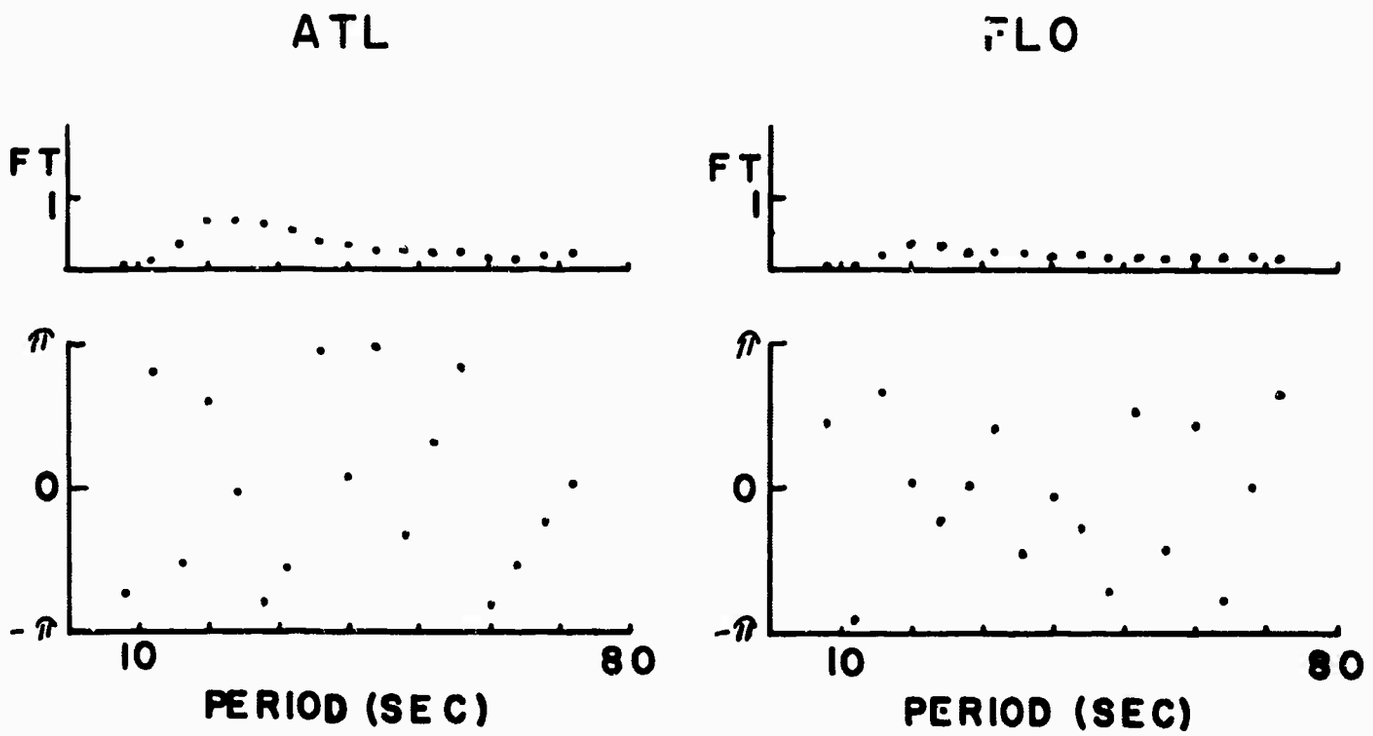
ATL
FLO
FT
1
π
0
-π
10
80
PERIOD (SEC)

Fig 1

angle is 2.2° and the maximum value of h/σ is 0.081.

The probable reason for this is the relatively low amplitudes of the surface waves. The possible range of the ramp angle and the value of the mean are much restrained.

2. Pair ATL-RTNM, 07 September 1963 (see Fig. 2).

Method 1. The curve is not so smooth as for the preceding pair. For ATL, $\theta = -2.5$ and $h/\sigma = 0.003$; for RTNM $\theta = 0.0$ and $h/\sigma = .25$.

Method 2. This method gives almost the same phase velocity curve as that from method 1, but smoother. For ATL $\theta = -5.8°$; for RTNM, $\theta = +4.1°$. The mean is zero. Evidently for the period range 8-72 seconds the effects of the ramp angles cancel and since the mean is zero a smoother phase velocity is obtained.

Methods 3 and 4. These methods each have $h/\sigma = 0.0$ and yield the same angles as above, thus giving the same phase velocities.

Method 5. Here $h/\sigma = 0.01$ for ATL and 0.236 for RTNM. The resulting phase velocity curve oscillates about the curve found by method 1. This may be caused by the different ramp angles.

3. Pair FRMA-BLWV, 06 November 1963 (see Fig. 3).

Method 1. For FRMA, $\theta = -0.1°$, and for BLWV $\theta = 0.1°$, $h/\sigma = 0.012$, and for BLWV $\theta = +0.1°$, $h/\sigma = 0.022$.

Method 2. The phase velocities match those of method 1. But for FRMA $\theta = 3.7°$ and for BLWV $\theta = 22.2°$, with zero means. The period range of interest (8-72 sec.) and the relative time durations of the data (FRMA, 579 sec; BLWV, 327 sec.) must account for the matching of the phase velocities. The angle of 22.2° would seem to be too large to allow reasonable results.

Method 3. The values of θ are -0.8° and -3.9°, respectively; the means are zero. The phase velocities are very nearly identical to those of method 1.

Method 4. Phase velocity curve is irregular.

Method 5. $\theta = 3.7°$ and 22.2°, respectively, and $h/\sigma = 0.138$ and 0.064. The respective means

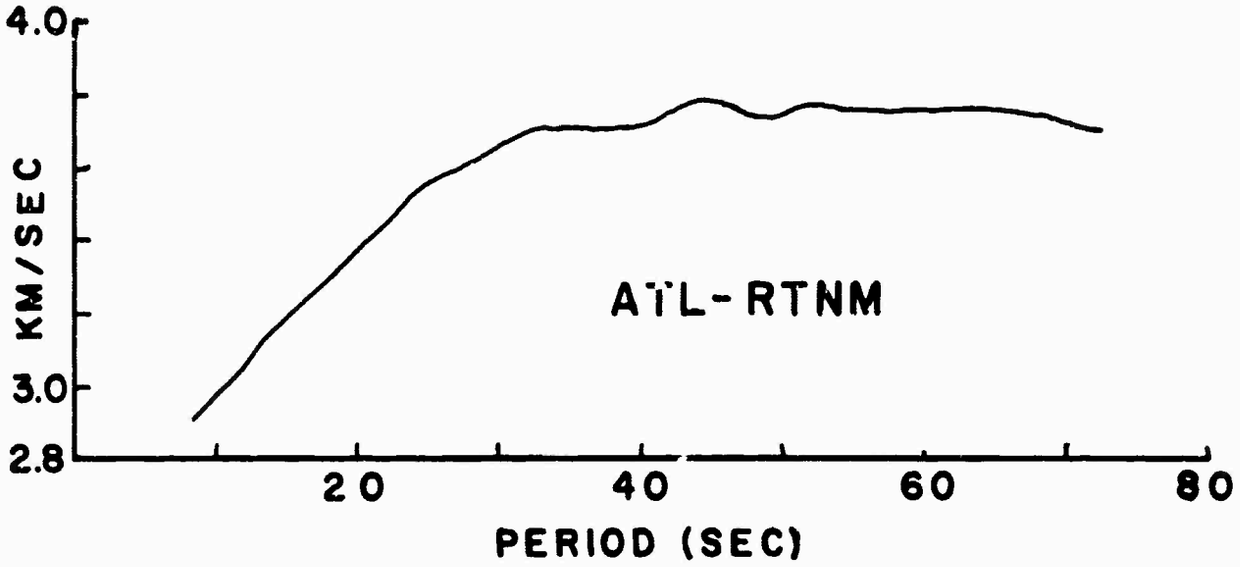
4.0
3.0
2.8
KM/SEC
ATL-RTNM
20
40
60
80
PERIOD (SEC)

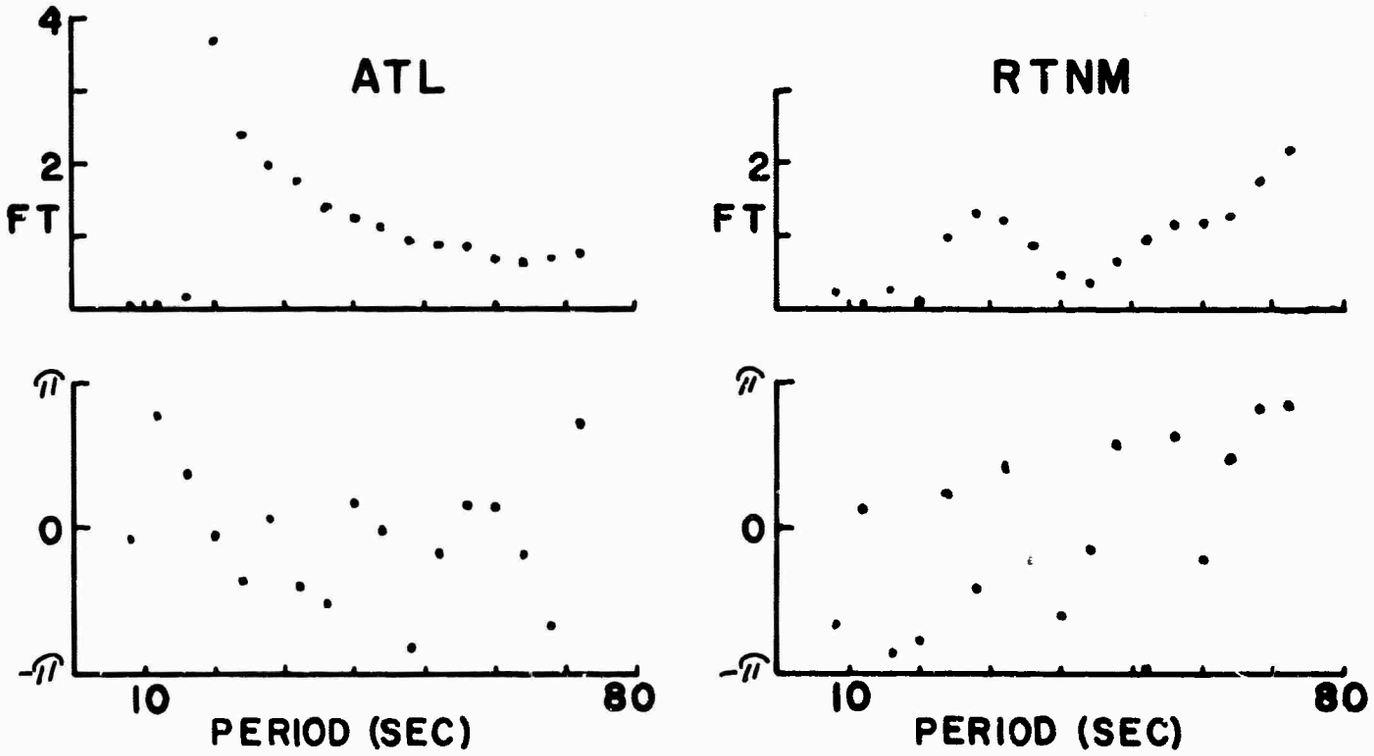
4
2
FT
ATL
RTNM
2
FT
π
0
-π
10
80
PERIOD (SEC)
π
0
-π
10
80
PERIOD (SEC)

Fig. 2

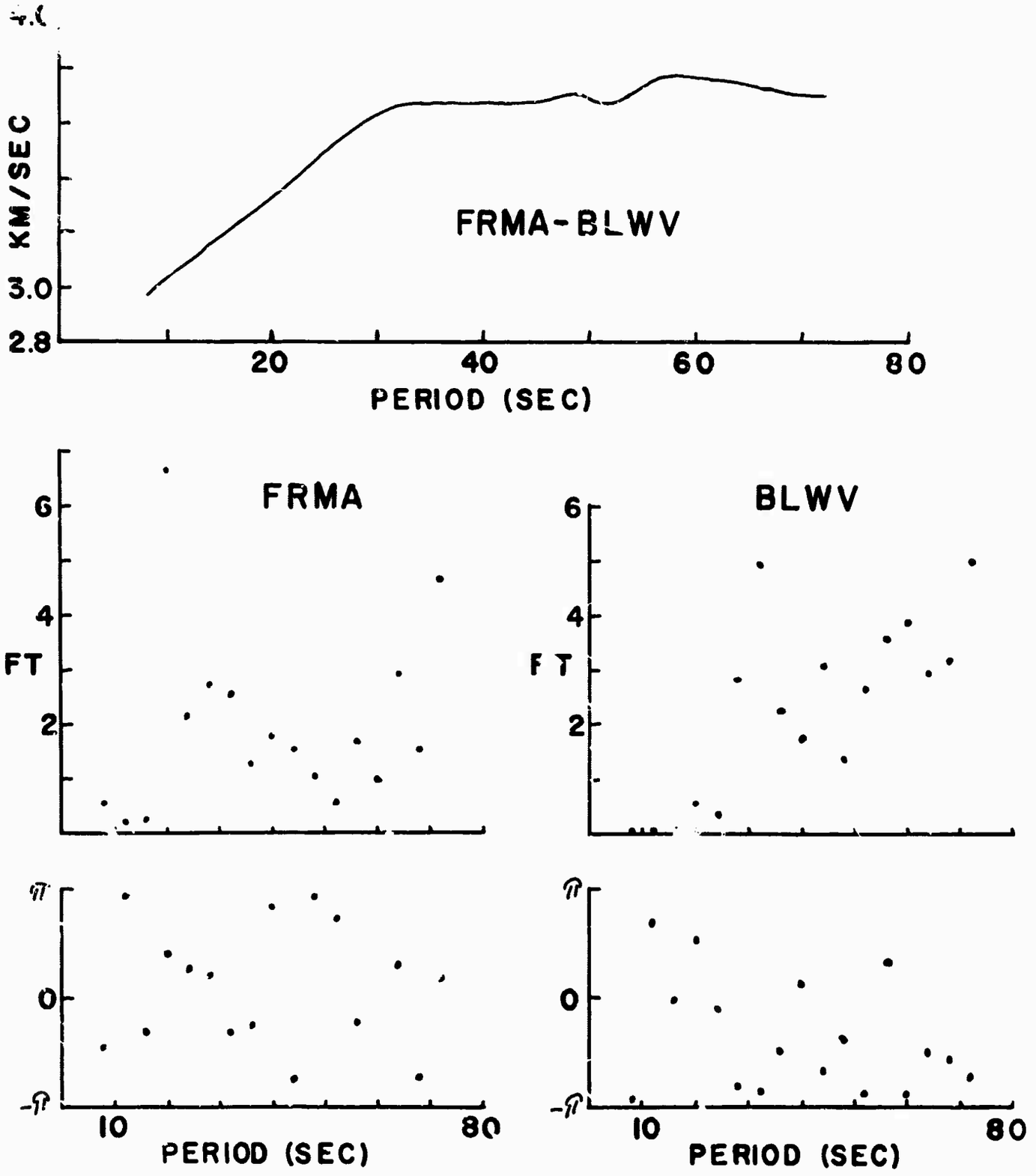
KM/SEC
3.0
2.8
FRMA-BLWV
20
40
60
80
PERIOD (SEC)
FRMA
BLWV
6
4
2
FT
π
0
-π
10
80
PERIOD (SEC)

Fig. 3

are -29.9 and +30.2. It appears that the effect of boxcar functions approximately equal in magnitude but opposite in sign cancel for the period range 8-72 sec.

4. Pair EBMT-BLA, 08 August 1963 (see Fig. 4).

Method 1. For EBMT $\theta = -7.2^{\circ}$ and $h/\sigma = 0.014$; for BLA $\theta = -0.4^{\circ}$ and $h/\sigma = 0.34$. The combination of the large θ at the first station and large h/σ at the second probably account for the appearance of the curve.

Methods 2-4. These methods give approximately the same type of oscillating curves. For all three methods ramp angles are -21.2° and $27\ 0^{\circ}$ with zero means.

Method 5. Ramp angles the same as in 2-4, but $h/\sigma = 0.027$ and 0.182, respectively.

Although the data from these pairs of stations are few, it is possible to propose some tentative results. If the maximum period of interest is approximately one-third or less of the time duration of the data, the effects of boxcar functions of about the same magnitude but of opposite sign at each of the two stations cancel when computing phase velocities. The same seems to be true of the ramp angle. It also appears that a boxcar of some relatively small amplitude and/or a small ramp angle may be allowable but the relation of the magnitudes of the two functions to other parameters is ambiguous.

Relatively low amplitude surface waves give the better results for the first five data processing methods. This is attributable to the restriction in the range of the mean and of the ramp angle.

The procedure of using the first half and the second half of the data to compute the ramp angle (to be called the half

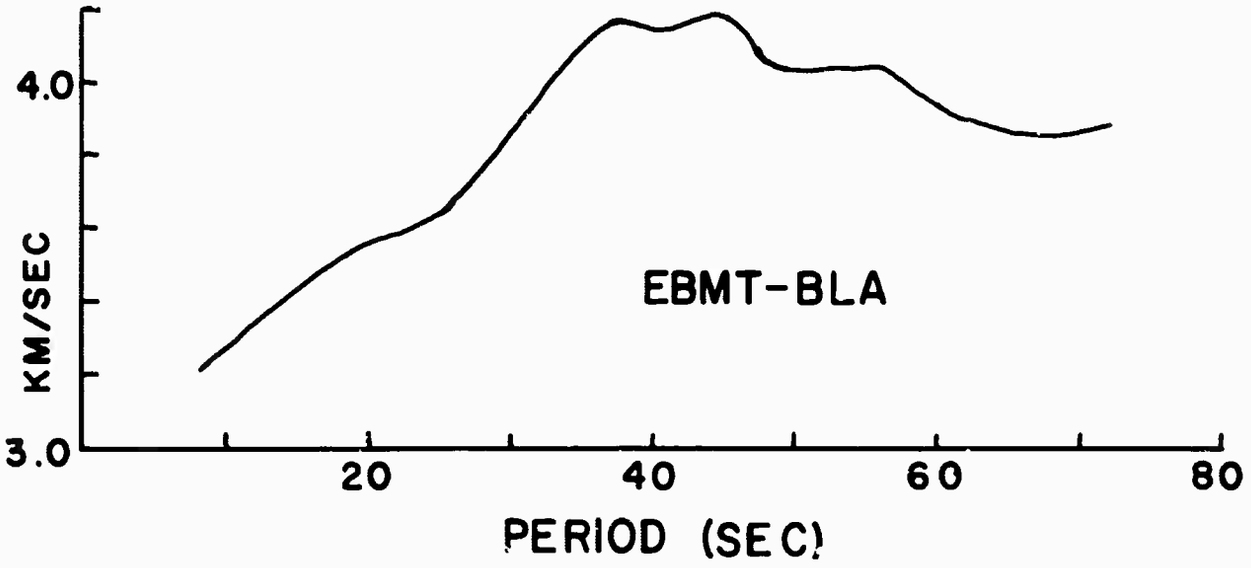
4.0
3.0
KM/SEC
EBMT-BLA
20
40
60
80
PERIOD (SEC)

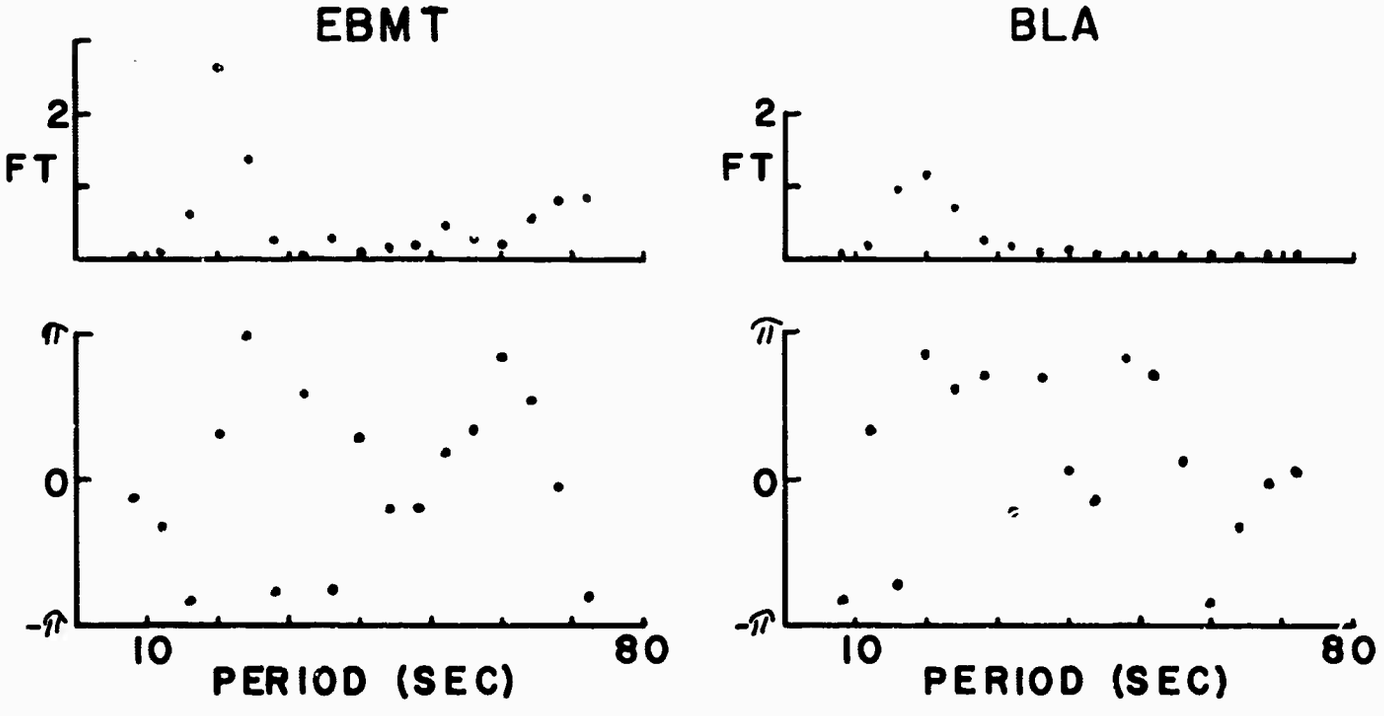
EBMT
BLA
2
FT
2
FT
π
0
-π
π
0
-π
10
80
PERIOD (SEC)
10
80
PERIOD (SEC)

Fig. 4

and half method) always gives angles larger than the least squares method. Filtering of the digitized data usually introduces a ramp angle large enough that subtracting the slope of the original data from the filtered data there still remains a ramp angle that is two to four times the ramp angle in the original (digitized) data. Thus the data that are Fourier analyzed often have a ramp angle larger than that in the original data. Note that these ramp angles are computed by the half and half method.

The ramp angle of the original data computed by the least squares method is always less than the ramp angle computed by the half and half method. With the least squares method, the ramp angles of the original and filtered data are within 0.2° of each other, so that the ramp angle of the data which are Fourier analyzed is less than $\pm 1.0^{\circ}$ in the majority of cases, and often less than $\pm 0.4^{\circ}$.

While the least squares method of computing the ramp angle was taken as the standard method against which the others were compared, this does not necessarily mean it is the best method. The half and half method often gave phase velocity curves whose shapes were very nearly the same as the curves from the least squares method, even though they did not agree in numerical value. Part of the reason for this is apparently compensating effects in each of the two sets of data. It may be that the half and half method gives a better representation of the base line thru the data because of its dependence upon the means of the first half and

and second half of the data series, whereas the least squares method is related to the mean of the entire data series. This comparison is complicated by the effect that the half and half method leaves large ramp angles in the data.

Another, and possibly more serious, problem is that of over correction. For some data sets that have small ramp angle, it was attempted to again remove the mean and ramp angle by the least squares method before Fourier analyzing. But, unexpectedly, the ramp angle increases, though the mean becomes closer to zero.

Intuitively, the least squares method would seem to be the best method for removing the ramp function from the data. Also, the ramp angles computed by the least squares technique are generally smaller, and therefore more acceptable, than the angles computed by the half and half technique. However, since neither of the methods is able to completely remove the ramp angle, more work in this area is required.

References

Sato, Yasuo (1955). Analysis of Dispersed Surface Waves by Means of Fourier Transform 1, BERI, 33, 33-48.

Hamming, R.W. (1962). Numerical Methods for Scientists and Engineers, McGraw-Hill, New York.

Blackman, R.B. and J. W. Tukey (1959). The Measurement of Power Spectra, Dover, New York.

B. Work already published or submitted for publication.

Work mentioned in this section has already been reported in detail. Consequently, by way of summary, abstracts of the papers in question are here presented.

1. "The Focal Mechanism of the Alaska Earthquake of 28 March 1964 and of Its Aftershock Sequence," William Stauder and G. A. Bollinger, Jour. Geophys. Res. 71, (1966): 5283-5296.

Abstract

Focal Mechanisms have been determined for one preshock, for the main shock, and for more than twenty-five aftershocks of the Alaska earthquake of 28 March 1964. For the main shock a single nodal plane with strike N66°E, dip 85° southeast is determinable from the polarity of the P wave. This plane may be taken either as a plane normal to the fault motion (thrust faulting) or as the fault plane (dip-slip motion on a near vertical plane). A combination of P wave first motion and S wave polarization data make possible the determination of both nodal planes in each shock studied of the aftershock sequence. One of these planes is near vertical and resembles closely the nodal plane of the main shock, the other dips 5° to 15° to the northwest or north. For earthquakes of the Kodiak Island region, the near vertical plane has the same orientation as that of the main shock. For earthquakes to the east of Prince William Sound, this plane shows a systematic change in orientation corresponding to the change in trend of the tectonic features. Three earthquakes, with foci at increasing depths along the line of greatest flexure of the tectonic features differ from the others. The difference in character of these foci probably provides an important clue to the right interpretation of the motion in the main shock. While the focal mechanism solutions for the shocks here studied are subject to the same ambiguity of the interpretation as that of the main shock, criteria which favor a thrust hypothesis are advanced from the inter-relation of the foci. From dislocation theory it is shown that differential slip and/or a dipping thrust plane explain satisfactorily the observed vertical displacements at the surface.

2. "The S-Wave Project for Focal Mechanism Studies, Earthquakes of 1963," William Stauder and G. A. Bollinger, Bull. Seism. Soc. Am. 56 (1966): 1363-1371.

Abstract

P and S wave data for thirty-five earthquakes selected from among the larger earthquakes of 1963 have been investigated. Focal mechanism determinations for twenty-six of these shocks are here presented. The solutions are based upon a combination of a graphical and a computer method for determining the poles of the nodal planes. In all cases it has been found that the mechanism may be adequately represented by a double couple as an equivalent point source of the focus, although in some few instances a single couple cannot be excluded as a possible alternate interpretation. The solution of a mid-Atlantic earthquake of November 17, 1963 is presented as an example of a focus which clearly conforms to the double couple model.

Special attention is called to the solutions for a series of earthquakes in the Kurile Islands, and to three earthquakes of the mid-Atlantic.

3. "Master Curves for the Response of Layered Systems to Compressional Seismic Waves." Luis M. Fernandez, Bull. Seism. Soc. Am. 56 (1966): 1363-1371.

Abstract

The layers of the earth's crust act as a filter with respect to seismic energy arriving at a given station. Consequently the motion recorded at the surface depends not only on the frequency content of the source and on the response characteristics of the recording instrument, but also on the elastic parameters and thicknesses of the transmitting layers. This latter dependence is the basis for a method of investigating the structure of the crust and upper mantle.

To facilitate this investigation a set of master curves for the transfer functions of the vertical and horizontal component of longitudinal waves and their ratios is presented. The calculation of these curves is in terms of a dimensionless parameter. This calculation allows one to group the curves corresponding to different crustal models into families of curves. The characteristics of these curves are discussed from the point of view of their "periodicity" in the frequency domain and of their amplitude in order to investigate

the influence of the layer parameters. Considerations, either of constructive interference or of Fourier analysis of a pulse multiply reflected within the layer system, reveal that the amplitudes of the transfer curves depend on the velocity contrasts at the interfaces of the system. The "periodicity" or spacing of the peaks depends on the time lags between the first arrivals and the arrivals of the different reverberations. Closely spaced fluctuations correspond to large time lags, and widely spaced fluctuations to short time lags.

4. "Model Investigation of Explosions in Prestressed Media," W. H. Kim and Carl Kisslinger, Geophysics, 32 (1967): 633-651.

Abstract

Seismic effects of explosions and rupture propagation in prestressed two-dimensional models (Plexiglas, aluminum) as well as anisotropy produced by the stress field are investigated. An explosion in a prestressed medium releases a portion of the stored strain energy by one or more of the following mechanisms: (1) formation of directional cracking, especially in brittle materials, (2) release of strain energy in the elastic zone outside the cavity, and (3) rupture propagation. Phenomena associated with all of these mechanisms were observed in the present investigation.

Explosions in prestressed Plexiglas produce cracks in preferred directions, the intensity of which increases with the applied stress. Explosions in prestressed aluminum sheets do not cause fracturing but rather plastic deformation about the explosion. Straight and branching modes of moving cracks initiated from explosions in prestressed Plexiglas can be explained on the basis of stress distribution ahead of the crack tips.

Observed radiation patterns resulting from explosions in prestressed media indicate asymmetrical radiation fields which are a direct consequence of strain energy release for the case of aluminum and by the combined effects of directional cracking and energy release in the elastic zone for the case of Plexiglas. Explosions in prestressed media generate shear waves. The observed S-wave magnitude increases sharply with the level of the existing stress field for a given amount of strain energy release. It is concluded that this phenomenon is attributable to the effective conversion of energy release to seismic radiation at high ambient stress fields. In other words, the effectiveness of S-wave generation is governed

by the rapidity with which the existing strain energy is released.

A definite anisotropy effect was observed in pre-stressed models, but this effect is not large enough to affect wave propagation in the range of the tensile loads applied.

5. "Ray Theory in an Anisotropic Inhomogeneous Elastic Medium," N. J. Vlaar, submitted to Bull. Seism. Soc. Am.

Abstract

A ray theory is developed for an inhomogeneous, anisotropic medium, based on the concept of a wave front as the carrier of a discontinuity in particle velocity. The discontinuity conditions of several field quantities involved are formulated and serve to cast the problem in terms of a partial differential equation. The characteristics of this equation subsequently are identified in terms of rays, represented in parametric form as space curves. The energy transport along the rays is formulated by means of transport equations.

The theory is applied in particular to the case of the transversely (horizontally) isotropic, vertically inhomogeneous medium. Equations for rays and travel times are obtained in the form of integrals, which are suited for serving the purpose of numerical computations.

6. "Determination of Earthquake Fault Parameters from Long Period P Waves," G. A. Bollinger, submitted to Journ. Geophys. Res.

Abstract

The theory for propagating earthquake sources predicts a "Doppler-type" effect in the time duration of the radiated body wave pulses. With the assumption of a constant fracture velocity the time duration of these pulses is directly related to the length of the fault but has different spatial patterns of variation for the unilateral and bilateral faulting cases. To relate this time duration of energy release to the observed long-period P waves, various pulseforms are postulated whose time history is controlled by the fault parameters of length and fracture velocity. These pulses are convolved

with the impulse response of a standard crust-seismograph system to yield theoretical P wave seismograms. A relation is thereby established between the time durations of the radiated pulses and those observed at the surface of the earth. This relationship is employed to correct the times of observed long period P waves so as to recover the original time-duration radiation pattern. By a minimum deviation technique the fault length and fracture velocity can be found that best fits this observed pattern. This procedure is shown to yield reasonable results for four different earthquakes from three different regions.

7. "The Thickness of the Crust in Central U.S. and La Paz, Bolivia, from the Spectrum of Longitudinal Seismic Waves" Luis M. Fernandez, submitted to Bull. Seism. Soc. Am.

Abstract

The ratio of the vertical and horizontal components of the P phase provides a crustal transfer function which is independent of the frequency content of the source and is a function only of the angle of incidence of the rays and the crustal parameters of the site where the observation is taken.

This ratio of the vertical and horizontal spectra corresponds to the tangent of the apparent angle of emergence and as such this apparent angle is a function of the frequency. Spectra of this type have been obtained in the Central U.S. and in La Paz, Bolivia, for large magnitude teleseisms. The observed curves have been compared with theoretical universal curves corresponding to one and two layer models.

Average results for several observations give a crustal thickness in the Central U.S. of 42 kilometers and a mean P velocity of 6.6 km/sec. For the Bolivian Andes at La Paz, the crustal thickness obtained is of 64 kms and the mean P velocity of 6.7 km/sec. These results are in good agreement with similar determinations obtained by independent methods.